

INFORMATION TO USERS

This manuscript has been reproduced from the microfilm master. UMI films the text directly from the original or copy submitted. Thus, some thesis and dissertation copies are in typewriter face, while others may be from any type of computer printer.

The quality of this reproduction is dependent upon the quality of the copy submitted. Broken or indistinct print, colored or poor quality illustrations and photographs, print bleedthrough, substandard margins, and improper alignment can adversely affect reproduction.

In the unlikely event that the author did not send UMI a complete manuscript and there are missing pages, these will be noted. Also, if unauthorized copyright material had to be removed, a note will indicate the deletion.

Oversize materials (e.g., maps, drawings, charts) are reproduced by sectioning the original, beginning at the upper left-hand corner and continuing from left to right in equal sections with small overlaps. Each original is also photographed in one exposure and is included in reduced form at the back of the book.

Photographs included in the original manuscript have been reproduced xerographically in this copy. Higher quality 6" x 9" black and white photographic prints are available for any photographs or illustrations appearing in this copy for an additional charge. Contact UMI directly to order.

UMI

A Bell & Howell Information Company
300 North Zeeb Road, Ann Arbor MI 48106-1346 USA
313/761-4700 800/521-0600

**Quantum Theory of a Hydrogen Atom
in a Circularly Polarized Electromagnetic Field
Near the Principal Resonance**

by
Maciej K. Kalinski

Submitted in Partial Fulfillment
of the
Requirements for the Degree
Doctor of Philosophy

Supervised by
Professor Joseph H. Eberly
Department of Physics and Astronomy
The College
Arts and Sciences

University of Rochester
Rochester, New York

1997

UMI Number: 9808888

**Copyright 1998 by
Kalinski, Maciej Konrad**

All rights reserved.

**UMI Microform 9808888
Copyright 1998, by UMI Company. All rights reserved.**

**This microform edition is protected against unauthorized
copying under Title 17, United States Code.**

UMI
**300 North Zeeb Road
Ann Arbor, MI 48103**

Curriculum Vitae

The author, Maciej K. Kalinski, was born in Warsaw, Poland on February 25, 1968. He attended Warsaw University of Technology from 1986 to 1991, and graduated with a Master of Science degree in 1991. He came to the University of Rochester in the Fall of 1992 and begin graduate studies in physics. He held various research and teaching assistantships and received the Agnes and George Messersmith Fellowship in 1996. He pursued his research in the field of atoms in strong fields under the direction of Professor Joseph H. Eberly.

Acknowledgments

Most of all I would like to thank Prof. Joseph Eberly for initiating and supervising my thesis project as well as for supporting this and my other research during my studies in Rochester.

I would also like to thank Prof. Iwo Bialynicki-Birula for his deep involvement at the initial stage of the project as well his constant valuable comments and suggestions.

The remarkably written and easy to modify computer program created by Prof. Rainer Grobe was essential to test our theoretical predictions during the project. Also his expert knowledge in numerical methods of time dependent quantum mechanics, which he never refused to share, was of a great help for me.

I would also like to thank other members of the quantum optics theory group, especially Chi-Kwong Law for valuable comments and suggestions related to my work.

Repeated interactions with Prof. Carlos Stroud and other members of his research group, especially Michael Noel and Jim West were, of a great help for me in realizing the connections between my work and other work related to electron wave packets in Rydberg atoms, as well as for better understanding of experimental reality of Rydberg systems.

Finally I would like to acknowledge the financial assistance of the Agnes and George Messersmith Fellowship at the University of Rochester.

Abstract

In this thesis we present the quantum theory of a hydrogen atom interacting strongly with a time dependent circularly polarized electromagnetic field. This is classically a non-integrable system. We demonstrate approximate integrability of the time dependent Schrödinger equation near the principal resonance, and by the proper choice of basis states we reduce the complicated nonseparable system to an effective quantum pendulum. For the class of quantum states discussed we also extend our theory to the case of a linearly polarized electromagnetic field within a modified Rotating Wave Approximation. Within the theory we are able to define and describe new so-called Trojan states, well-localized packets moving on classical trajectories which can also be predicted within a simpler harmonic approximation discussed in the thesis. We also predict other well localized packet states without a classical origin, so-called anti-Trojan states.

Numerical solutions of the time-dependent and field-dependent Schrödinger equation are used to confirm the validity of these approximations even in the range of relatively low principal quantum numbers ($n = 10-20$). An adiabatic extension of the theory allows us to work out the method for generating well localized states from circular Rydberg states, which can be produced under contemporary experimental conditions. We present the results of numerical simulations showing that well localized Trojan states can be generated from the circular states by the right adjustment of the external field frequency to the principal quantum number of the initial state. The adiabatic extension of the theory allows us to predict the uncertainty of the position of the packet as well as its distance from the atomic nucleus. Therefore the size of the atom can be further controlled with the use of a field with a time dependent frequency.

We also discuss a possible detection method by a use of very short half-cycle

laser pulses, which is a reasonable method for time and space dependent analysis of atomic quantum states.

Table of Contents

1	Introduction	1
2	Hydrogen Atom in Circularly Polarized Field as Nonseparable System	6
2.1	Classical dynamics	6
2.2	Approximate separability in the low frequency limit	11
2.3	Related quantum systems	15
3	Harmonic Approximations	20
3.1	General stability of rotating extremum	20
3.2	Energies and states in Cartesian coordinates	24
3.3	Energies and states in cylindrical coordinates	30
3.4	Nonlinear corrections to harmonic approximation	35
4	Energies and States within Nonlinear Theory	38
4.1	Overview	38
4.2	Energies and states of the quantum pendulum	39
4.3	High n expansion and resonant approximation	44
4.4	Energies and states	49
4.5	Analytic, asymptotic and numerical tests of pendular versus harmonic approximation	53
4.6	Relation to Stark effect	59
4.7	Corrections by small detuning and quantum defect	66
5	Importance of Localized States and Numerical Confirmations	71
5.1	Trojan wavepackets	71

5.2 Anti-Trojan wavepackets	77
6 The Case of Linear Polarization	86
6.1 Corrected RWA approximation	86
6.2 Three-dimensional Schrödinger's cat states	94
7 Application to Quantum Control	96
7.1 Adiabatic connection to zero-field states	96
7.2 Three-dimensional localization of Rydberg electron	97
7.3 Expansion and compression of Rydberg atom	104
8 Theory of Detection of Localized States	112
8.1 Effect of a short pulse on the quantum state	112
8.2 Scattering cross section for δ -pulse ionization	113
9 Summary	119
References	121

List of Figures

Figure	Page
2.1 Classical trajectories of the electron in C.P. field obtained from a small perturbation of the circular trajectory. The classical equations of motion depend only on scaled variables $\mathbf{r}_{sc} = \mathbf{r}\omega^{2/3}$, $t_{sc} = \omega t$, $\mathcal{E}_{sc} = \mathcal{E}\omega^{-4/3}$. The upper plot shows a weakly perturbed circular trajectory when it is stable for ($\mathcal{E}_{sc} = 0.044$) and the lower plot when unstable (for $\mathcal{E}_{sc} = 0.228$).	10
2.2 The electron probability density in the elliptical state (2.52) for $n = 20$ and $\varepsilon = 0.7$. The charge distribution is being polarized with respect to the nucleus ($x = y = 0$), as it is localized around the classical elliptical orbit with the eccentricity ε	16
3.1 The islands of stability (shaded areas) in the plane of parameters a and b where both ω_+ and ω_- are real. In the parabolic triangle the potential has a saddle point. Points lying on the lines $a + 2b = 0$ and $2b + a = 0$, which intersect the stability region, correspond to the atom in a C.P. field, and the line $a + b = -1$ to the gravitational three-body problem of Trojan asteroids.	22
3.2 Real and imaginary parts of the eigenfrequencies ω_+ and ω_- of the hamiltonian (3.31) scaled to the frequency of the C.P. field ω . The imaginary parts vanish in a tiny stability zone for $8/9 < q < 1$. . .	27

- 3.3 Real parts of the parameters A , B , and C of the pseudo ground state wave function (3.48) plotted as functions of the parameter q . Note that the real part of A is much smaller than the real part of B in the stability region $8/9 < q < 1$ and has a maximum for $q \approx 0.9562$ 31
- 3.4 Imaginary parts of the parameters A , B , and C of the pseudo ground state wave function (3.48) plotted as functions of the parameter q . The imaginary parts vanish in a tiny stability zone for $8/9 < q < 1$ which provides the wave function to be square integrable. 32
- 4.1 Levels of scaled energy $-\alpha$ (corresponding to symmetric Mathieu functions) as functions of the parameter p . The value $-\alpha = 2p$ corresponds to Trojan states. States with scaled energy in the vicinity of the line $-\alpha = -2p$ are anti-Trojan states. Note that anti-Trojan states do not belong to a single energy line but to different lines close to the spectrum folding around $\alpha = 2p$ 41
- 4.2 A few of the lowest eigenfunctions of the quantum pendulum (π -periodic Mathieu functions) labeled in order of the excitation for $p = 60$. For this choice of the parameter p they resemble the eigenfunctions of the harmonic oscillator. 42
- 4.3 Probability density of one of the higher excited states of the quantum pendulum (6-th, even) as a function of both the angle ϕ and the parameter p . Note the change from the plane-wave-like behaviour for low p characteristic of the rigid rotor to oscillator-like behaviour for high p . The change of behavior occurs near separatrix $\alpha = 2p$ near $p = 60$, where the wave function strongly peaks around $\phi = \pi$ 43

- 4.4 Examples of the eigenfunctions (4.37) for the scaled field $\mathcal{E}_{sc} = 0.016$ and $n_0 = 20$ corresponding to even-order Mathieu functions and the circular-states manifold ($k = 1, s = 0$): (a) $jks=010$, pure Trojan packet-state, (b) $jks=210$, oscillatory-like, from above the separatrix, (c) $jks=410$, near the separatrix, (d) $jks=610$, (e) $jks=810$, (f) $jks=1010$, rotational-like, below the separatrix. 52
- 4.5 Eigenfrequencies of the harmonic hamiltonian (3.11) as functions of the parameter q and the spacing σ obtained from formula (4.38). Note that generally $\omega_o \approx \omega_+ \approx \omega$ and $\sigma \approx \omega_-$, so the energy spectra obtained from the basis expansion method with the assumption about noninteracting manifolds and from the harmonic approximation approximately coincide. For lower field strengths (larger q) the agreement is better. 55
- 4.6 Parameters of the pseudo ground state wave function (3.58) obtained from the harmonic approximations as functions of the parameters q and β given by (4.42) from the noninteracting manifolds model. For larger q we have $B \approx C \approx D \approx 1$ and also $A \approx \beta$, and therefore the harmonic wave function agrees approximately with the one obtained from the basis expansion for lower field strengths (however fields strong enough to permit the harmonic approximation in the Mathieu equation as given by the condition (4.43). 58
- 4.7 Energy spectrum as a function of scaled electric field in the vicinity of the $n_0 = 10$ circular state for $\omega = 1/n_0^3$. The marker points belong to the Trojan lines. One can see two doublets on the diagram separated by approximately $\omega = 0.001$. The large marker point corresponds to Gaussian-like Trojan packet for $\mathcal{E}_{sc} = 0.016$ 60

4.8	Energy spectrum as a function of scaled electric field in the vicinity of the $n_0 = 20$ circular state for $\omega = 1/n_0^3$. The marker points belong to the Trojan lines. One can see two tripets on the diagram separated by approximately $\omega = 0.000125$. The large marker point corresponds to the Gaussian-like Trojan packet for $\mathcal{E}_{sc} = 0.016$. . .	61
4.9	Doublets obtained from the expression (4.31) within nonlinear theory for $\omega = 1/10^3$. The large point corresponds to the Gaussian-like Trojan packet for $\mathcal{E}_{sc} = 0.016$	62
4.10	Triplets obtained from the expression (4.31) within nonlinear theory for $\omega = 1/20^3$. The large point corresponds to the Gaussian-like Trojan packet for $\mathcal{E}_{sc} = 0.016$	63
5.1	Lagrange equilibrium points in celestial mechanics. The collinear points L_1 , L_2 and L_3 are always unstable. The equilateral points L_4 and L_5 are stable for $\mu(1 - \mu) < 1/27$ and they are the points of accumulation of Trojan asteroids in the sun-Jupiter system. . .	74
5.2	Time evolution of the wave packet in the laboratory frame prepared at $t = 0$ according to (3.47) for $\omega = 1/60^3$ and $q = 0.9562$, i.e, for the maximum of $A(q)$. Snapshots of the contour lines of the probability distribution are taken three times per cycle for the cycles 1, 2, 3, 5, 7, and 10. Each square covers the space region of the size 11250×11250 atomic units.	76

5.3	Time evolution of the wave packet in the laboratory frame prepared at $t = 0$ according to (3.63) for $l_0 = 60$, $\omega = 1.09/60^3$ and $\mathcal{E}_{sc} = 0.050$, i.e., for the maximum of A obtained numerically from the modified Gaussian approximation. Snapshots of the contour lines of the probability distribution are taken three times per cycle for the cycles 1, 2, 3, 5, 7, and 10. Each square covers the space region of the size 11250×11250 atomic units.	78
5.4	Values of $P(t)$, the total probability inside the circle with radius approximately twice the radius of the classical orbit for the time evolution plotted in Fig. 5.3.	79
5.5	Values of the correlation function $C(t)$, defined in (5.7) as the absolute value of the scalar product between the theoretical and numerical solutions for the time evolution plotted in Fig. 5.4. . . .	80
5.6	Trojan wave packet for $\mathcal{E}_{sc} = 0.016$ and $\omega = 1/10^3$ obtained from (a) harmonic approximation from formula (3.58), (b) modified Gaussian approximation given by (3.63), (c) Mathieu functions approach from expression (4.37), and (d) the numerical solution in the aligned states basis (4.9). Functions (c) and (d) correspond to the two large points on the energy diagrams in Figs. 4.7 and 4.9. The black dot in the center indicates the position of the nucleus ($x = y = 0$).	81

5.7	Trojan wave packet for $\mathcal{E}_{sc} = 0.016$ and $\omega = 1/20^3$ obtained from (a) harmonic approximation from formula (3.58), (b) modified Gaussian approximation given by (3.63), (c) Mathieu functions approach from expression (4.37), and (d) the numerical solution in the aligned states basis (4.9). Functions (c) and (d) correspond to the two large points on the energy diagrams in Figs. 4.8 and 4.10. The black dot in the center indicates the position of the nucleus ($x = y = 0$).	82
6.1	Contour plot of the probability density for the single packet in the lab-stationary frame prepared at $t = 0$ according to the modified RWA formula (6.13) and $l_0 = 60$, $\omega = 1.09/60^3$ and $\mathcal{E}_{sc} = 0.050$. Snapshots are plotted every $1/3$ of the optical cycle for cycles number 1, 2, 3, 5, 7 and 10. Each square covers the space region of the size 11250×11250 atomic units.	91
6.2	Values of $P(t)$, the total probability inside the circle with radius approximately twice the radius of the classical orbit for the time evolution plotted in Fig. 6.1.	92
6.3	Values of the correlation function $C(t)$, defined in (5.7) between the theoretical solution (6.13) and the numerical solution for the time evolution plotted in Fig. 6.1.	93
6.4	Typical one cycle steady field ($\mathcal{E}_{sc} = 0.016$) evolution of two-packet state (6.17) ($\omega = 1/20^3$) obtained in numerical simulation. Strong interference pattern appears twice a period when the two packet components pass through each other.	95

7.1	Adiabatic angular localization of electron probability density. Snapshots of $ \Phi ^2$ at $t = 0$ and after 6, 14 and 20 cycles show increasing angular bunching during exponential switching of the field. The initial state is the circular state for $n_0 = 20$. The black dot in the center indicates the position of the nucleus ($x = y = 0$).	101
7.2	Correlation function $C(t)$ defined in (5.7) between the numerical solution Φ and the predicted solution from the modified Gaussian approximation (3.63).	102
7.3	Total electron probability $P(t)$ as defined in (5.6). The values along the P axis emphasize the negligible loss to ionization. . . .	103
7.4	Trojan versus anti-Trojan wave packet formation. (a) The initial state is a circular state with $n_0 = 20$. (b) Anti-Trojan wave packet formation. The initial state is a circular state with $n_0 = 19$. Note that localization occurs at the oposite side of the nucleus from the Trojan case. In both (a) and (b) the CP field was switched on quasi-adiabatically and $\omega = 1/20^3$	105
7.5	Energy spectrum as a function of frequency between two resonant values $\omega = 1/21^3$ and $\omega = 1/20^3$ for the fixed electric field strenght $\mathcal{E} = 0.016/20^4$. Trojan lines can be identified from their proper connection with triplets for the resonant values (Figs. 7.5 and 7.6).	108
7.6	Energy spectrum as a function of electric field scaled to $\omega = 1/20^3$ for the lower frequency boundary of Fig. 7.5 $\omega = 1/21^3$. The energies along the horizontal line coinside with the energies for the lower boundary frequency in Fig. 7.5. The crossing between the horizontal line and Trojan triplets determine starting points for Trojan lines in frequency domain in Fig. 7.5.	109

- 7.7 Energy spectrum as a function of electric field scaled to $\omega = 1/20^3$ for the upper frequency boundary of Fig. 7.5 $\omega = 1/20^3$ (same like Fig. 4.8). The energies along the horizontal line coincide with the energies for the upper boundary frequency in Fig. 7.5. The crossing between the horizontal line and Trojan triplets determine ending points for Trojan lines in frequency domain in Fig. 7.5. . . 110
- 7.8 Adiabatic compression of Trojan wave packet. The frequency of the C.P. field is growing linearly from the resonant $\omega = 1/24^3$ to the resonant $\omega = 1/18^3$ during 60-ty optical cycles for the initial frequency. The last plot shows again the packet at $t = 0$ for comparison with compressed proceeding packet at the end of compression. The field strength is $\mathcal{E} = 0.016/24^4$ all the time during frequency chirping. Each square covers the region 1800×1800 atomic units. 111
- 8.1 Normalized differential cross section (8.6) (divided by the density of levels) in the direction parallel to the ionizing δ -pulse calculated with the plane-wave continuum and Gaussian wave function (3.47) for $\omega = 1/20^3$ and $\mathcal{E}_{sc} = 0.016$ as a function of time during one optical cycle. Note that single flash appears during the cycle in each direction. One unit of the wave vector k_x is the momentum of Trojan packet ωr_0 116

- 8.2 Normalized differential cross section from the expansion (8.12) (divided by the density of levels) in the direction parallel to the ionizing δ -pulse calculated with the plane-wave continuum and the Trojan state within nonlinear approach (4.37) for $\omega = 1/20^3$ and $\mathcal{E}_{sc} = 0.016$ as a function of time during one optical cycle. The deviation of the packet from the Gaussian in Cartesian coordinates leads to broadening of the peaks in time domain. One unit of the wave vector k_x is the momentum of Trojan packet ωr_0 117
- 8.3 Normalized differential cross section (8.5) (divided by the density of levels) in the direction parallel to the ionizing δ -pulse calculated numerically with the plane-wave continuum for $\omega = 1/20^3$ and $\mathcal{E}_{sc} = 0.016$ as a function of time during one optical cycle (between $t = 20$ and $t = 21$) for the wave packet generated in adiabatic turn-on shown in Fig. 7.1. One unit of the wave vector k_x is the momentum of Trojan packet ωr_0 118

Chapter 1

Introduction

We present here the analytical form of non-perturbative rotating-frame energies and states of a hydrogen atom in a circularly polarized (C.P.) field near the principal resonance, when the frequency of the C.P. field is approximately equal to the spacing between unperturbed hydrogenic energy levels in the limit of large angular momentum. Our treatment is nonlinear but quantum-mechanical. For the better understanding of this new result it is helpful to mention previous work to which it is related.

Fundamental quantum systems in the presence of strong external perturbations are of wide interest in physics. Fast development of new experimental techniques which allow atomic electrons to be subjected to external forces of the order of atomic Coulomb forces created a new need for theoretical studies of atomic systems under strong external perturbations. These have come from experiments in laser fields [1], in static electric and magnetic fields [2], time-dependent microwave fields as well as strong field preparation of field-free wave packets [3]. The discovery of Above Threshold Ionization (ATI) [4] and atomic stabilization [5] in strong time dependent fields finally excluded one of the most powerful theoretical methods for studies of quantum systems, time-dependent perturbation theory [6]. The reason is that when the radiation force on the atomic electron is comparable to the Coulomb force no clear small perturbation can be identified since both parts of the system are equally important. The only known case when the quantum mechanical wave function in the presence of a plane-wave radiation field can be found for a single electron is when there is no atomic potential [7]. The lack of analytical approaches has also created a new field in theoretical studies of those

systems, a field of numerical experiments with use of supercomputers [8] conducted by a direct integration of the time dependent Schrödinger equation on numerical grids or using basis expansions.

A consistent framework for calculations in the domain of strong time dependent perturbation is important not only from the point of view of fundamental studies of those systems but also from the point of view of optimum control theory [9] whose ultimate goal is to generate arbitrary states of the electron system as a gateway for control of physical properties of matter. Therefore the knowledge of a particular method of generation of quantum states with some interesting properties is of great importance as a special solution of the optimum control theory problem [9] without solving the inverse problem for the propagation of the wave function.

Since the work of Volkov [7] various approximate analytical methods have been developed to deal with the problem of the atom in a strong time dependent field but approximate Coulomb-Volkov wave functions have been found only for the continuum states [10]. The most powerful replacement for time dependent perturbation theory has been found in the form of the Rotating Wave Approximation (RWA) [11] where the importance of terms is evaluated according to the classification of speed of their time dependence. Great progress in understanding of the quantum dynamics of atoms in strong high frequency fields has been made by realizing that it is useful to change the reference frame to one which is moving with the classical electron when there is no atom but only the laser present [12]. This so-called Kramers-Henneberger frame allows one to construct dressed approximate solutions of the Schrödinger equation with respect to which the time dependent perturbation theory can be further applied. When the influence of the atomic potential on the electron dynamics can be reduced only to the initial

condition the Strong Field Approximation (SFA) based on the extension of the scattering matrix formalism to treat atom-laser interaction was able successfully explain strong field ionization of atoms in the ultra-strong field regime [13].

Rydberg atoms (atoms excited to high n states [14]) provide a unique opportunity for achieving the strong field non-perturbative regime with modest absolute power of the laboratory source of the time dependent field. Although experimental [15] and theoretical work [16] has been performed on Rydberg atoms with low angular momentum in strong linearly polarized electromagnetic fields the interaction of high angular momentum Rydberg states with both C.P. and linearly polarized fields remains almost unexplored.

Great experimental progress in generation of circular Rydberg states [17] suggests a new class of experiments with large angular momentum states when those states can be subjected to strong fields and justifies the need for detailed theoretical studies.

The hydrogen atom in a C.P. electromagnetic field has a unique property. Unlike any other driven atomic system the exact solutions for its classical equations of motion are known to be circular orbits [18]. On the other hand another class of approximate solutions of the Schrödinger equations in the limit of large principal quantum number has been known for the hydrogen atom [19]. These correspond to initially localized wave packets moving while spreading along classical Keplerian orbits. The association of those two facts motivated us to construct the nonlinear albeit quantum mechanical theory presented here.

In this thesis we present our analytic quantum theory of a single-electron Rydberg atom interacting with a C.P. time dependent electromagnetic field near the principal resonance, (when the field frequency is nearly equal to unperturbed level spacing of the atom). We also demonstrate that within its adiabatic extension,

the theory can be used for generation and control of well localized electron wave packets in Rydberg atoms. The theory is non-perturbative and also cannot be obtained within the time-average Kramers-Hennenberger approach. Numerical calculations are used to show that our analytic approximations which are better for higher orbits, are confirmed even for orbits with principal quantum number in the range $n = 10 - 20$.

The thesis is organized as follows: In Chapter 2 we discuss the classical equations of the motion for the hydrogen atom in a C.P. field and the special classical analytical solutions of these equations which have motivated us to construct quantum-mechanical wave functions within a unified approach. We also discuss special approximate quantum mechanical solutions of the Schrödinger equation limit in the context of approximate invariants of motion, and we review some of the properties of related quantum systems with similar hamiltonians.

Chapter 3 is devoted to the harmonic approach to the solution of the Schrödinger equation. We discuss generally the quantum stability of quadratic hamiltonians, derive the appropriate harmonic hamiltonians of our system in Cartesian and cylindrical coordinates, and discuss their energy spectra and wave functions.

Chapter 4 deals with the most important result of this work, the analytic, nonlinear quantum theory of the hydrogen atom in a C.P. electromagnetic field near the principal resonance. We construct the approximate solutions of the rotating-frame Schrödinger equation analytically and compare the energy spectra and the wave functions with the spectra and wave functions obtained from the harmonic approximation. We also find the connection with perturbation theory and the quadratic and linear Stark effects and extend the theory to the case when the quantum condition of the principal resonance cannot be strictly fulfilled.

In Chapter 5 we discuss a special class of the quantum states, so-called Trojan

states, which have classical, particle-like behavior and we show the results of numerical simulations which confirm their existence. We also discuss other states, so called-anti Trojan states, which are highly localized but have a non-classical origin.

Chapter 6 deals with the extension of our theory in the case when the external field is linearly polarized within the corrected RWA. We also show a numerical simulation of an atomic analog of Schrödinger cat states constructed within this extension.

In Chapter 7 we discuss the implications of our theory for the quantum control of an atomic electron. We show how the localization properties of certain wave functions of our system can be used for the generation of well localized atomic wave packets and how the adiabatic connection of certain hydrogenic eigenstates with Trojan and anti-Trojan states can be used to control the relative phase between the motion of a localized electron and the driving C.P. field. In Chapter 7 we also show how the atom can be expanded and compressed by a C.P. field with a chirped frequency. Finally in Chapter 8 we present the theory of detection of localized states and calculate both theoretically and from numerical simulations the differential cross sections for Trojan packet ionization by a short pulse. We conclude our thesis in Chapter 9.

Chapter 2

Hydrogen Atom in a Circularly Polarized Field as a Nonseparable System

2.1 Classical dynamics

It is useful to describe the classical equations of motion for the hydrogen atom in a circularly polarized field rotating with the angular frequency ω in a spherical coordinate system which can be derived from the following hamiltonian

$$\mathcal{H} = \mathcal{H}_0 + \mathcal{E} r \sin \theta \cos(\phi - \omega t) \quad (2.1)$$

(we always assume $\mathcal{E} > 0$ for convenience), where H_0 is the hamiltonian for the classical Kepler problem [20]

$$\mathcal{H}_0 = \frac{1}{2} \left(p_r^2 + \frac{p_\theta^2}{r^2} + \frac{p_\phi^2}{r^2 \sin^2 \theta} \right) - \frac{1}{r} \quad (2.2)$$

One can simplify the problem by performing the classical coordinate transformation

$$\phi \rightarrow \phi + \omega t \quad (2.3)$$

which represents the change of the coordinate system to the one rotating with the electric field vector of the circularly polarized electromagnetic wave. In the rotating frame the equations of motion can be obtained from the hamiltonian

$$\mathcal{H}_R = \mathcal{H}_0 + \mathcal{E} r \sin \theta \cos \phi - \omega p_\phi. \quad (2.4)$$

The complexity of this system originates from the fact that the corresponding stationary Hamilton-Jacobi equation [20] for the generating function W

$$\begin{aligned} \frac{1}{2} \left(\frac{\partial W}{\partial r} \right)^2 + \frac{1}{r^2} \left(\frac{\partial W}{\partial \theta} \right)^2 + \frac{1}{r^2 \sin^2 \theta} \left(\frac{\partial W}{\partial \phi} \right)^2 - \omega \frac{\partial W}{\partial \phi} - \frac{1}{r} \\ + \mathcal{E} r \sin \theta \cos \phi = \mathcal{K} \end{aligned} \quad (2.5)$$

does not separate in any of the known coordinate systems. As a result $\mathcal{H}_R = \mathcal{K}$ is the only classical constant of motion and the classical equation of motion cannot be solved analytically.

The classical equations of motion are

$$\frac{dr}{dt} = p_r, \quad (2.6)$$

$$\frac{dp_r}{dt} = -\frac{1}{r^2} + \frac{p_\theta^2}{r^3} + \frac{p_\phi^2}{r^3 \sin^2 \theta} - \mathcal{E} \cos \phi \sin \theta, \quad (2.7)$$

$$\frac{d\theta}{dt} = \frac{p_\theta}{r^2}, \quad (2.8)$$

$$\frac{dp_\theta}{dt} = \frac{p_\phi^2 \cos \theta}{2r^2 \sin^3 \theta} - \mathcal{E} \cos \phi \cos \theta, \quad (2.9)$$

$$\frac{d\phi}{dt} = -\omega + \frac{p_\phi}{r^2 \sin^2 \theta}, \quad (2.10)$$

$$\frac{dp_\phi}{dt} = \mathcal{E} \sin \phi \sin \theta. \quad (2.11)$$

A whole class of simplified solutions of equations (2.11) exists for which

$$\theta = \frac{\pi}{2}, \quad (2.12)$$

$$p_\theta = 0,$$

since those conditions make equations (2.8) and (2.9) automatically fulfilled. They correspond to the classical situation when the electron motion takes place in the plane of polarization of the circularly polarized field. The simplified equations of motion for this class of solutions

$$\frac{dr}{dt} = p_r, \quad (2.13)$$

$$\frac{dp_r}{dt} = -\frac{1}{r^2} + \frac{p_\phi^2}{r^3} - \mathcal{E} \cos \phi, \quad (2.14)$$

$$\frac{d\phi}{dt} = -\omega + \frac{p_\phi}{r^2}, \quad (2.15)$$

$$\frac{dp_\phi}{dt} = \mathcal{E} \sin \phi \quad (2.16)$$

can now be derived from the two-dimensional version \mathcal{H}_{2D} of the hamiltonian (2.4) which is

$$\mathcal{H}_{2D} = \frac{1}{2} \left(p_r^2 + \frac{p_\phi^2}{r^2} \right) - \frac{1}{r} + \mathcal{E} r \cos \phi - \omega p_\phi. \quad (2.17)$$

The unique property of this system is that while nonseparable, special analytical solutions exist within this planar class described by the equations (2.16) [18]. These are the circular solutions

$$r = r_c = \text{const}, \quad (2.18)$$

$$p_r = 0, \quad (2.19)$$

$$\phi = \frac{\pi}{2}(1 \pm 1), \quad (2.20)$$

$$p_\phi = \omega r_c^2, \quad (2.21)$$

where the classical radius of the orbit r_c can be found from equation (2.14) as a solution of the cubic equation

$$\omega^2 r_c^3 \pm \mathcal{E} r_c^2 - 1 = 0. \quad (2.22)$$

Equation (2.22) can be solved using the well known Cardano formulas [21] and has two physical solutions

$$r_c^\pm = \mp \frac{\mathcal{E}}{3\omega^2} + \frac{2^{1/3}\mathcal{E}^2}{3\omega^2 g^\pm(\mathcal{E}, \omega)} + \frac{1}{3} \frac{g^\pm(\mathcal{E}, \omega)}{2^{1/3}\omega^2}, \quad (2.23)$$

where

$$g^\pm(\mathcal{E}, \omega) = \left(\mp 2\mathcal{E}^3 + 27\omega^4 + 3\sqrt{3}\omega^2 \sqrt{\mp 4\mathcal{E}^3 + 27\omega^4} \right)^{1/3} \quad (2.24)$$

In the limit $\mathcal{E} \rightarrow 0$ they obviously reduce to the circular Kepler orbit with the radius r_0

$$r_0 = \omega^{-2/3} \quad (2.25)$$

and for finite \mathcal{E} we have

$$r_c^+ < r_0, \quad (2.26)$$

$$r_c^- > r_0$$

Classical stability analysis [18] shows that the smaller orbit is always unstable, while the larger is stable if the field strength of a circularly polarized field does not exceed a critical value

$$\mathcal{E} < (1/9)(8/9)^{-1/3}\omega^{4/3} \quad (2.27)$$

Fig. 2.1 shows a trajectory which is a small perturbation of the circular trajectory when the field strength is above and below the stability threshold. Also other periodic trajectories other than circular ones has been found numerically [22].

Despite of the presence of periodic trajectories the most striking consequence of the nonseparability of the system is its classically chaotic behavior. Depending on the field strength \mathcal{E} the phase space can exhibit mixed structure, namely semi-regular zones surrounded by stochastic layers [22, 23] as well as it can be totally chaotic [22, 23, 24]. The transition to globally chaotic behavior can be investigated with the heuristic Chirikov overlap criterion [24, 25, 26] which rigorously is neither necessary or sufficient and gives only a rough and usually too severe estimate of the global transition to chaos [26].

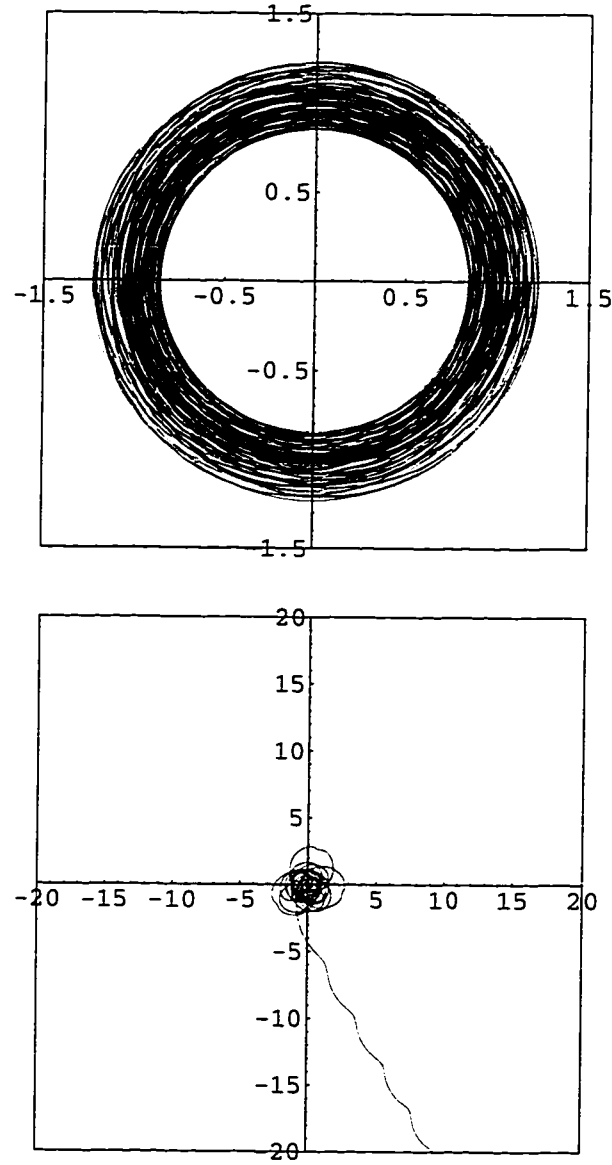


Fig. 2.1. Classical trajectories of the electron in C.P. field obtained from a small perturbation of the circular trajectory. The classical equations of motion depend only on scaled variables $\mathbf{r}_{sc} = \mathbf{r}\omega^{2/3}$, $t_{sc} = \omega t$, $\mathcal{E}_{sc} = \mathcal{E}\omega^{-4/3}$. The upper plot shows a weakly perturbed circular trajectory when it is stable for ($\mathcal{E}_{sc} = 0.044$) and the lower plot when unstable (for $\mathcal{E}_{sc} = 0.228$).

2.2 Approximate separability in the low frequency limit

The direct consequence of the lack of separability of the Hamilton-Jacobi equation (2.5) is that the corresponding Schrödinger equation

$$H\Psi = E\Psi \quad (2.28)$$

with the quantum-mechanical hamiltonian of the system in the rotating frame

$$H = \frac{\mathbf{p}^2}{2} - \frac{1}{r} + \mathcal{E}x - \omega L_z \quad (2.29)$$

is also nonseparable, where L_z is the z component of the angular momentum operator

$$\begin{aligned} L_z &= (xp_y - yp_x), \\ \mathbf{p} &= [p_x, p_y, p_z]. \end{aligned} \quad (2.30)$$

The hamiltonian H can be also formally obtained from the original quantum-mechanical hamiltonian in the laboratory frame

$$H_L = \frac{\mathbf{p}^2}{2} - \frac{1}{r} + \mathcal{E}(x \cos \omega t + y \sin \omega t) \quad (2.31)$$

within the framework of quantum mechanics and with the use of the time dependent unitary transformation

$$U(t) = e^{i\omega t L_z} \quad (2.32)$$

as

$$H = U H_L U^\dagger \quad (2.33)$$

This eliminates the time dependence of the hamiltonian H_L . Therefore for two time-dependent solutions of the Schrödinger equation, one in the laboratory frame

Ψ_L and the other Ψ_R in the rotating frame

$$H\Psi_L(t) = i\frac{d\Psi_L(t)}{dt}, \quad (2.34)$$

$$H_L\Psi_L(t) = i\frac{d\Psi_R(t)}{dt} \quad (2.35)$$

one has the following relation

$$\Psi_L(t) = U(t)\Psi_R(t) \quad (2.36)$$

which is just a formal expression of the fact that the one wave function is the time dependent rotation of the other.

For a frequency ω which is low compared to the Kepler frequency of hydrogenic eigenstates with a fixed principal quantum number n

$$\omega \ll \omega_c = \frac{1}{n^3} \quad (2.37)$$

the hamiltonian (2.29) can be simplified. We define $|nlm\rangle$ as hydrogenic eigenstates by the stationary Schrödinger equation for the hydrogen atom

$$H_0|nlm\rangle = -\frac{1}{2n^2}|nlm\rangle \quad (2.38)$$

with

$$H_0 = \frac{\mathbf{p}^2}{2} - \frac{1}{r}. \quad (2.39)$$

Within the Coulomb manifold of a fixed energy associated with n , the simplification of the hamiltonian (2.29) can be done using the known Pauli equality [27]

$$\mathbf{r} = -\frac{3}{2}n\mathbf{A}. \quad (2.40)$$

The \mathbf{A} is the Runge-Lenz vector-operator given by

$$\mathbf{A} = n\frac{\mathbf{p} \times \mathbf{L} - \mathbf{L} \times \mathbf{p}}{2} - \frac{\mathbf{r}}{r}. \quad (2.41)$$

Therefore within a single n manifold the energies can be found as solutions of the stationary Schrödinger equation with the effective hamiltonian [28]

$$H_n = H_0 + \omega L_z - \frac{3}{2}n\mathcal{E}A_x \quad (2.42)$$

This can be simplified to the form

$$H_n = H_0 - \sqrt{\omega^2 + \frac{9}{4}n^2\mathcal{E}^2}(\Lambda \cdot \mathbf{e}), \quad (2.43)$$

where \mathbf{e} is a unit vector

$$\mathbf{e} = [\sin \gamma, 0, \cos \gamma], \quad (2.44)$$

and Λ is a vector built from three of the six generators of the $O(4)$ dynamical symmetry group of the hydrogen atom [29]

$$\Lambda = [A_x, A_y, L_z] \quad (2.45)$$

and

$$\tan \gamma = \frac{3n\mathcal{E}}{2\omega} \quad (2.46)$$

Using the commutation relations for the generators of the $O(4)$ group

$$[A_x, A_y] = iL_z, \quad (2.47)$$

$$[L_z, A_x] = iA_y,$$

$$[L_z, A_y] = -iA_x,$$

one can calculate

$$e^{i\gamma A_y} A_x e^{-i\gamma A_y} = L_z \sin \gamma + A_x \cos \gamma \quad (2.48)$$

$$e^{i\gamma A_y} L_z e^{-i\gamma A_y} = L_z \cos \gamma - A_x \sin \gamma, \quad (2.49)$$

which immediately implies the eigenstates $|nlm\rangle$ of the hamiltonian (2.43) as [31]

$$|nlm\rangle \equiv e^{-i\gamma A_y} |nlm\rangle \quad (2.50)$$

with the eigenvalues [28]

$$E_{nlm} = -\frac{1}{2n^2} + m\sqrt{\omega^2 + \frac{9}{4}n^2\mathcal{E}^2}. \quad (2.51)$$

The states (2.50) are the hydrogenic states changed by a generalized rotation $e^{-i\gamma A_y}$. They are obviously also the eigenstates of the hamiltonian H_0 of the bare hydrogen atom and can be considered as coherent states of the $O(4)$ symmetry group [31]. For $l = m = n - 1$, i.e., when the rotated hydrogenic state is a circular state, a direct decomposition on the hydrogenic eigenstates is known [31]

$$|nll\rangle = \sum_{\mu=-n+1}^{\mu=n-1} c_{n\mu}(\varepsilon) |n|\mu|\mu\rangle, \quad (2.52)$$

where

$$c_{n\mu}(\varepsilon) = \left[\frac{1}{2^{n-1}} \frac{[2(n-1)]!}{(n+\mu-1)!(n-\mu-1)!} \right]^{\frac{1}{2}} \left[\frac{1 + \sqrt{1-\varepsilon^2}}{1 - \sqrt{1-\varepsilon^2}} \right]^{\frac{\mu}{2}} \varepsilon^{n-1} \quad (2.53)$$

and ε is the eccentricity parameter of the hydrogenic eigenstate related to its average angular momentum

$$\varepsilon = \sin \gamma = \sqrt{\left(1 - \frac{\langle L_z \rangle^2}{n^2}\right)}.$$

The round-bracket states (2.52) exhibit localization properties to some extent (Fig. 2.2). They are localized in the plane of circular polarization of the C.P. field and also exhibit weak angular localization while confined along an ellipse. Physically they represent elliptical hydrogenic states, with the parameters tuned to the frequency and the field strength of the C.P. field through formula (2.46). Those elliptical states adiabatically follow the external C.P. field.

The method of solution of the Schrödinger equation presented here implies that in the low frequency limit the operator of the perturbation to H_0

$$W = \omega L_z - \frac{3}{2}n\mathcal{E}A_x$$

commutes approximately with the exact hamiltonian H in this regime and therefore is an approximate constant of motion [28], namely

$$\frac{dW}{dt} = i[W, H] \approx 0 \quad (2.54)$$

This result reflects the fact that the approximate eigenvalues (2.51) have well defined quantum numbers generated by W in analogy to hydrogenic quantum numbers l and m generated by the angular momentum operator \mathbf{L} and its z component L_z .

2.3 Related quantum systems

It is worth to mention a few other quantum systems with hamiltonians somehow related to the rotating frame hamiltonian (2.29).

The simplest and best known is the hydrogen atom in a static electric field with the hamiltonian

$$H_S = H_0 + \mathcal{E}x \quad (2.55)$$

obtained from the hamiltonian (2.29) of our system by formally putting $\omega = 0$. This is relevant to the Stark effect [29].

There are two interesting theoretical facts about the Stark hamiltonian (2.55). First, the perturbation expansion of the eigenvalues in terms of the field strength \mathcal{E} is divergent for arbitrary small \mathcal{E} . Nevertheless the stationary perturbation theory [29] applied formally gives the right answer for the eigenvalues for moderate field

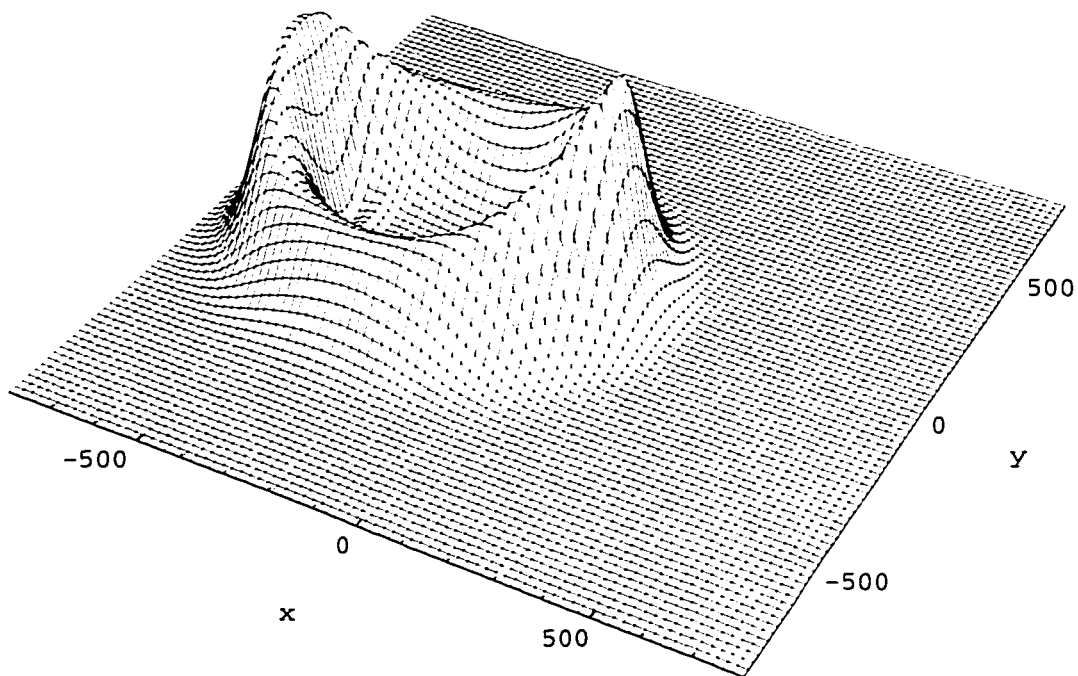


Fig. 2.2. The electron probability density in the elliptical state (2.52) for $n = 20$ and $\varepsilon = 0.7$. The charge distribution is being polarized with respect to the nucleus ($x = y = 0$), as it is localized around the classical elliptical orbit with the eccentricity ε .

strength depending on the order of the perturbation expansion [32, 33]. Second, besides the obvious constant of motion for the hamiltonian (2.55) which is L_x

$$[L_x, H_S] = 0, \quad (2.56)$$

there is an additional constant of motion \mathbf{B} analogical to the Runge-Lenz vector \mathbf{A} for the Coulomb problem given by (2.41). For the hamiltonian (2.55) one gets [34]

$$\mathbf{B} = \mathbf{A} + \frac{\mathcal{E}}{2}(z^2 + y^2), \quad (2.57)$$

$$[\mathbf{B}, H_S] = 0. \quad (2.58)$$

An additional constant of motion must exist since the Stark problem separates in parabolic coordinates [35]. The result for eigenvalues of the hamiltonian (2.55) within first order perturbation theory coincides with the formula (2.51) in the limit $\omega = 0$ and $k = n_1 - n_2$ and one gets [35]

$$E_{nn_1n_2} = -\frac{1}{n^2} + \frac{3}{2}n(n_1 - n_2). \quad (2.59)$$

The numbers $n_1 = 0, 1, \dots, n-1$ and $n_2 = 0, 1, \dots, n-1$ are the quantum numbers for the hydrogenic eigenfunctions in a parabolic coordinate system [29, 35].

Another interesting related quantum system is the hydrogen atom in a magnetic field of strength B with the cyclotronic frequency $\omega_c = B$ in atomic units, and a hamiltonian denoted by H_B . For the magnetic field parallel to the z axis H_B can be obtained from (2.29) by putting $\mathcal{E} = 0$ and $\omega = \omega_c/2$ and adding a diamagnetic term quadratic in ω_c

$$H_B = H_0 - \frac{\omega_c}{2}L_z + \frac{\omega_c^2}{8}(x^2 + y^2). \quad (2.60)$$

With the diamagnetic term neglected one obtains the standard Zeeman splitting of the hydrogenic energy levels [29]

$$E_{nlm} = -\frac{1}{2n^2} - m\frac{\omega_c}{2} \quad (2.61)$$

The full problem with the diamagnetic term present is nontrivial, since L_z is the only exact constant of the motion besides H_B itself

$$[L_z, H] = 0, \quad (2.62)$$

and the Schrödinger equation with H_B cannot be fully separated. However the approximate constant of motion exists in analogy to the case discussed in Section 2.2 which allows one to calculate approximate eigenvalues of the Schrödinger equation for moderate field strength B with well defined quantum numbers [36]. An interesting fact is that this approximate separability was first discovered experimentally by observing the regularity in measured energy spectra as a function of the magnetic field [37].

The approximate constant of motion can be constructed from the components of the Runge-Lenz vector \mathbf{A} as [38, 39]

$$\Sigma = 4\mathbf{A}^2 - 5A_z^2, \quad (2.63)$$

and the approximate eigenvalues of H_B are [40, 41]

$$E_{n\lambda m} = -\frac{1}{2n^2} - m\frac{\omega_c}{2} + \frac{\omega_c^2 n^2}{32} [n^2 + 9 + 9\lambda(\lambda + 1) - 16m^2] \quad (2.64)$$

with $\lambda = 0 \dots n - 1$, and n and m hydrogenic quantum numbers.

The hamiltonian (2.29) of the hydrogen atom in a C.P. field in a rotating frame obviously describes also the hydrogen atom in crossed electric and magnetic fields in the case when the diamagnetic term in (2.60) is absent. The approximate separability of our system for low frequencies discussed in Section 2.2 was first discovered for the case of crossed fields [42].

There is a characteristic common feature of all the related systems discussed in this section as well as the low frequency case of our system. For all the cases discussed, the Coulomb manifold of quantum states associated with the principal

quantum number n spans the quantum states of the approximate hamiltonians and this quantum number remains a good one for the eigenvalues of the dressed system. As we will see later, in our non-perturbative quantum theory of hydrogen in C.P. field, the quantum number n is no longer a good quantum number even for small strengths of the electric field \mathcal{E} .

Chapter 3

Harmonic Approximations

3.1 General stability of rotating extremum

Within this section we discuss the classical and quantum stability of the system described by the two dimensional hamiltonian which is the following quadratic form in the spatial coordinates and momenta

$$H_{OSC} = \frac{P_X^2 + P_Y^2}{2} + \frac{a\omega^2 X^2 + b\omega^2 Y^2}{2} - \omega(XP_Y - YP_X). \quad (3.1)$$

Thus the hamiltonian for $a > 0, b > 0$ describes a rotating quadratic minimum, and for $a < 0, b < 0$, a rotating maximum, and when $ab < 0$ a rotating saddle-shaped potential. The corresponding classical equations of motion

$$\frac{dX}{dt} = P_x + \omega Y, \quad (3.2)$$

$$\frac{dP_X}{dt} = -a\omega^2 X + \omega P_Y, \quad (3.3)$$

$$\frac{dY}{dt} = P_Y - \omega X, \quad (3.4)$$

$$\frac{dP_Y}{dt} = -b\omega^2 Y - \omega P_X, \quad (3.5)$$

have stable oscillatory solutions when the stability matrix \mathbf{K}

$$\mathbf{K} = \begin{bmatrix} 0 & 1 & \omega & 0 \\ -a\omega^2 & 0 & 0 & \omega \\ -\omega & 0 & 0 & 1 \\ 0 & -\omega & -b\omega^2 & 0 \end{bmatrix} \quad (3.6)$$

has purely imaginary eigenvalues λ

$$\text{Det}[\mathbf{K} - \lambda \mathbf{I}] = 0. \quad (3.7)$$

The eigenvalues of M can be found as

$$\lambda_+ = \pm i\omega_+, \quad (3.8)$$

$$\lambda_- = \pm i\omega_-,$$

where ω_+ , ω_- are the natural frequencies of the system and they can be found as

$$\omega_+ = \omega \sqrt{2 + a + b + \sqrt{(a - b)^2 + 8(a + b)}/\sqrt{2}}, \quad (3.9)$$

$$\omega_- = \omega \sqrt{2 + a + b - \sqrt{(a - b)^2 + 8(a + b)}/\sqrt{2}}. \quad (3.10)$$

Fig. 3.1 shows the regions in the $a - b$ plane for which ω_+ and ω_- are real, so λ_+ and λ_- are purely imaginary and therefore the classical motion is stable. As can be seen from Fig. 3.1, the rotation of the potential can cause the minimum to be unstable and can stabilize the saddle point, but cannot stabilize the maximum. The case of the saddle point stabilization is the most interesting one since the stability zone is quite tiny and as we describe further, the saddle point case will be relevant to our hamiltonian of a hydrogen atom in C.P. field.

The hamiltonian (3.1) after quantization can be transformed to the diagonal form

$$H_{OSC} = \omega_+(a_+^\dagger a_+ + 1/2) \pm \omega_-(a_-^\dagger a_- + 1/2), \quad (3.11)$$

where the plus sign with ω_- corresponds to $ab > 0$, and the minus sign to $ab < 0$.

We use the canonical transformation

$$a_+ = \alpha_1 X + \alpha_2 P_X + \alpha_3 Y + \alpha_4 P_Y \quad (3.12)$$

$$a_- = \beta_1 X + \beta_2 P_X + \beta_3 Y + \beta_4 P_Y,$$

where a_+ , a_- fulfill the standard commutation relations for a harmonic oscillator

$$[a_+, a_+^\dagger] = 1 \quad (3.13)$$

$$[a_-, a_-^\dagger] = 1$$

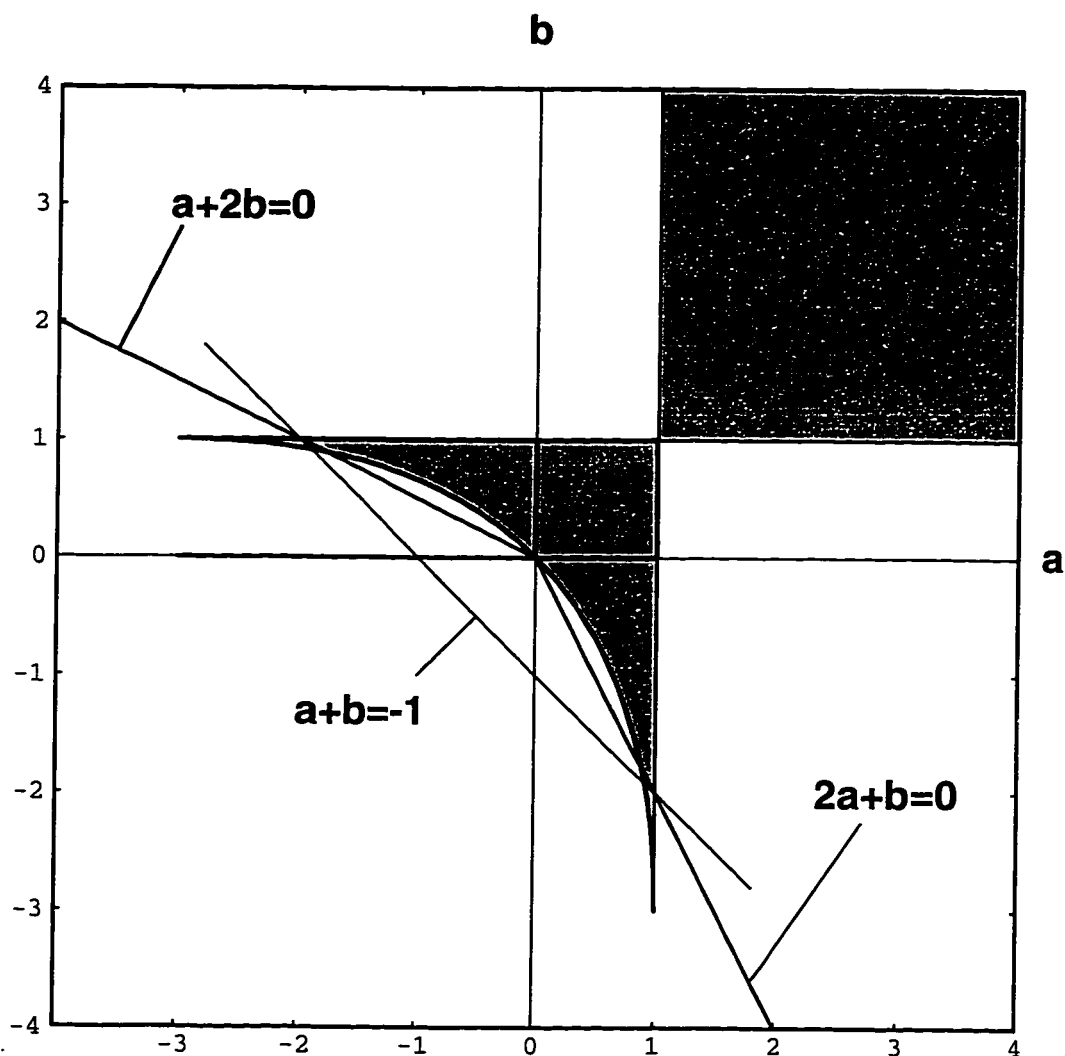


Fig. 3.1. The islands of stability (shaded areas) in the plane of parameters a and b where both ω_+ and ω_- are real. In the parabolic triangle the potential has a saddle point. Points lying on the lines $a + 2b = 0$ and $2b + a = 0$, which intersect the stability region, correspond to the atom in a C.P. field, and the line $a + b = -1$ to the gravitational three-body problem of Trojan asteroids.

and all the other commutators between them vanish. The coefficients α_i and β_i can be found from the operator equations

$$\begin{aligned} [a_+, H_{OSC}] &= \omega_+ a_+ \\ [a_-, H_{OSC}] &= \pm \omega_- a_- \end{aligned} \quad (3.14)$$

which is the eigenvalue problem for the transposed stability matrix \mathbf{K}

$$\begin{aligned} -i\mathbf{K}^T \vec{\alpha} &= \omega_+ \vec{\alpha} \\ -i\mathbf{K}^T \vec{\beta} &= \pm \omega_- \vec{\beta} \end{aligned} \quad (3.15)$$

where $\vec{\alpha}$, $\vec{\beta}$ are the vectors built from the coefficients of the canonical transformation (3.12).

$$\begin{aligned} \vec{\alpha} &= [\alpha_1, \alpha_2, \alpha_3, \alpha_4], \\ \vec{\beta} &= [\beta_1, \beta_2, \beta_3, \beta_4]. \end{aligned} \quad (3.16)$$

The components of the vectors $\vec{\alpha}$ and $\vec{\beta}$ must further satisfy the conditions which follow directly from the commutation relations (3.13) and the canonical commutation relations for the canonical variables of the hamiltonian (3.1). These are

$$[X, P_X] = [Y, P_Y] = i, \quad (3.17)$$

and all the other commutators between them vanish. Relations (3.13) can be written in the compact form [43]

$$-i\mathbf{T}_1 = \mathbf{T}_2^{-1} \quad (3.18)$$

where the matrices \mathbf{T}_1 and \mathbf{T}_2 are

$$\mathbf{T}_1 = \begin{bmatrix} \alpha_1 & \alpha_2 & \alpha_3 & \alpha_4 \\ \beta_1 & \beta_2 & \beta_3 & \beta_4 \\ \alpha_1^* & \alpha_2^* & \alpha_3^* & \alpha_4^* \\ \beta_1^* & \beta_2^* & \beta_3^* & \beta_4^* \end{bmatrix}$$

$$(3.19)$$

and

$$\mathbf{T}_2 = \begin{bmatrix} \alpha_2^* & \beta_2^* & -\alpha_2 & -\beta_2 \\ -\alpha_1^* & -\beta_1^* & \alpha_1 & \beta_1 \\ \alpha_4^* & \beta_4^* & -\alpha_4 & -\beta_4 \\ -\alpha_3^* & -\beta_3^* & \alpha_3 & \beta_3 \end{bmatrix} \quad (3.20)$$

The hamiltonian (3.11) has square-normalizable eigenstates for real ω_+ , ω_- , i.e., when the corresponding classical motion is also stable.

3.2 Energies and states in Cartesian coordinates

In this section we will apply the harmonic approximation in Cartesian coordinates to the stationary Schrödinger equation with the hamiltonian (2.29) of our system [44]

$$H\psi = \left[\frac{p_x^2 + p_y^2 + p_z^2}{2} - \frac{1}{r} + \mathcal{E}x - \omega(xp_y - yp_x) \right] \psi = E\psi. \quad (3.21)$$

The harmonic hamiltonian can be obtained from the Taylor expansion up to second order of the Coulomb potential $1/r$ around the circular classical trajectory described in Section 2.1, which in the rotating frame reduces to a stationary point with the coordinates

$$x_0 = \mp r_c^\pm, \quad y_0 = 0, \quad z_0 = 0, \quad (3.22)$$

This leads to the corresponding quadratic hamiltonian

$$\begin{aligned} H_Q &= E_0 + \frac{p_x^2 + (p_y - \omega x_0)^2 + p_z^2}{2} - \frac{2x^2}{|x_0|^3} + \frac{y^2}{|x_0|^3} + \frac{z^2}{|x_0|^3} \\ &\quad - \omega[(x - x_0)(p_y - \omega x_0) - yp_x] + x(\omega^2 x_0 + \mathcal{E} - \frac{1}{x_0^2}) \\ &= E_0 + \frac{p_x^2 + (p_y - \omega x_0)^2 + p_z^2}{2} - \frac{2x^2}{|x_0|^3} + \frac{y^2}{|x_0|^3} + \frac{z^2}{|x_0|^3} \\ &\quad - \omega[(x - x_0)(p_y - \omega x_0) - yp_x], \end{aligned} \quad (3.23)$$

where E_0 is the classical energy of the circular trajectory in the rotating frame

$$E_0 = -\frac{\omega^2 x_0^2}{2} - \frac{1}{|x_0|} + \mathcal{E}x_0, \quad (3.24)$$

which is a sum of the centrifugal energy, Coulomb energy and the electrostatic energy in the C.P. field, which is static in the rotating frame. The term which is linear in x vanishes since its coefficient is equal to zero as a result of the equilibrium of classical forces (2.22). Therefore H_Q can be written as

$$H_Q = E_0 + H_{OSC} + \frac{p_z^2}{2} + \frac{c\omega^2 z^2}{2} \quad (3.25)$$

where H_{OSC} is the hamiltonian of the rotating extremum (3.1) with

$$\begin{aligned} X &= x - x_0 \\ P_X &= p_x \\ Y &= y \\ P_Y &= p_y - \omega x_0 \end{aligned} \quad (3.26)$$

The coefficients a , b , and c can be expressed in terms of a dimensionless parameter q

$$a(q) = -2q, \quad b(q) = q, \quad c(q) = q \quad (3.27)$$

where

$$q = \frac{1}{\omega^2 |x_0|^3} = \frac{1}{\omega^2 r_c^3}, \quad (3.28)$$

which is a ratio between the Coulomb force and the centrifugal force for the circular trajectory. The equilibrium of forces (2.22) can be written in terms of q as

$$\mathcal{E} = |1 - q|q^{-1/3}\omega^{4/3}. \quad (3.29)$$

Hamiltonian (3.25) can be now transformed to diagonal form using the general method described in the previous section

$$H_Q = E_0 + \omega_+(a_+^\dagger a_+ + 1/2) - \omega_-(a_-^\dagger a_- + 1/2) + \omega_0(a_0^\dagger a_0 + 1/2), \quad (3.30)$$

with the frequencies

$$\begin{aligned} \omega_+ &= \omega \sqrt{2 - q + \sqrt{9q^2 - 8q}} / \sqrt{2}, \\ \omega_- &= \omega \sqrt{2 - q - \sqrt{9q^2 - 8q}} / \sqrt{2}, \\ \omega_0 &= \omega \sqrt{q}. \end{aligned} \quad (3.31)$$

The frequencies are real when the parametric line $[a(q), b(q)]$ intersects the stability zone in the $a - b$ plane (Fig. 3.1) which restricts the value of q

$$8/9 < q < 1. \quad (3.32)$$

This restriction leads to limitation of the field strength \mathcal{E} which causes the hamiltonian (3.11) to have discrete spectrum within the harmonic approximation:

$$\mathcal{E} < (1/9)(8/9)^{(-1/3)} \omega^{4/3}, \quad (3.33)$$

which by the construction coincides with the early result of reference [18] for the stability of the classical circular trajectories. Fig. 3.2 shows the dependence of real and imaginary parts of $\omega_+(q)$ and $\omega_-(q)$ for the physical q values.

We have found the explicit form of the diagonalizing transformation (3.12), and obtain these canonical lowering operators for the atom-field system [45]:

$$\begin{aligned} a_+ &= \left(-\frac{i}{M_Y} X + v P_X - u Y + i \frac{v}{M_Y} P_Y \right) \sqrt{N_+}, \\ a_- &= \left(u X - i \frac{v}{M_X} P_X + \frac{i}{M_X} Y - v P_Y \right) \sqrt{N_-}, \\ a_0 &= (i p_z + \omega_0 z) / \sqrt{\omega_0}, \end{aligned} \quad (3.34)$$

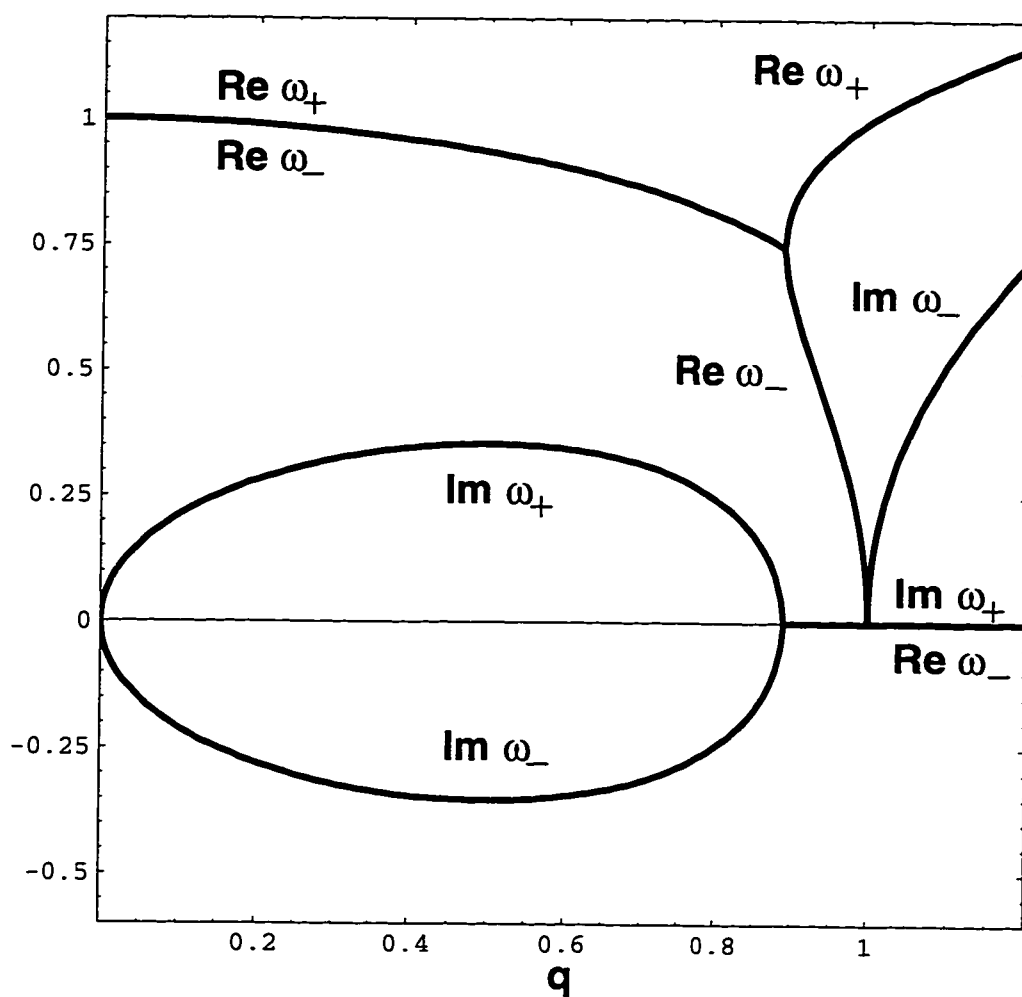


Fig. 3.2. Real and imaginary parts of the eigenfrequencies ω_+ and ω_- of the hamiltonian (3.31) scaled to the frequency of the C.P. field ω . The imaginary parts vanish in a tiny stability zone for $8/9 < q < 1$.

with

$$N_- = 2 \frac{v}{M_X} (1 - u), \quad (3.35)$$

$$N_+ = 2 \frac{v}{M_Y} (1 - u),$$

$$M_X = \left(\frac{1 - 2v\omega - 2qv^2\omega^2}{u^2 + 2uv\omega + qv^2\omega^2} \right)^{1/2},$$

$$M_Y = \left(\frac{1 + 2v\omega + qv^2\omega^2}{u^2 - 2uv\omega - 2qv^2\omega^2} \right)^{1/2}, \quad (3.36)$$

where

$$u = [(9q - 4) - 3\sqrt{9q^2 - 8q}]/4,$$

$$v = [-3q - \sqrt{9q^2 - 8q}]/2q\omega. \quad (3.37)$$

The explicit form of a_+ and a_- in terms of the original coordinates allows us to find the eigenstates of H_Q using the generating algebra of a harmonic oscillator in a well known way

$$|m_+, m_-, m_0\rangle = a_+^{\dagger m_+} a_-^{\dagger m_-} a_0^{\dagger m_0} |0, 0, 0\rangle, \quad (3.38)$$

where the pseudo-vacuum is defined by

$$a_+ |0, 0, 0\rangle = a_- |0, 0, 0\rangle = a_0 |0, 0, 0\rangle = 0, \quad (3.39)$$

and the eigenvalues are given by

$$E_{m_+, m_-, m_0}(\mathcal{E}) = E_0 + (m_+ + \frac{1}{2})\omega_+ - (m_- + \frac{1}{2})\omega_-$$

$$+ (m_0 + \frac{1}{2})\omega_0. \quad (3.40)$$

We call the state $|0, 0, 0\rangle$ a pseudo-vacuum because it is algebraically the simplest, although it is not the lowest energy eigenstate of the hamiltonian H_Q . This property is implied by the negative sign near ω_- in (3.11).

It is worth pointing out here that a system with the hamiltonian

$$H_- = -\omega_- a_-^\dagger a_- \quad (3.41)$$

which is a part of H_Q should not be confused with the hamiltonian of a particle on the top of a quadratic potential hill which is

$$H_{TOP} = \frac{\pi_x^2}{2} - \frac{\omega_-^2 x^2}{2}, \quad (3.42)$$

and which does not have normalizable eigenstates. In contrast to (3.42) H_- corresponds to a particle with negative mass on the top of the hill which is perfectly stable and has square-normalizable eigenfunctions and the hamiltonian in space variables

$$H_- = -\frac{\pi_x^2}{2} - \frac{\omega_-^2 x^2}{2} \quad (3.43)$$

with a discrete spectrum not bounded from below. The reason why H_Q does not have a ground state is that as an effective harmonic hamiltonian it was constructed by expansion around the classical trajectory with a finite energy and there should exist quantum states with lower energy.

The set of equations (3.39) for a_+ , a_- , and a_0 in a spatial representation is a set of linear partial differential equations for the wave function

$$\psi_0(\mathbf{r}) = \langle \mathbf{r} | 0, 0, 0 \rangle, \quad (3.44)$$

since

$$p_x = -i\partial_x \quad (3.45)$$

$$p_y = -i\partial_y. \quad (3.46)$$

The wave function (3.44) can be found analytically and is the one of two eigenstates of the greatest importance. It is given by a Gaussian wave function [44, 45]

$$\psi_0(x, y, z) = N e^{i\omega x_0 y} e^{-\frac{\omega}{2}[Ay^2 + B(x-x_0)^2 + 2iC(x-x_0)y + Dz^2]}, \quad (3.47)$$

with coefficients A , B , C and D dependent on the parameter q

$$\begin{aligned} A(q) &= \sqrt{(1-q)(8+4q-9q^2-8s(q))}/(3q), \\ B(q) &= s(q)A(q)/(1-q), \\ C(q) &= (2+q-2s(q))/(3q), \\ D(q) &= \sqrt{q}, \end{aligned} \tag{3.48}$$

where

$$s(q) = \sqrt{(1-q)(1+2q)}. \tag{3.49}$$

We will discuss this solution in more detail in Chapter 5. Figs. 3.3 and 3.4 show the real and imaginary parts of parameters A , B and C as functions of parameter q . The imaginary parts vanish within the stability interval of q to provide the square-integrability of the wave function ψ_0 .

3.3 Energies and states in cylindrical coordinates

In this section we show how to obtain the harmonic approximation in cylindrical coordinates, related to the Cartesian coordinates by

$$\begin{aligned} x &= r \cos \phi, \\ y &= r \sin \phi, \\ z &= z. \end{aligned} \tag{3.50}$$

Since this transformation is nonlinear the wave functions obtained using the harmonic approximation in different coordinates differ even when the harmonic hamiltonians are stable for the same parameter range. As we will see in Chapters 5 and 6 the wave functions obtained in the cylindrical coordinate system are more

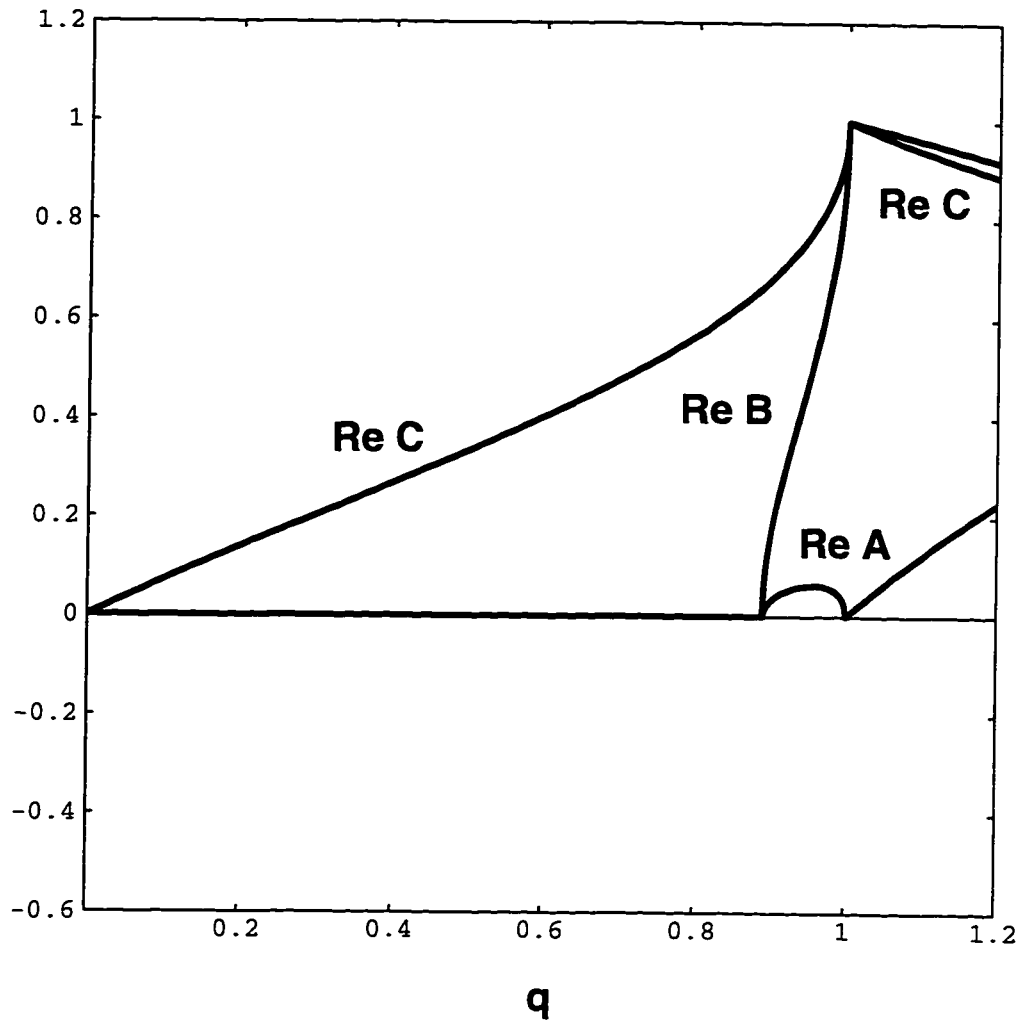


Fig. 3.3. Real parts of the parameters A , B , and C of the pseudo ground state wave function (3.48) plotted as functions of the parameter q . Note that the real part of A is much smaller than the real part of B in the stability region $8/9 < q < 1$ and has a maximum for $q \approx 0.9562$.

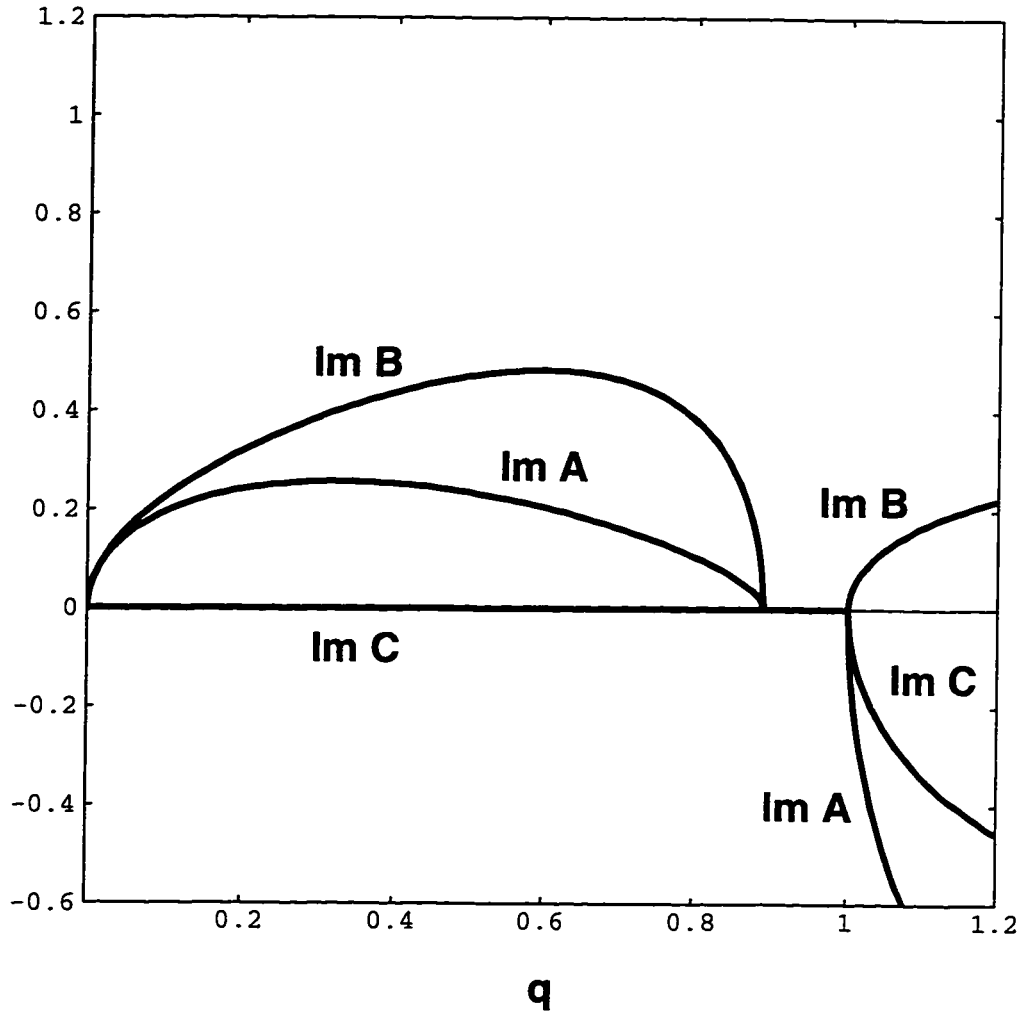


Fig. 3.4. Imaginary parts of the parameters A , B , and C of the pseudo ground state wave function (3.48) plotted as functions of the parameter q . The imaginary parts vanish in a tiny stability zone for $8/9 < q < 1$ which provides the wave function to be square integrable.

accurate than those obtained in Cartesian coordinates. That is why we discuss this coordinate dependence in detail.

The hamiltonian H when written in cylindrical coordinates is

$$H = -\frac{1}{2}(\partial_r^2 + \frac{1}{r}\partial_r + \frac{1}{r^2}\partial_\phi^2 + \partial_z^2) - \frac{1}{\sqrt{r^2 + z^2}} + \mathcal{E}r \cos \phi + i\omega\partial_\phi. \quad (3.51)$$

After the transformation of the wave function $\Psi(r, \phi, z) = \Phi(r, \phi, z)/\sqrt{r}$ the hamiltonian for the function Φ becomes

$$H = -\frac{1}{2}[\partial_r^2 + \frac{1}{r^2}(\partial_\phi^2 + \frac{1}{4}) + \partial_z^2] - \frac{1}{\sqrt{r^2 + z^2}} + \mathcal{E}r \cos \phi + i\omega\partial_\phi. \quad (3.52)$$

After dropping $1/4$ in (3.52), performing the first unitary transformation $U_1 = e^{i l_0 \phi}$ and then expanding the resulting hamiltonian $H_1 = U_1^\dagger H U_1$ around the stable circular classical orbit [18] up to second order in the operators ∂_r and ∂_ϕ , and the variables $\delta r = (r - r_c)$, ϕ and z , we obtain the following quadratic hamiltonian

$$H_1 = E_0 - \frac{1}{2}(\partial_r^2 + \frac{1}{r_c^2}\partial_\phi^2 + \partial_z^2) + \frac{\omega_r^2 \delta r^2}{2} - \frac{\omega_\phi^2 r_c^2 \phi^2}{2} - 2i\omega \frac{1}{r_c} \partial_\phi \delta r + \frac{\omega_z^2 z^2}{2}. \quad (3.53)$$

The classical condition of equilibrium of forces expressed by the equation

$$\omega^2 r_c + \mathcal{E} = \frac{1}{r_c^2} \quad (3.54)$$

implies vanishing of the linear terms and leads to the requirement $l_0 = \omega r_c^2$. The frequencies ω_ϕ , ω_r and ω_z are defined by the relations

$$\begin{aligned} \omega_\phi^2 &= \frac{\mathcal{E}}{r_c}, \\ \omega_r^2 &= \omega^2 + 2\omega_\phi^2, \\ \omega_z^2 &= \omega^2 - \omega_\phi^2 \end{aligned} \quad (3.55)$$

and E_0 is the classical energy of the electron shifted by the rotation of the coordinate system

$$E_0 = \frac{\omega^2 r_c^2}{2} - \frac{1}{r_c} + r_c \mathcal{E} - l_0 \omega. \quad (3.56)$$

A second unitary transformation $U_2 = e^{i\omega r_c \phi \delta r}$ next transforms the hamiltonian (3.53) into

$$\begin{aligned} H_{QC} &= U_2^\dagger H U_2 = E_0 + \frac{\pi_r^2 + \pi_\phi^2}{2} + \frac{-2q\omega^2 X_r^2 + q\omega^2 X_\phi^2}{2} \\ &\quad - \omega(X_r \pi_\phi - X_\phi \pi_r) + \frac{\pi_z^2}{2} + \frac{\omega_z^2 z^2}{2} \end{aligned} \quad (3.57)$$

where we defined $X_r = \delta r$, $X_\phi = r_c \phi$, $\pi_r = -i\partial_r$, $\pi_\phi = (-i/r_c)\partial_\phi$ and $\pi_z = -i\partial_z$.

The second unitary transformation U_2 proves the equivalence of the stability in two different systems of coordinates since the hamiltonian H_{QC} is the identical quadratic form in the operators X_r , π_r , X_ϕ , π_ϕ as the hamiltonian H_Q in X , P_X , Y , P_Y . When obtaining the pseudo ground state wave function of H one must not forget about the unitary transformations U_1 , U_2 . Also for well confined wave functions the factor \sqrt{r} multiplying the function Ψ can be replaced by $\sqrt{r_c}$ and the harmonic approximation gives the following expression for the wave function Ψ .

$$\begin{aligned} \Psi_0(r, \phi, z) &= N e^{i l_0 \phi} e^{-\frac{\omega}{2} [A(r_c \phi)^2 + B(r - r_c)^2 + 2i(C-1)(r - r_c)r_c \phi]} \\ &\quad \times e^{-\frac{\omega}{2} D z^2}. \end{aligned} \quad (3.58)$$

with A , B , C and D given by (3.48).

The wave function (3.58) can be formally obtained from the wave function (3.47) in Cartesian coordinates by the coordinate transformation (3.51) approximated up to second order

$$x - x_0 \approx r - r_0, \quad (3.59)$$

$$y = r_0 \phi + (r - r_0) \phi. \quad (3.60)$$

However for lower angular momenta l_0 , functions (3.47) and (3.58) may differ significantly enough to provide improvement in approximation when using cylindrical coordinates.

3.4 Nonlinear corrections to harmonic approximation

We have developed another approximation for the pseudo ground state wave function Ψ_0 which includes some terms of the order of $1/l_0$ and leads to modification of the angular spread coefficient A as a function of the field strength [46]. In the limit of large l_0 this approximation is reduced to the harmonic approximation described in the previous section.

The approximation modifies only that part of the wave function Ψ_0 which depends on the variables ϕ and r , so it is enough to discuss it for the planar part of the hamiltonian (3.51)

$$H_{2D} = -\frac{1}{2}(\partial_r^2 + \frac{1}{r}\partial_r + \frac{1}{r^2}\partial_\phi^2) - \frac{1}{r} - \mathcal{E}r \cos \phi + i\omega\partial_\phi. \quad (3.61)$$

Following the harmonic approximation we search for a pseudo ground state solution of the eigenvalue problem for the hamiltonian (3.61) in Gaussian form. However this time we do not use Gaussians of the polar angle ϕ because such functions are not single valued. Instead, we use Gaussians of trigonometric functions of ϕ in the form

$$\Psi(r, \phi) = Ne^{l_0[i\phi - K(r, \phi)]}, \quad (3.62)$$

where l_0 is an integer and $K(r, \phi)$ is a periodic function of ϕ .

The periodic function $K(r, \phi)$ in (3.62) can be expanded into an infinite Fourier series but in the spirit of our Gaussian approximation we keep only the lowest two

terms. In this way we arrive at the following approximation for our initial wave function

$$\begin{aligned}
\Psi(r, \phi) &= Ne^{il_0\phi} \exp\{-(l_0/2r_c^2)[2r_c^2A(1 - \cos \phi) \\
&\quad + B(r - r_c)^2 + 2iCr_c(r - r_c) \sin \phi]\} \\
&= Ne^{il_0\phi} \exp\{-(l/2r_c^2)[4r_c^2A \sin^2(\phi/2) \\
&\quad + B(r - r_c)^2 + 4iCr_c(r - r_c) \sin(\phi/2) \\
&\quad \times \sqrt{1 - \sin^2(\phi/2)}]\}.
\end{aligned} \tag{3.63}$$

It is clear from the second form of the wave function that the role of ϕ is now being played by $2 \sin(\phi/2)$. We have not kept any terms higher than quadratic in this variable except where such terms are needed to secure periodicity of the wave function. That is why we could not drop the quadratic term under the square root. This procedure can, in principle, be extended to higher orders by keeping more powers of $\sin(\phi/2)$ in the wave function.

After substituting the wave function (3.63) into the equation $H_{2D}\Psi = E\Psi$ we perform all the differentiations, divide by the wave function, expand the resulting equation into a power series in $r - r_c$ and in $\sin(\phi/2)$ and drop all terms higher than quadratic. Collecting the coefficients of different powers of the variables $r - r_c$ and $\sin(\phi/2)$ we arrive at five equations for the five unknown coefficients A, B, C, r_c , and l_0 appearing in the wave function (3.63).

The linear terms give the first two of the five equations,

$$\frac{r_c^3}{l_0^2} \left(\frac{1}{r_c^2} + \mathcal{E} - \frac{l_0^2}{r_c^3} \right) = \frac{2A - B + 2C(l_0 - k)}{2l_0}, \tag{3.64}$$

$$1 - k/l_0 = -\frac{C}{2Al_0}, \tag{3.65}$$

where $k = \omega r_c^2$. If it were not for the quantum corrections of the order of $1/l_0$ that we placed on the right hand side of these equations, we would obtain the classical

values of the orbit radius and the angular momentum. Note that according to Eq. (3.65) l_0 differs by $C/(2A)$ from its classical value ωr_c^2 due to the quantum corrections appearing on the right hand side. Also the equilibrium radius r_c is slightly shifted. The quadratic terms lead to the remaining three equations,

$$A^2 - C^2 + 1 - q = -\frac{3A - B + 2C(l_0 - k)}{2l_0}, \quad (3.66)$$

$$B^2 - C^2 - 4C - 3 + 2q = \frac{3A - B}{l_0}, \quad (3.67)$$

$$(A + B)C + 2A = -\frac{C}{l_0}, \quad (3.68)$$

with $q = r_c/l_0^2$. In the classical limit, when $l_0 \rightarrow \infty$, the right hand sides vanish and our equations have analytic solutions which coincide with (3.49) obtained from the previously discussed harmonic approximation in cylindrical coordinates as well as those obtained in an early WKB approach in reference [18]. The wave function (3.63) coincides with the two dimensional part of the wave function (3.58) in this limit after expanding $\sin \phi$ and $\cos \phi$ up to second order in the polar coordinate ϕ . As we will show in Chapter 5 this method gives a very good approximation to the exact pseudo ground state solution.

Chapter 4

Energies and States within Nonlinear Theory

4.1 Overview

In this chapter we present the most important result of our work, the analytic, nonlinear quantum theory of the hydrogen atom in C.P. field near the principal resonance. By the proper rearrangement of the bare hydrogenic basis states we are able to achieve an approximate separability of the Schrödinger equation. This is based on our new view of the bare hydrogenic quantum numbers. We have found that in contrast to perturbative approaches it is not the principal quantum number n which labels the manifolds of strongly interacting states but new quantum numbers k and s which represent the deviation of a given state from circularity.

In contrast to non-perturbative harmonic approaches described in Chapter 3 this theory provides an explicit decomposition of dressed states in term of hydrogenic eigenstates, has well defined zero field limit, and predicts new states which cannot be described within harmonic theory. By the approximate block-diagonalization of the hamiltonian of our system we are able to look on a hydrogen atom in C.P. field as a system of non-interacting quantum pendula. This provides analytic expressions for both the energies and the wave functions of the rotating frame hamiltonian. The main advantage of this analytic theory is that among thousands of eigenstates it allows us to identify two classes of quantum states well localized in all spatial dimensions. Those states are of special importance since their adiabatic connection to circular states, well described within our the-

ory, implies new experimental methods of creating and controlling atoms with highly localized electrons. These special states have been denoted Trojan states for reasons that will be made clear later in Chapter 5.

4.2 Energies and states of the quantum pendulum

In this section we discuss the stationary solutions of the Schrödinger equation with the hamiltonian

$$H_P = -\frac{1}{2ml^2} \frac{\partial^2}{\partial \phi^2} + lg \cos \phi \quad (4.1)$$

It describes a quantized pendulum with mass m in a gravity field g and length l . An understanding of this simple quantum system is essential for our nonlinear quantum theory of hydrogen in the C.P. field and it is worth discussing its properties in detail. Defining $\xi = (\phi - \pi)/2$, the Schrödinger equation

$$H_P \psi = E \psi \quad (4.2)$$

can be transformed to the well known Mathieu equation [47]

$$\frac{\partial^2 \psi}{\partial \xi^2} + [\alpha - 2p \cos 2\xi] \psi = 0, \quad (4.3)$$

where

$$\alpha = 8mr_0^2 E, \quad p = -4mgl^3 \quad (4.4)$$

The periodic solutions of equation (4.3) are the Mathieu functions e_j with periodicity π and 2π . The periodic boundary conditions for the wave function ψ

$$\psi(\phi + 2\pi) = \psi(\phi) \quad (4.5)$$

allow only 2π periodic solutions for the wave functions. The invariance of the pendulum hamiltonian (4.1) under the transformation $\phi \rightarrow -\phi$ implies that the eigenfunctions ψ_j are either odd or even. Fig. 4.1 shows the scaled pendular energies α_i corresponding to even eigenfunctions and Fig. 4.2 a few lowest eigenstates of the hamiltonian (4.1).

There are two physically different kinds of solutions of the Schrödinger equation (4.2) depending on the relation of the energy of a given eigenstate with respect to the classical energy of unstable equilibrium of the up-side-down position $\alpha = 2p$ which defines the separatrix in the pendular phase-space [20].

The states with energies above the pendulum separatrix, $\alpha^j(p) > 2p$, are closer to the eigenstates of a rigid rotor with the hamiltonian

$$H_R = -\frac{1}{2ml^2} \frac{\partial^2}{\partial \phi^2} \quad (4.6)$$

with comparatively flat dispersion $\alpha(p)$. (Fig. 4.1). They correspond to the classical situation when the pendulum is so excited that it almost steadily rotates around its pivot-point. The states with energies below the separatrix, $\alpha^j(p) < 2p$ are of a different kind, corresponding to oscillatory-like motions of the pendulum around the stable equilibrium point. Then the pendular hamiltonian can be approximated by the hamiltonian of a harmonic oscillator

$$H_H = -\frac{1}{2ml^2} \frac{\partial^2}{\partial \phi^2} + \frac{\omega_H l^2 (\phi - \pi)^2}{2} \quad (4.7)$$

with the frequency $\omega_H = \sqrt{g/l}$. As a result of localization of those states around $\phi = \pi$ pendulum equilibrium position their energies exhibit almost linear growth as functions of the parameter p . This transition can be best seen by following the behavior of a selected Mathieu function as a function of both the parameter p and the normal angular variable ϕ , as shown in Fig. 4.3.

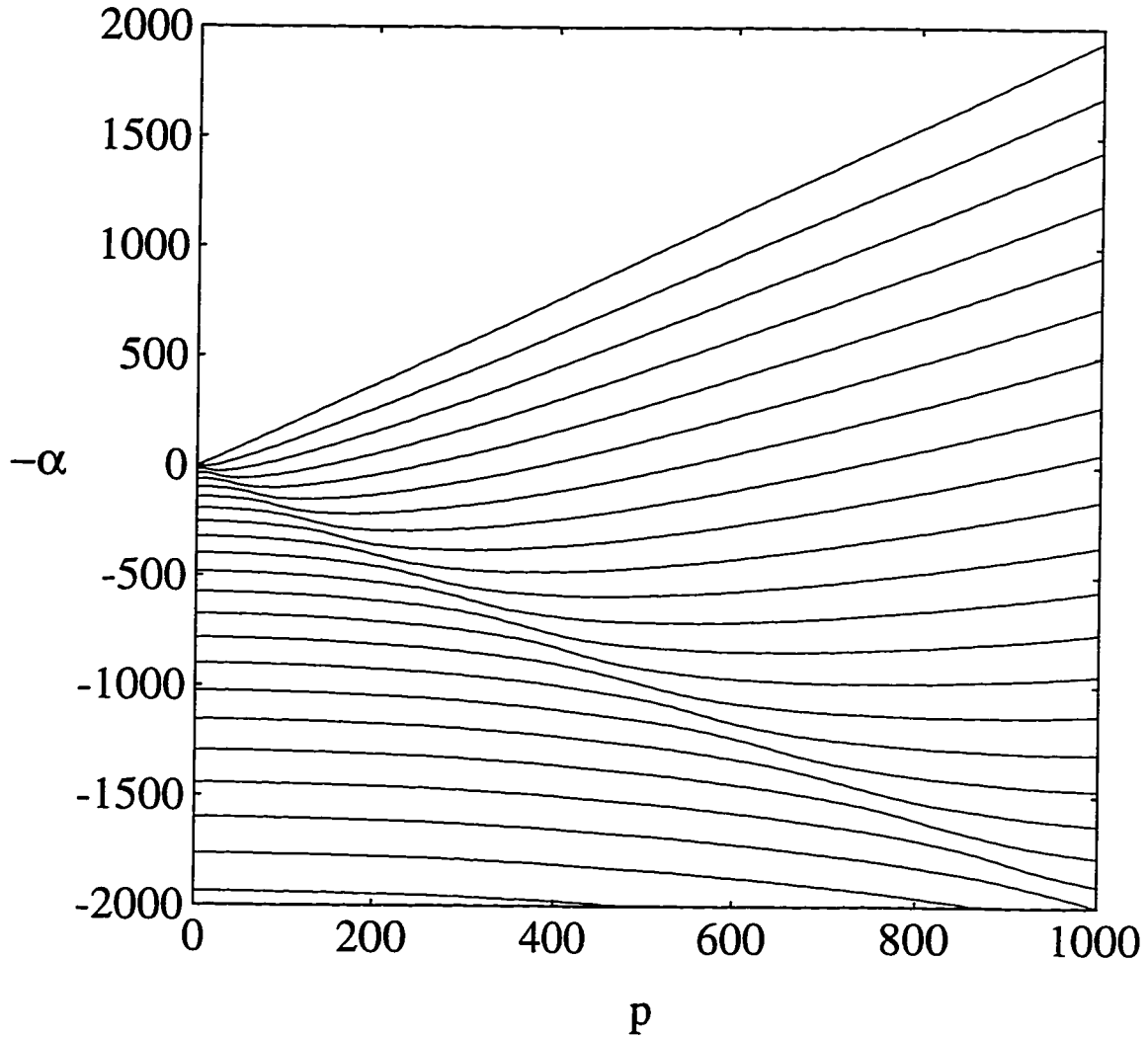


Fig. 4.1. Levels of scaled energy $-\alpha$ (corresponding to symmetric Mathieu functions) as functions of the parameter p . The value $-\alpha = 2p$ corresponds to Trojan states. States with scaled energy in the vicinity of the line $-\alpha = -2p$ are anti-Trojan states. Note that anti-Trojan states do not belong to a single energy line but to different lines close to the spectrum folding around $\alpha = 2p$.

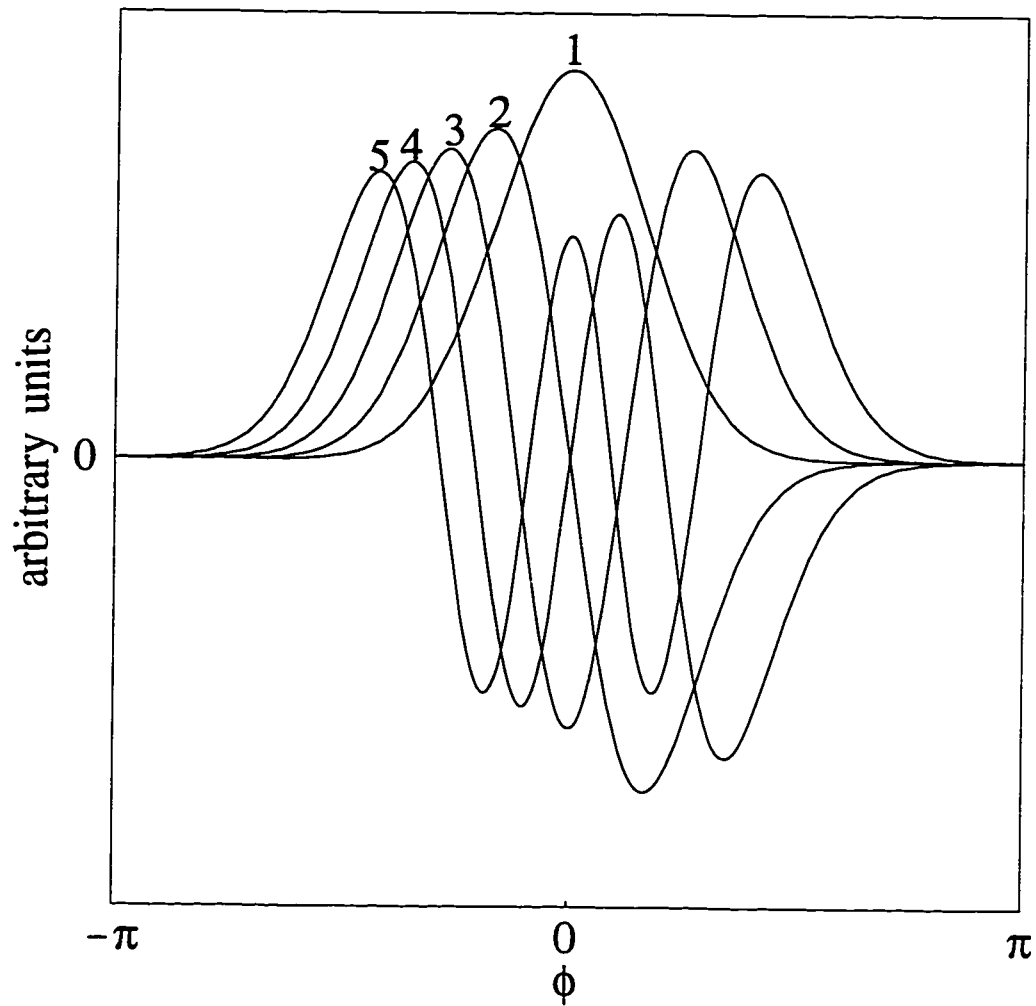


Fig. 4.2. A few of the lowest eigenfunctions of the quantum pendulum (π -periodic Mathieu functions) labeled in order of the excitation for $p = 60$. For this choice of the parameter p they resemble the eigenfunctions of the harmonic oscillator.

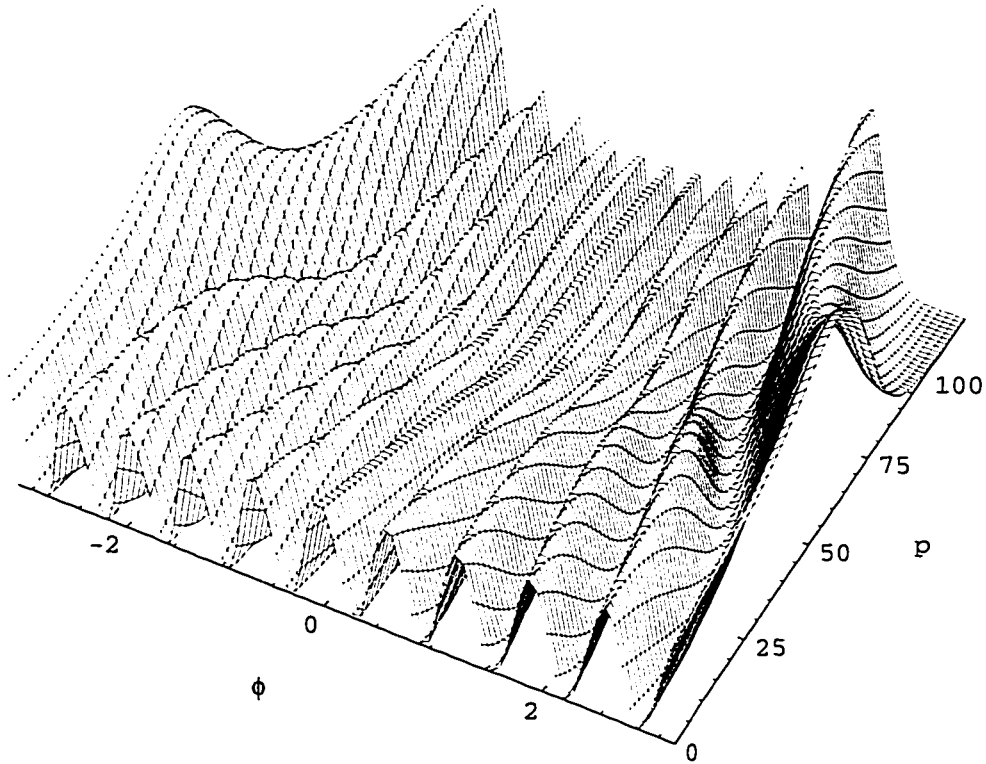


Fig. 4.3. Probability density of one of the higher excited states of the quantum pendulum (6-th, even) as a function of both the angle ϕ and the parameter p . Note the change from the plane-wave-like behaviour for low p characteristic of the rigid rotor to oscillator-like behaviour for high p . The change of behaviour occurs near separatrix $\alpha = 2p$ near $p = 60$, where the wave function strongly peaks around $\phi = \pi$.

4.3 High n expansion and resonant approximation

There are two main disadvantages of the harmonic approaches discussed in the previous chapter. First, the wave functions obtained within the harmonic approximation do not have a strict mathematical limit with a clear physical interpretation when the field strength \mathcal{E} goes to zero, since they are no longer well localized and the harmonic approximation is not well justified in this limit. Second, those approaches are not giving an explicit decomposition of the dressed eigenstates on the hydrogenic eigenstates, which is of special importance for lower field strengths when the spectrum of the rotating frame hamiltonian of our system should smoothly approach the hydrogenic levels in the rotating frame. In this section we discuss the essential ingredients which allow us to construct the nonlinear effective hamiltonian for a hydrogen atom in a C.P. field. This hamiltonian will generate energies and eigenstates free of those limitations.

We start from the Schrödinger equation with the hamiltonian (2.29)

$$\left(\frac{\mathbf{p}^2}{2} - \frac{1}{r} + \mathcal{E}x - \omega L_z \right) \Psi_E = E^j(\mathcal{E}) \Psi_E \quad (4.8)$$

where j labels the exact (discrete) eigenvalues of (2.29). We assume that an eigenfunction Ψ_E can be expanded as

$$\Psi_E(r, \theta, \phi) = \sum_{nlm} c_{nlm}(E) R_{nl}(r) Y_{lm}(\theta, \phi), \quad (4.9)$$

where $R_{nl}(r)$ is the radial part of the hydrogenic eigenfunction and Y_{lm} is a spherical harmonic. In this basis the stationary Schrödinger equation with the hamiltonian (2.29) takes the form

$$\mathcal{E} \sum_{n'l'm'} x_{nlm}^{n'l'm'} c_{n'l'm'}^j = [E^j(\mathcal{E}) - E_n + m\omega] c_{nlm}^j, \quad (4.10)$$

where $E_n \equiv -1/2n^2$, and the hydrogenic dipole matrix elements

$$x_{nlm}^{n'l'm'} = \langle n, l, m | x | n', l', m' \rangle \quad (4.11)$$

are known analytically [48] and the only nonvanishing ones are

$$\langle n, l, m | x | n', l+1, m+1 \rangle = \frac{1}{2} \sqrt{\frac{(l+m+2)(l+m+1)}{(2l+3)(2l+1)}} R_{nl}^{n'l+1}, \quad (4.12)$$

$$\langle n, l, m | x | n', l+1, m-1 \rangle = -\frac{1}{2} \sqrt{\frac{(l-m+2)(l-m+1)}{(2l+3)(2l+1)}} R_{nl}^{n'l+1}, \quad (4.13)$$

$$\langle n, l, m | x | n', l-1, m+1 \rangle = -\frac{1}{2} \sqrt{\frac{(l-m)(l-m-1)}{(2l+1)(2l-1)}} R_{nl}^{n'l-1}, \quad (4.14)$$

$$\langle n, l, m | x | n', l-1, m-1 \rangle = \frac{1}{2} \sqrt{\frac{(l+m)(l+m-1)}{(2l+1)(2l-1)}} R_{nl}^{n'l-1}, \quad (4.15)$$

where $R_{nl}^{n'l'}$ is the radial part of the elements given for $n' \neq n$ by [48]

$$\begin{aligned} R_{nl}^{n'l-1} &= \int_0^\infty R_{nl} R_{n',l-1} r^3 dr = \\ &= \frac{(-1)^{n'-1}}{4(2l-1)!} \sqrt{\frac{(n+l)!(n'+l-1)!(4nn')^{l+1}(n-n')^{n+n'-2l-2}}{(n-l-1)!(n'-l)! (n+n')^{n+n'}}} \times \\ &\quad \{F[-n_r, -n'_r, 2l, -\frac{4nn'}{(n-n')^2}] \\ &\quad - \left(\frac{n-n'}{n+n'}\right)^2 F[-n_r-2, -n'_r, 2l, -\frac{4nn'}{(n-n')^2}]\}. \end{aligned} \quad (4.16)$$

where F is the hypergeometric function and $n_r = n-l-1$, $n'_r = n'-l$. For $n = n'$ one gets [48]

$$R_{nl-1}^{nl} = -\frac{3}{2} n \sqrt{n^2 - l^2} \quad (4.17)$$

The matrix equation (4.10) can be solved only numerically and the crucial point for further processing is to reduce the hamiltonian matrix

$$\langle n, l, m | H | n', l', m' \rangle = \mathcal{E} x_{nlm}^{n'l'm'} + E_n - m\omega \quad (4.18)$$

to an approximate, simplified form.

We have found the clue to this simplification. We divide the $\{|nlm\rangle\}$ basis into the following manifolds $\{|n, n-1, n-1\rangle\}$, $\{|n, n-1, n-2\rangle\}$, ..., $\{|n, n-k, n-k-s\rangle\}$, The first manifold represents circular states, the second all states with angular momentum L_z one atomic unit lower, etc. Note that all of these manifolds are infinitely large. The simplification can be performed because for $k \ll n$ and $s \ll n$ (states with angular momentum quantum numbers close to circular) matrix elements between states within a particular manifold labeled by $k > 0$ and $s \geq 0$ are much larger than those between states which belong to two different manifolds. This can be checked directly by inspecting the analytical form of the matrix elements of the coordinate x between two different hydrogenic eigenfunctions (4.15), but also can be estimated from the large- n approximate expression for the radial matrix elements (4.16). This is [49, 50]

$$|R_{nl}^{n'l'}| \simeq \left| \frac{n^2}{2s} \left[\left(1 + \Delta l \frac{l}{n} \right) J_{s+1}(s\varepsilon) - \left(1 - \Delta l \frac{l}{n} \right) J_{s-1}(s\varepsilon) \right] \right| \quad (4.19)$$

where $\Delta l = l' - l = \pm 1$, $s = n - n' > 0$, J_s is the Bessel function of the s -th order and

$$\varepsilon = \sqrt{1 - \frac{l^2}{n^2}}. \quad (4.20)$$

Let us consider all the matrix elements (4.19) between the state $|n, n-k, n-k-s\rangle$ from a fixed manifold k, s and fixed n and other states which are not zero. Those will be $|n', n'-k', n'-k'-s'\rangle$ for which $n \neq n'$

$$n - k = n' - k' \pm 1, \quad (4.21)$$

$$n - k - s = n' - k' - s' \pm 1. \quad (4.22)$$

For $k' \ll n$, $k \ll n$ also $s = n - n' = k - k' \mp 1 \ll n$ and the argument of the Bessel functions J_{s-1} and J_{s+1} is also small $s\varepsilon \ll 1$, also $l \approx n$. One can now

expand those functions [21] and get

$$|R_{nl}^{n'l'}(s)| \simeq \left| \frac{n^2}{2s} \left[(1 \pm 1) \left(\frac{s\varepsilon}{2} \right)^{s+1} \frac{1}{(s+1)!} - (1 \mp 1) \left(\frac{s\varepsilon}{2} \right)^{s-1} \frac{1}{(s-1)!} \right] \right| \quad (4.23)$$

For $s\varepsilon \ll 1$ expression (4.23) is a fast decreasing function of s with a maximum at $s = 1$, i.e., $|R_{nl}^{n'l'}(1)| \simeq n^2$, and this establishes an approximate block diagonal form in k, k' . For $n = n'$ this can be seen directly from the exact expression (4.17) since $l \approx n$. The approximate diagonal form in s, s' follows directly from the consideration above, since those matrix elements which could be large, i.e., for $k = k'$ are restricted by the second of the transition rules (4.22) to $n - s = n' - s' \pm 1$.

As the result, in our first principal approximation, the interaction between different manifolds $\{k, s\}$ can be neglected. Additionally, we concentrate on rotating-frame eigenfunctions that are well localized in angular momentum space, namely those requiring only a limited number of significant terms in the expansion (4.9), centered around some particular value of n denoted n_0 . Because of the assumption of the localization of the wave function in angular momentum space we will put all matrix elements between states within a particular manifold equal. The conditions $k \ll n$ and $s \ll n$ allow us to take the value $x_{nlm}^{n'l'm'} = n_0^2/2 = r_0/2$ for all matrix elements assumed to be nonzero. Under these assumptions equation (4.10) is block-diagonal with blocks labeled by k and s . The assumption about the localization in n allows us to expand the hydrogenic energy around n_0 up to second order, namely

$$E_n = -\frac{1}{2n_0^2} + \omega_c \delta n - \frac{3}{2} \frac{\delta n^2}{r_0^2}, \quad (4.24)$$

where $\omega_c = 1/n_0^3$ is the Kepler frequency corresponding to the quantum number n_0 , and $\delta n \equiv n - n_0$.

Now we impose our second principal assumption. By assuming $\omega_c = \omega$, the principal resonance condition, the Schrödinger equation (4.10) for the particular

block then takes the simple form

$$\begin{aligned} \frac{\mathcal{E}}{2} r_0 (a_{n-1ks}^j + a_{n+1ks}^j) &= [E^j(\mathcal{E}) - E_{n_0} + (n_0 - k - s)\omega \\ &+ \frac{3}{2} \frac{\delta n^2}{r_0^2}] a_{nks}^j \end{aligned} \quad (4.25)$$

with $a_{nks} \equiv c_{n,n-k,n-k-s}$. This simplification follows directly from the fact that dipole matrix elements between states within a single manifold $\{|n, n-k, n-k-s\rangle\}$ are zero except between two consecutive states $|n, n-k, n-k-s\rangle$ and $|n-1, n-1-k, n-1-k-s\rangle$.

For n and l much larger than 1 we can assume that there is no boundary restriction for the variables n and δn . Under this assumption equation (4.25) becomes the Schrödinger equation for a quantum pendulum, but with a negative mass $-1/3$. In real space it becomes

$$\begin{aligned} \left[\frac{3}{2} \frac{1}{r_0^2} \frac{\partial^2}{\partial \phi^2} + \mathcal{E} r_0 \cos \phi \right] f &= [E^j(\mathcal{E}) - E_{n_0} \\ &+ (n_0 - k - s)\omega] f, \end{aligned} \quad (4.26)$$

where

$$f(\phi) = \sum_{\delta n} a_{nks}^j e^{i\delta n \phi} \quad (4.27)$$

Therefore it can be written in the standard Mathieu form [compare (4.3) with $\phi = 2\xi + \pi$]:

$$\alpha = -(8r_0^2/3)[E^j - E_{n_0} + (n_0 - k - s)\omega] \quad (4.28)$$

and

$$p = \frac{4}{3} \frac{(e\mathcal{E}/m\omega^2)}{(\hbar^2/me^2)} = \frac{4}{3} \frac{\mathcal{E}}{\omega^2} \quad (4.29)$$

Thus the dimensionless parameter p in our theory has a physical interpretation. It is proportional to the ratio between the radius of the orbit of a free electron in

the presence of a circularly polarized light field (Volkov problem) and the Bohr radius (Coulomb problem). Note that equation (4.26) implies that the operator

$$H_{EFF} = -\frac{3}{2} \frac{1}{r_0^2} L_z^2 + \mathcal{E} r_0 \cos \phi \quad (4.30)$$

is an approximate constant of motion for quantum states from within given k, s manifold in the analogy to approximate constants of motion discussed in Chapter 2.

4.4 Energies and states

The energies of our systems can be now expressed in terms of the eigenvalues α^j of the Mathieu equation as

$$E_{ks}^j(\mathcal{E}) = -\frac{1}{2n_0^2} - (n_0 - 1 - k - s)\omega - \frac{3}{8r_0^2} \alpha^j(p) \quad (4.31)$$

For the discrete set of eigenvalues α_μ of the Mathieu equations (4.3) two analytic asymptotic expressions are known [47]. For $p \ll \mu$ one gets

$$\alpha_\mu(p) \approx \mu^2 + \frac{p^2}{2(\mu^2 - 1)} \quad (4.32)$$

and in the opposite case for $\mu \ll p$ the asymptotic expression is

$$\alpha_\mu(p) \approx -\frac{[(2\mu + 1)^2 + 1]}{8} + 2(2\mu + 1)\sqrt{p} - 2p. \quad (4.33)$$

The corresponding eigenfunctions of equation (4.26) are obviously also Mathieu functions and because of periodic boundary conditions, only those with periodicity π are permitted. This implies that in the case of formula (4.32) only every second eigenvalue can be permitted, namely $\mu = 2j, j = 0, 1, \dots$ since the eigenfunctions of (4.3) corresponding to odd μ have period 2π in the variable ξ and lead to nonphysical wave functions. In case of formula (4.33), μ can be either even or

odd since the solutions with periodicity π become approximately degenerate [47] with those with periodicity 2π , and one corresponding to a physical solution can always be found.

The coefficients a_{nks}^j from equation (4.25) can be found as

$$a_{nks}^j = \int e_{2j}(\xi) e^{-2i\xi} d\xi, \quad (4.34)$$

where $e_{2j}(\xi)$ is the j -th Mathieu function of period π . Expressions (4.32) and (4.33) allow us to obtain two asymptotic expressions for the field-dependent energy levels of the hamiltonian. For low values of the electric field we obtain

$$\begin{aligned} E^j(\mathcal{E}) &\equiv E_{ks}^j(\mathcal{E}) \\ &= E_{n_0} - (n_0 - k - s)\omega - \frac{3}{2} \frac{j^2}{r_0^2} - \frac{\mathcal{E}^2 r_0^4}{4j^2 - 1}. \end{aligned} \quad (4.35)$$

For larger field strengths we use (4.33) and get

$$\begin{aligned} E_{ks}^j(\mathcal{E}) &= E_{n_0} - (n_0 - k - s)\omega \\ &+ \frac{3}{32} \frac{(2j^2 + 2j + 1)}{r_0^2} - (j + \frac{1}{2}) \sqrt{\frac{3\mathcal{E}}{r_0}} + r_0 \mathcal{E}. \end{aligned} \quad (4.36)$$

The spectrum is labeled by three quantum numbers s , k , and j . The first two are associated with the angular momentum quantum numbers of hydrogen and the third with excitations of the quantum pendulum.

The corresponding eigenfunctions directly from (4.9) can be written

$$\Psi_{jks}(r, \theta, \phi) = \sum_n a_{nks} R_{n,n-k}(r) Y_{n-k,n-k-s}(\theta, \phi). \quad (4.37)$$

When the summation in (4.37) is restricted to n around some particular value n_0 , as we assume for the expansion of hydrogenic energy (4.24), the radial functions $R_{n,n-k}$ and $Y_{n-k,n-k-s}$ can be replaced by those for $n = n_0$. This is a result of the fact that for fixed s and k they have the same spatial character or, in other words,

they are slowly varying functions of n . Under this assumption we get from (4.37)

$$\begin{aligned}\Psi_{jks}(r, \theta, \phi) &= N_{n_0-k, n_0-k-s} e^{i(n_0-k-s)\phi} R_{n_0, n_0-k}(r) \\ &\times P_{n_0-k, n_0-k-s}(\theta) \sum_{\delta n} a_{nks} e^{i\delta n\phi},\end{aligned}\quad (4.38)$$

where we wrote explicitly spherical harmonics Y_{lm} as products of Legendre polynomials P_{lm} , exponentials $e^{il\phi}$ and normalization factors N_{lm} . Note that now because of relation (4.34) the sum over δn can be reduced back to the Mathieu function and therefore the wave function has a nice analytical form

$$\begin{aligned}\Psi_{jks}(r, \theta, \phi) &= N_{n_0-k, n_0-k-s} e^{i(n_0-k-s)\phi} R_{n_0, n_0-k}(r) \\ &\times P_{n_0-k, n_0-k-s}(\theta) e_{2j}((\phi - \pi)/2).\end{aligned}\quad (4.39)$$

The pendular-like character of the wave functions (4.39) immediately implies two physically different kinds of solutions analogical to those of the quantum pendulum. The states with energies below the pendulum separatrix, $\alpha^j(p) > 2p$ (note the negative mass of the pendulum which causes levels to be inverted), are closer to the circular states of bare hydrogen and they are delocalized angularly with a weak angular periodic modulation (Fig. 4.4 (d)-(f)). As a result of nonlocalization, the eigenvalues corresponding to those states exhibit weak dependence on the field strength Fig. 4.1. They correspond to near-circular classical orbits with angular velocities larger or smaller than the frequency of the external field [22].

The states with energies above the separatrix, $\alpha^j(p) < 2p$, correspond to oscillatory-like motions around the stable classical orbit [18, 51] and as we discuss in the next section in the limit of large n_0 can be well represented by our harmonic approximations discussed in Chapter 2. As a result of localization their energy exhibits an almost linear growth as a function of the external field (Fig. 4.1). Special attention should be given to two special kinds of states, those with their

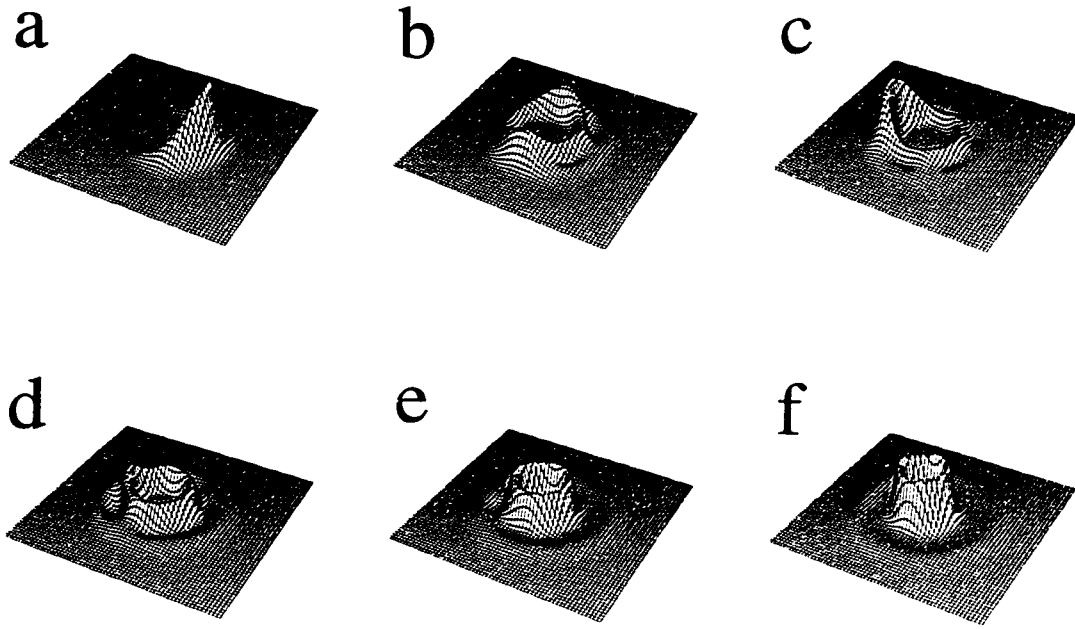


Fig. 4.4. Examples of the eigenfunctions (4.37) for the scaled field $\mathcal{E}_{sc} = 0.016$ and $n_0 = 20$ corresponding to even-order Mathieu functions and the circular-states manifold ($k = 1, s = 0$): (a) $jks=010$, pure Trojan packet-state, (b) $jks=210$, oscillatory-like, from above the separatrix, (c) $jks=410$, near the separatrix, (d) $jks=610$, (e) $jks=810$, (f) $jks=1010$, rotational-like, below the separatrix.

energies around the separatrix, i. e., $\alpha^j(p) \approx 2p$, and those with $\alpha^j(p) \approx -2p$ (Fig. 4.4). These are so-called Trojan and anti-Trojan states [44, 45, 46, 52] which we will discuss in detail in Chapter 5.

Equations (4.31), (4.34) and (4.37) contain one of the most important results of our work presented in this thesis, namely the analytical form of non-perturbative, rotating-frame energies and states of the hydrogen atom in a circularly polarized field near the principal resonance treated within the nonlinear theory. This result supplies the limited list of results for atoms in various strong external fields when the approximate spectra can be found analytically.

4.5 Analytic, asymptotic and numerical tests of pendular versus harmonic approximation

It is interesting to compare the spectra obtained within the harmonic approximation (3.40) with the result of the nonlinear approach (4.31). The connection comes directly from the approximate formula (4.36). For the field strengths which guarantee classical stability the parameter q satisfies the condition (3.32), namely $(8/9) < q < 1$, so $q \approx 1$ and we have $\omega_+ \approx \omega$ and $\omega_0 \approx \omega$. For \mathcal{E} large enough for fixed k and s , the energy levels given by expression (4.36) are equally spaced with the spacing

$$\sigma = \sqrt{(3\mathcal{E}/r_0)}. \quad (4.40)$$

The behavior of σ as a function of the parameter q (shown in Fig. 4.5) allows us to associate this spacing with the frequency ω_- from the harmonic approximation. Note additionally that $E_0 \approx E_{n_0} + \mathcal{E}r_0 - (n_0 - 1)\omega$, since the radius of the classical orbit r_c is only very little different than the radius of the corresponding Kepler orbit $r_0 = n_0^2$. The small difference between those two radii is given by the

relation $r_c = r_0 q^{-1/3}$ which follows directly from (3.28). This connection between the basis expansion method and the harmonic approximation allows us to tell which Rydberg manifolds contribute most in creating the eigenfunctions of the harmonic hamiltonian (3.53). The quantum number m_0 from the formula (3.40) associated with the excitation perpendicular to the plane of the motion of the packet obviously corresponds to the quantum number s in the expression (4.36). The quantum number m_+ in (3.40) corresponds to k in (4.36) and finally the Mathieu function index j corresponds to the index m_- in (3.40). Therefore the eigenstate of hamiltonian (3.53) with the eigenvalue E_{m_+, m_-, m_0} is built mainly from the hydrogenic eigenfunctions which belong to the $\{|n, n-1-m_+, n-1-m_+-m_0\rangle\}$ manifold with n in the vicinity of n_0 , which is defined by the resonance condition $\omega = 1/n_0^3$.

Also the simplest possible eigenfunction (4.37) ($j = 0, k = 1, s = 0$) can be compared directly with the pseudo ground state wave function obtained within the harmonic approximation in cylindrical coordinates (3.58). In this case the functions R_{n_0, n_0-1} , P_{n_0-1, n_0-1} and e_0 have Gaussian-like shapes in their coordinates [47, 19]. For n_0 large enough and for appropriate field strengths the function (4.39) can be written as

$$\begin{aligned} \Psi_{jks}(r, \theta, \phi) &= N e^{i(n_0-1)\phi} e^{-\frac{\omega}{2}(r-r_0)^2} e^{-\frac{\omega}{2}r_0^2\theta^2} \\ &\times e^{-\beta\frac{\omega}{2}r_0^2\phi^2}, \end{aligned} \quad (4.41)$$

where the expression for the coefficient β is given by

$$\beta = \sqrt{\mathcal{E}_{sc}/3}. \quad (4.42)$$

Here \mathcal{E}_{sc} is the electric field scaled to the Coulomb field at the distance r_0 from the nucleus, $\mathcal{E}_{sc} = \mathcal{E}\omega^{1/3}$.

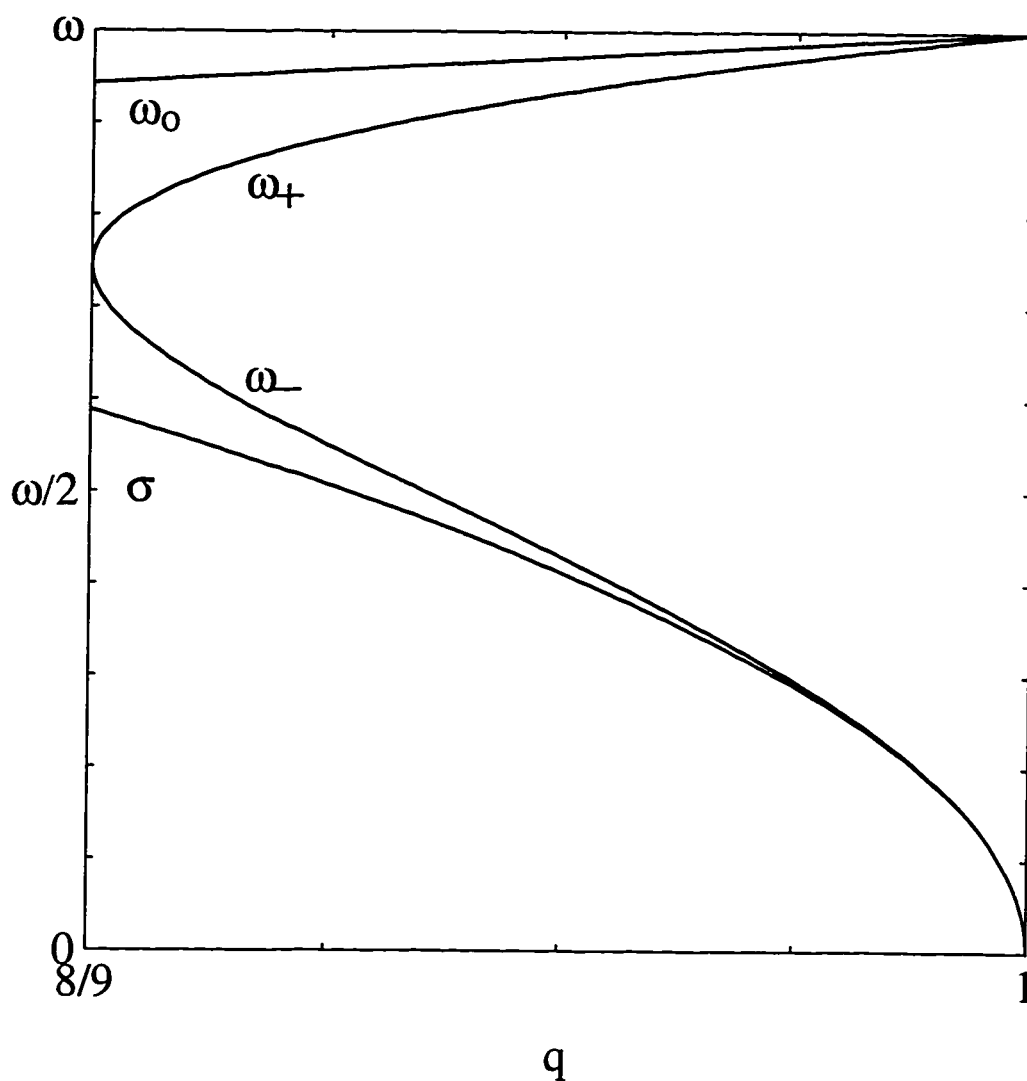


Fig. 4.5. Eigenfrequencies of the harmonic hamiltonian (3.11) as functions of the parameter q and the spacing σ obtained from formula (4.38). Note that generally $\omega_0 \approx \omega_+ \approx \omega$ and $\sigma \approx \omega_-$, so the energy spectra obtained from the basis expansion method with the assumption about noninteracting manifolds and from the harmonic approximation approximately coincide. For lower field strengths (larger q) the agreement is better.

The Gaussian approximation of the zero order Mathieu function e_0 originates directly from the fact that the $\cos 2\xi$ in equation (4.3) can be replaced by its expansion up to second order in ξ when the wave function is compact enough to permit a small- ξ approximation. This occurs whenever p is large enough compared to μ . As we pointed out in Section 4.1 the Mathieu equation in this case becomes the Schrödinger equation of a harmonic oscillator. The quantum mechanical condition for this replacement can be found from the requirement that if one wants the harmonic approximation to be valid for the j -th eigenstate in equation (4.26) the amplitude of the cosine term in (4.26) must be larger than the energy of the j -th level obtained from the harmonic approximation. This self-consistent requirement means that the cosine potential must be deep enough to bind j states in the harmonic portion of the potential well. This requirement gives the constraint for the scaled electric field, which is

$$\mathcal{E}_{sc} > 3 \frac{(j+1)^2}{n_0^2}. \quad (4.43)$$

This implies that for very small field strengths the harmonic approximation holds for the particular eigenfunctions (4.37) with $j = 0$, and for j not far from the lowest the energy levels are almost equally spaced as predicted by formula (4.36). Note that wave function (4.41) approximately satisfies periodic boundary conditions with respect to the variable ϕ only when it is well localized around $\phi = 0$. On the other hand the function (4.39) is free from this restriction since the Mathieu function e_0 has period π . For large enough r_c and appropriate field strengths the z -dependent parts of the wave functions (3.58) and (4.41) can also be compared directly with the expression using the approximate relation $z = r_c \theta$. Note that when this approximation holds (for wave functions well localized around the plane of orbital motion) the circular coordinate r is approximately the same as the

cylindrical r and a comparison is possible.

For lower field strengths when q is very close to 1 (Fig. 4.6) we have $B \approx 1$, $C \approx 1$, $D \approx 1$ and also $A \approx \beta$, so those two wave functions do not differ too much from each other, which confirms the applicability of our approximation of noninteracting manifolds. The deviation for higher field strengths is a result both of the assumption of the lack of the interaction between manifolds as well as the fact that the basis of hydrogenic bound states is not a complete basis. The orthogonal space of the continuum states also exists but the interaction with the continuum has been totally neglected. The interaction with the continuum states will lead to a small amount of ionization, and this contributes to a non-zero width of the energy levels.

Note that in the limit $l_0 \rightarrow \infty$ the harmonic approximation becomes exact while the model of noninteracting manifolds does not, and for very large l_0 the harmonic approximation should be used as a test of the former model rather than vice versa. For lower values of l_0 and lower field strengths, when the harmonic theory predicts weak radial confinement of the electron wave function, we can expect that the noninteracting manifolds model works better. In the limit $\mathcal{E} \rightarrow 0$ it recovers the quadratic nonlinearity of the Coulomb spectrum and the exact hydrogenic eigenfunctions.

Finally we can resort to purely numerical calculations as a strict test of our analytic results for finite (non-asymptotic) values of principal quantum number and angular momentum. We have solved the stationary Schrödinger equation numerically using only aligned states (states with $l = m$) in the expansion of the wave function (4.9), which is approximately equivalent to considering a two dimensional hydrogen atom [53]. This corresponds to taking into account all (numerically truncated) states from $\{|n, n-1, n-1\rangle, \dots, |n, n-k, n-k\rangle\}$

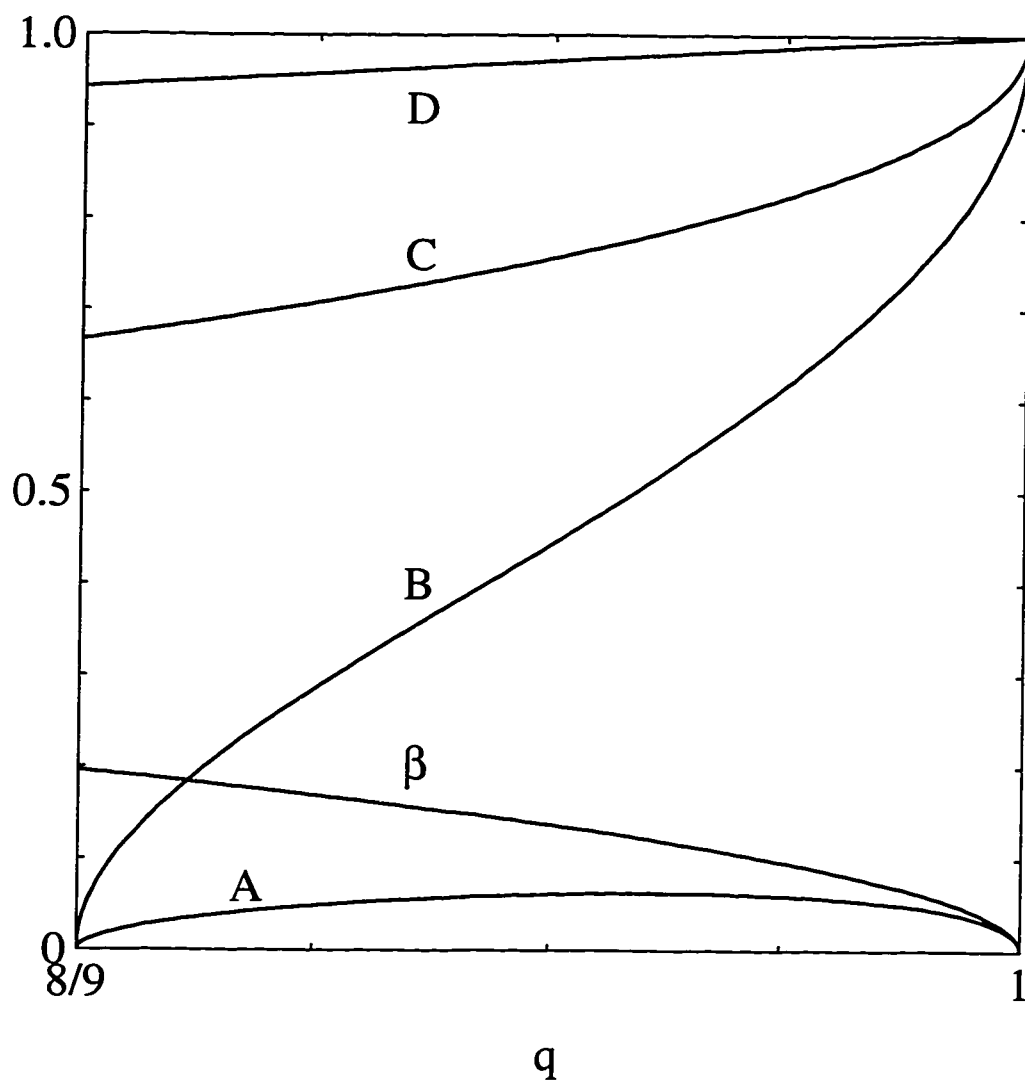


Fig. 4.6. Parameters of the pseudo ground state wave function (3.58) obtained from the harmonic approximations as functions of the parameters q and β given by (4.41) from the noninteracting manifolds model. For larger q we have $B \approx C \approx D \approx 1$ and also $A \approx \beta$, and therefore the harmonic wave function agrees approximately with the one obtained from the basis expansion for lower field strengths (however fields strong enough to permit the harmonic approximation in the Mathieu equation as given by the condition (4.43)).

manifolds, with all interactions between those states governed by the values of the exact matrix elements between them.

Figs. 4.7 and 4.8 show the rotating frame energy spectra as functions of the scaled electric field for the frequency $\omega = 1/n_0^3$, for $n_0 = 10$ and $n_0 = 20$. One can barely identify two doublets in Fig. 4.7 but two triplets can be picked out in Fig. 4.8 consisting of energy lines almost linearly proportional to the field strength. This is the imprint of the harmonic spectrum. Note that from condition (4.43) one gets the maximum number of levels contributing to a harmonic-like structure within a single bunch as $n_{max} = n_0(\mathcal{E}_{sc}/3)^{1/2}$. For the maximum value of the scaled field $\mathcal{E}_{sc} = 0.05$ and $n_0 = 20$ we get $n_{max} = 2.58$, so one should expect about three harmonic energy lines as one sees in Fig. 4.8. For $\mathcal{E}_{sc} = 0.1$ and $n_0 = 10$ we have $n_{max} = 1.83$, so one expects to see up to two lines as can be identified in Fig. 4.7. If the identification of the harmonic energies is not totally obvious, reference to Figs. 4.9 and 4.10 which show the corresponding energy lines obtained from the eigenvalues of Mathieu equation (4.3), is helpful. One can see very satisfactory agreement between analytical and numerical results for $n_0 = 20$ and still satisfactory for $n_0 = 10$.

4.6 Relation to Stark effect

We want to point out here that the stationary Schrödinger equation for our system (4.8) can be considered as a Stark problem with the paramagnetic hamiltonian

$$H_P = \frac{\mathbf{p}^2}{2} - \frac{1}{r} - \omega L_z, \quad (4.44)$$

since

$$H = H_P + \mathcal{E}x \quad (4.45)$$

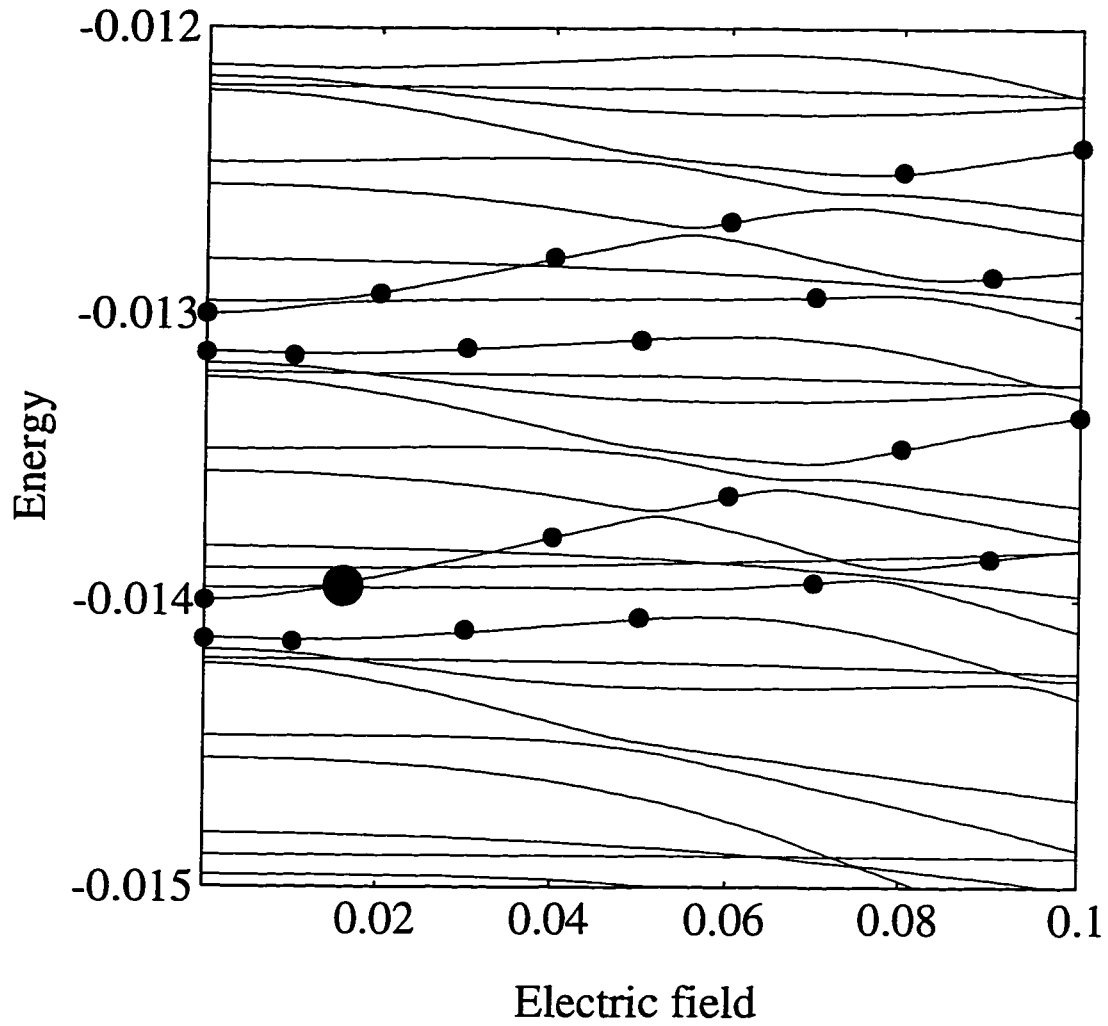


Fig. 4.7. Energy spectrum as a function of scaled electric field in the vicinity of the $n_0 = 10$ circular state for $\omega = 1/n_0^3$. The marker points belong to the Trojan lines. One can see two doublets on the diagram separated by approximately $\omega = 0.001$. The large marker point corresponds to the Gaussian-like Trojan packet for $\mathcal{E}_{sc} = 0.016$.

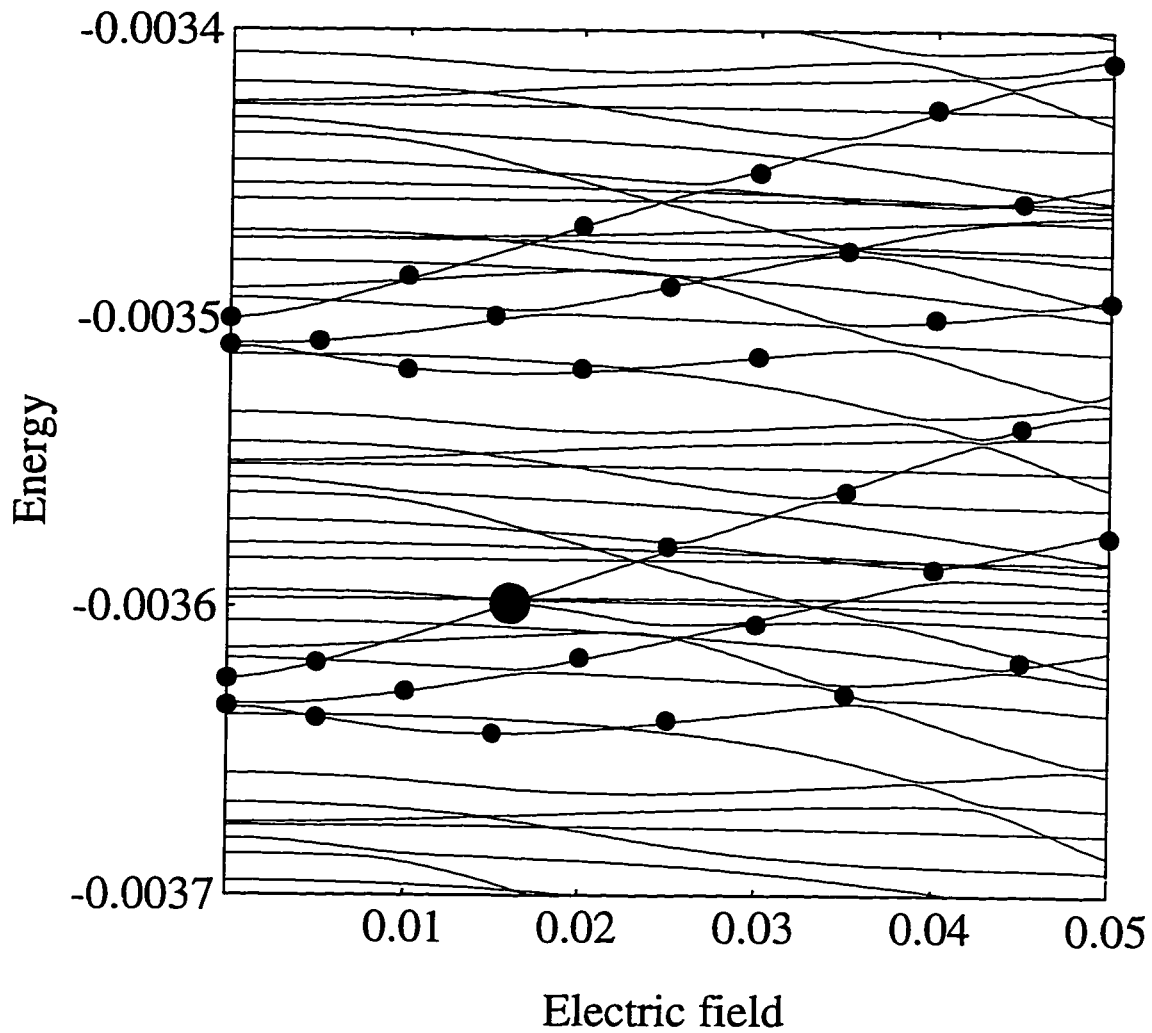


Fig. 4.8. Energy spectrum as a function of scaled electric field in the vicinity of the $n_0 = 20$ circular state for $\omega = 1/n_0^3$. The marker points belong to the Trojan lines. One can see two triplets on the diagram separated by approximately $\omega = 0.000125$. The large marker point corresponds to the Gaussian-like Trojan packet for $\mathcal{E}_{sc} = 0.016$.

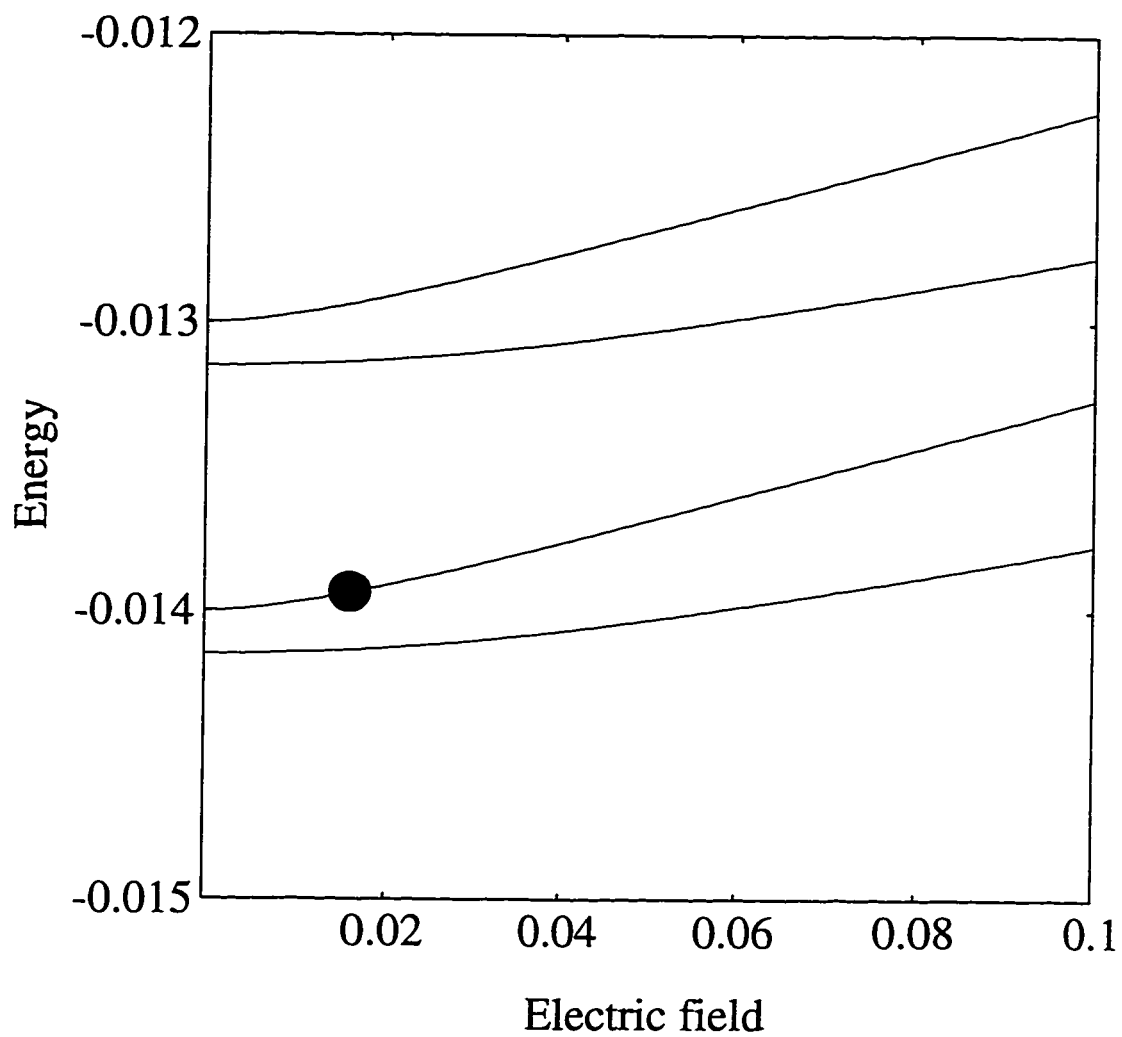


Fig. 4.9. Doublets obtained from the expression (4.31) within nonlinear theory for $\omega = 1/10^3$. The large point corresponds to the Gaussian-like Trojan packet for $\mathcal{E}_{sc} = 0.016$.

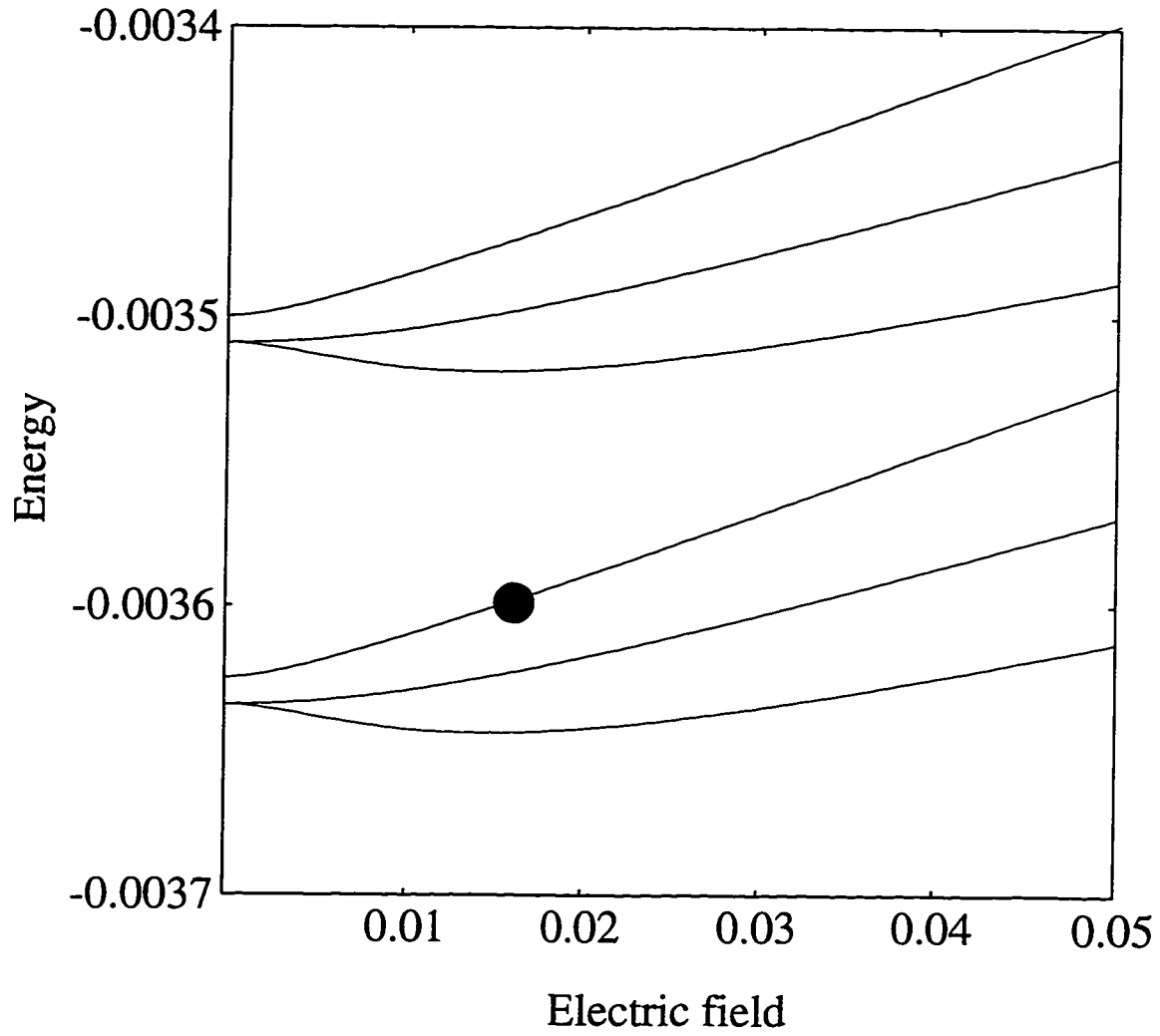


Fig. 4.10. Triplets obtained from the expression (4.31) within nonlinear theory for $\omega = 1/20^3$. The large point corresponds to the Gaussian-like Trojan packet for $\mathcal{E}_{sc} = 0.016$.

For the bare hydrogenic eigenstates which are obviously also the eigenstates of H_P for weak field strength one can use the stationary perturbation calculus treating $\mathcal{E}x$ as a perturbation to H_P . The energies of the hamiltonian are however different then the energies of the hydrogen and the standard perturbation calculus for degenerate n manifold used for normal Stark effect [35] no longer can be used. The results from the Section 4.1 show that near the principal resonance $\omega = 1/n^3$ one should use the new quantum numbers s, k as a guidance for perturbation theory [54]. Within a single $\{s, k\}$ manifold no states are strictly degenerated. The first order correction to the energy vanishes [55]

$$\delta E^1 = \mathcal{E} \langle n, n-k, n-k-s | x | n, n-k, n-k-s \rangle = 0 \quad (4.46)$$

The second order correction is given by [55]

$$\delta E^2 = \mathcal{E}^2 \sum_{n \neq n'} \frac{|\langle n, n-k, n-k-s | x | n', n'-k, n'-k-s \rangle|^2}{E_{nks}^0 - E_{n'ks}^0} \quad (4.47)$$

with

$$E_{nks}^0 = -\frac{1}{2n^2} - (n-k-s)\omega. \quad (4.48)$$

The infinite sum over n in (4.47) reduces only to two components with $n' = n \pm 1$ from the construction of the $\{s, k\}$ manifolds and the angular momentum transition rules, so

$$\begin{aligned} \delta E^2 = \mathcal{E}^2 \times & \quad (4.49) \\ & \left\{ \frac{|\langle n, n-k, n-k-s | x | n+1, n-k+1, n-k-s+1 \rangle|^2}{E_{n+1ks}^0 - E_{n+1ks}^0} \right. \\ & + \left. \frac{|\langle n, n-k, n-k-s | x | n+1, n-k-1, n-k-s-1 \rangle|^2}{E_{n-1ks}^0 - E_{n-1ks}^0} \right\} \end{aligned}$$

Using the expansion of the bare energies (4.24) up to second order in $n - n_0$ and the approximate resonant value $r_0^2/2$ for the dipole matrix elements the expression

(4.47) reduces to

$$\delta E^2 = -\frac{1}{3} \frac{\mathcal{E}^2 r_0^4}{(4\delta n^2 - 1)} \quad (4.50)$$

Note that the second order perturbation energy with expanded zero-order part of the energy E_{n+1ks}^0

$$E^2(\mathcal{E}) = -\frac{1}{2n_0^2} - (n_0 - k - s)\omega - \frac{3}{2} \frac{\delta n^2}{r_0^2} + \delta E^2 \quad (4.51)$$

for $j = |\delta n|$ coincides exactly with the low field limit (4.35) obtained within our nonlinear theory which we obtained using known [47] low- p expression (4.32) for characteristic value of the Mathieu equation $\alpha(p)$. Thus the weak field result can be interpreted as second order Stark effect for the paramagnetic Kepler problem with the cyclotronic frequency $\omega/2$.

The nonperturbative strong-field limit (4.36) can be interpreted as an approximately linear Stark effect since for low quantum number j in the expression the term linear in \mathcal{E} is dominant. Note that this transition from quadratic to approximately linear Stark effect is exactly inverse of that for the normal Stark effect for a hydrogen since the lowest order effect is linear [35]. This can be understood from the fact that in our case the essential states which are mixed by the electric field are not degenerated, but on the larger energy scale they look approximately degenerated since the centrifugal term in the hamiltonian H cancels the linear contribution to the spacing between the energy levels. However even for larger fields this lack of degeneracy remains important enough to induce an additional term in (4.36) which is proportional to $\sqrt{\mathcal{E}}$ and is a peculiarity of our case. Also one may notice that because of small deviation from circularity k and s of the manifolds we consider, the dipole matrix elements which are responsible for state mixing in case of the normal Stark effect (those between states with the same principal n), within our approximation of noninteracting manifolds can be totally

neglected which also confirms that the nature of our dressed states is very different then the normal Stark states.

4.7 Corrections by small detuning and quantum defect

Within this section we will discuss a modification of our nonlinear theory in the case where the resonant condition $\omega = 1/n_0^3$ is not strictly satisfied [30]. This may obviously happen since n_0 is an integer. We will incorporate also the case when the hydrogen atom is replaced by another atom with an active single electron, for example by sodium. This is important since atoms other than hydrogen are more feasible from the experimental point of view.

When the single electron potential of the atom differs from the Coulombic $1/r$ potential the energies of the atom no longer are described by the Rydberg series. When the potential remains spherical the angular momentum quantum numbers l and m still remain a good quantum numbers however the energies become l dependent. The energies may be written as

$$E_{nl} = -\frac{1}{2(n - \delta_l)^2}. \quad (4.52)$$

The l dependent parameter δ_l which represents the deviation of the spectrum from being hydrogenic is called the quantum defect [14] and can be found within the quantum defect theory [56] from the phase shift of a radial part of single electron wave function. It may also be found directly from an experiment from the deviation of the transitions from the Rydberg series. For large angular momenta this correction is small, however as we will show, the generation of certain dressed eigenstates of our system is very sensitive to the resonance condition and even small corrections to this condition may be significant. Since the quantum numbers

n , l and m are preserved even when the hydrogenic l degeneracy is removed we still can divide the eigenstates into the manifolds $\{s, k\}$ described in Section 4.2. Since for the large angular momenta the radial wave functions do not deviate much from hydrogenic as they do not penetrate the core region where the deviation of the potential from $1/r$ dependence is the largest [14], we can assume the same conditions for smallness and magnitudes of the matrix elements. We also assume $\delta_l = \delta$ as a constant analogically to previous assumption about all nonnegligible matrix elements. Since δ is small we can now expand $E_n = E_{nl}$ around fixed n_0 with respect to $\delta n - \delta$

$$E_n = -\frac{1}{2n_0^2} + \omega_c(\delta n - \delta) - \frac{3}{2} \frac{(\delta n - \delta)^2}{r_0^2}, \quad (4.53)$$

where we keep the definition $\omega_c = 1/n_0^3$. Note that because we allow any ω and also because of the presence of the quantum defect δ the term linear in δn no longer vanishes. To be as close as possible to the resonant case we define n_0 through the generalized detuning

$$\Delta = \omega_c - \omega + 3\frac{\delta}{r_0^2} \quad (4.54)$$

as near resonant, such that Δ is the smallest possible for all n_0 .

In the pure hydrogenic case for $\delta = 0$, Δ represents just normal detuning between the frequency of the external field and the closest near-resonant Kepler frequency. The definition of Δ implies

$$|\Delta| < \frac{1}{2} \left\{ \frac{1}{n_0^3} - \frac{1}{(n_0 + 1)^3} \right\} \approx \frac{1}{2} \left\{ \frac{1}{(n_0 - 1)^3} - \frac{1}{n_0^3} \right\} \approx \frac{3}{2r_0^2} \quad (4.55)$$

The presence of the term linear in δn modifies the equation (4.26) for the generating function f to

$$\begin{aligned} \left[\frac{3}{2} \frac{1}{r_0^2} \frac{\partial^2}{\partial \phi^2} - i\Delta \frac{\partial}{\partial \phi} + \mathcal{E} r_0 \cos \phi \right] f &= [E^j(\mathcal{E}, \Delta) - E_{n_0} + \frac{3}{2} \frac{\delta^2}{r_0^2} - \omega_c \delta \\ &+ (n_0 - k - s)\omega] f \end{aligned} \quad (4.56)$$

which upon the substitution $\tilde{f} = e^{-i\kappa\phi} f$, $\kappa = \Delta^2 r_0^2/3$ reduces to the previous form

$$\begin{aligned} \left[\frac{3}{2} \frac{1}{r_0^2} \frac{\partial^2}{\partial \phi^2} + \mathcal{E} r_0 \cos \phi - \frac{1}{6} \Delta^2 r_0^2 \right] \tilde{f} &= [E^j(\mathcal{E}, \Delta) - E_{n_0} + \frac{3}{2} \frac{\delta^2}{r_0^2} - \omega_c \delta \\ &+ (n_0 - k - s)\omega] \tilde{f} \equiv \tilde{E}^j(\mathcal{E}, \Delta) \tilde{f} \end{aligned} \quad (4.57)$$

Equation (4.57) however now can be considered as the Schrödinger equation for the one dimensional solid [57], rather than a quantum pendulum since the function \tilde{f} is no longer periodic since the function f must be 2π -periodic and κ is noninteger. Nonperiodic solutions of the equation (4.57) are fractional Mathieu functions [47] and they are also Bloch functions for the one dimensional solid with harmonic periodic potential [57]. The correction to the energies can be found using known results for the one dimensional solid or the Josephson junction [21]. Using the notation of Josephson junction we define the critical energy

$$E_C = \frac{3}{8r_0^2} \quad (4.58)$$

and

$$E_J = \mathcal{E} r_0 \quad (4.59)$$

In a weak-binding limit $E_J \ll E_C$ [65] we obtain

$$\tilde{E}^j(\mathcal{E}, \Delta) = \tilde{E}^j(\mathcal{E}, 0) \pm j\Delta - \frac{\Delta^2 r_0^2}{6} \quad (4.60)$$

In the tight-binding limit $E_J \ll E_C$ we obtain sinusoidal bands

$$\begin{aligned} \tilde{E}^j(\mathcal{E}, \Delta) &= \tilde{E}^j(\mathcal{E}, 0) \\ &- \frac{1}{2} (-1)^j \frac{2^{1/2}}{\pi} E_C \frac{E_J}{2E_Q} \frac{j/2+3/4}{j!} 2^{4s+5} \exp[-(8E_J/E_C)] \\ &\times [\cos(2\pi\kappa) - 1] \end{aligned} \quad (4.61)$$

In the tight-binding limit we get the approximation for the pseudo ground state wave function \tilde{f} as

$$\tilde{f}(\phi) = \sum_n g_0(\phi - 2\pi n) e^{i2\pi n \kappa}, \quad (4.62)$$

where

$$g_0(\phi) = e^{-\beta(\omega/2)r_0^2\phi^2} \quad (4.63)$$

is the ground state of the harmonic oscillator obtained by the expansion of the $\cos \phi$ up to second order in ϕ (Section 4.2). The generating function f is the periodic part of the tight-binding Bloch function (Wannier function) with the Bloch vector $-\kappa$

$$f(\phi) = \sum_n g_0(\phi - 2\pi n) e^{i(\phi - 2\pi n)\kappa}. \quad (4.64)$$

The pseudo ground state wave function in the approximation leading to (4.42) is now

$$\begin{aligned} \Psi_{jks}(\tau, \theta, \phi) &= N e^{i(n_0-1)\phi} e^{-\frac{\omega}{2}(r-r_0)^2} e^{-\frac{\omega}{2}r_0^2\theta^2} \\ &\times \sum_{\nu} e^{-\beta\frac{\omega}{2}r_0^2(\phi-2\pi\nu)^2} e^{i(\phi-2\pi\nu)\kappa}. \end{aligned} \quad (4.65)$$

For the larger field strength g_0 is well localized so only the term with $\nu = 0$ gives a significant contribution so the full wave function (4.65) is well localized and does not differ much from the resonant case. Note that for larger field strength the “bands” in the parameters Δ , $E^j(\mathcal{E}, \Delta)$ are almost equally spaced since the band width is exponentially decaying. This is consistent with the result from the harmonic approximations in Chapter 3 where no discrete parameter appears. This can be understood since in the resonant case $\Delta = 0$ discussed in the previous section the condition (4.43) for good quality of the harmonic approximation implies automatically the tight-binding condition $E_J > E_C$ which translated in the scaled field is just

$$\mathcal{E}_{sc} \gg \frac{3}{8n_0^2} \quad (4.66)$$

This condition also implies that for strong fields $\mathcal{E}_{sc} > 0.01$ the energies and states are well described within the tight-binding approximation since we expect our nonlinear theory to be valid for the lowest states for $n_0 > 10$.

Chapter 5

Importance of Localized States and Numerical Confirmations

5.1 Trojan wavepackets

The common prediction of both the harmonic approximations from Chapter 3 and the nonlinear theory from Chapter 4 is that the algebraically simplest eigenfunction of the rotating frame hamiltonian (2.29) is a Gaussian, well-localized wave function as given by the formulas (3.47), (3.58) and (4.39). Within the harmonic approximation this state has the highest energy for $m_+ = m_0 = 0$, i.e., the one with $m_- = 0$. Within the nonlinear theory this is the highest energy eigenstate spanned by the manifold $s = 1, k = 0$ of circular states. In the laboratory frame it represents a well localized wave packet moving around the classical circular orbit without changing the shape. The harmonic approximation within nonlinear Mathieu theory (4.39) through the unitary transformation to the laboratory frame (2.33) gives the time dependent solution

$$\begin{aligned} \Psi_{010}(r, \theta, \phi; t) = & N e^{-iE_{010}t} e^{i(n_0-1)(\phi-\omega t)} e^{-\frac{\omega}{2}(r-r_0)^2} e^{-\frac{\omega}{2}r_0^2\theta^2} \\ & \times e^{-\beta\frac{\omega}{2}r_0^2(\phi-\omega t)^2}, \end{aligned} \quad (5.1)$$

The expectation values of the coordinates and momenta

$$\begin{aligned} \langle r \rangle & \approx r_c \\ \langle p_r \rangle & \approx 0 \\ \langle \phi \rangle & \approx \omega t \\ \langle L_z \rangle & \approx \omega r_c^2 \end{aligned} \quad (5.2)$$

are approximately equal to its corresponding classical values. Therefore the packet is obeying Newtonian dynamics and from this aspect is the cardinal example of the quantum versus classical correspondence. The essential point is that this state does not change its semi-classical character with time since the packet remains shape-invariant.

The search for this kind of quantum state for hydrogen without any external field has a long history. Schrödinger and Lorentz sought to construct such a state from wave mechanics without success [58]. The reason why it is not possible to construct a quantum state for the hydrogen atom which follows a classical trajectory for the arbitrary long time is the nonlinearity of the Coulomb spectrum, which is also the source of the negative and fractional electron mass in the equation (4.26). The approximate time evolution of the state $\Psi_{010}(r, \theta, \phi; 0)$ in the hydrogen atom was found in early searches for wave packets moving on the circular orbits [19]

$$e^{-iH_0t}\Psi_{010}(r, \theta, \phi; 0) = Ne^{-iE_{n_0}t}e^{i(n_0-1)\phi}e^{-\frac{\omega}{2}(r-r_0)^2}e^{-\frac{\omega}{2}r_0^2\theta^2} \\ \times \exp\left[\frac{-(\phi - \omega t)^2}{2\sigma_\phi^2 - \frac{6i\omega t}{l_0}}\right], \quad (5.3)$$

with $\sigma_\phi = 1/r_0\sqrt{\beta\omega}$. This is a Gaussian wave packet moving around a classical circular orbit and spreading angularly three times faster than a free wave function of a one dimensional particle with the same mass. This acceleration of spreading compared to the free particle case can be explained as a direct consequence of the fractional mass in (4.26). Formula (5.3) also describes the situation when the hydrogen atom was originally in the pseudo ground state but the external field has been abruptly turned off, and shows the importance of the external field for the suppression of spreading. The result (5.3) is valid only for $t < T_c \approx Tn^{1/2}/3\beta^{1/2}$, where $T = 2\pi/\omega$. After T_c the packet spreads so much that it covers the 2π angle.

For larger times it undergoes fractional revivals [59] - it splits into smaller packets which are similar to the one at $t = 0$ and approximately recovers completely after a full revival time $T_R \approx T n_0/3$. This time evolution does not correspond to any single classical trajectory and from this aspect is purely quantum mechanical.

Another interesting aspect of the states (3.47), (3.58), (4.39) is that they are the direct quantum analogs of so-called Trojan asteroids, two cluster of asteroids orbiting the sun near the stable Lagrange points denoted L_4 and L_5 of the sun-Jupiter system [44]. That is why they have been called Trojan wavepackets. Lagrange points L_1, \dots, L_5 are the points of equilibrium in the restricted three-body problem of celestial mechanics at which the centrifugal forces are exactly balanced by the gravitational attraction of the two orbiting bodies (Fig. 5.1). These points have fixed positions in the coordinate frame co-rotating with the two bodies around their center of mass. Around the each Lagrange point the motion of the particle can be derived from the hamiltonian of the rotating extremum (3.1) discussed in Section 3.1. The three collinear points lying on the line connecting the centers of the two bodies are unstable. The two equilateral points, lying on the vertices of two equilateral triangles based on the line segment connecting the centers of the bodies are stable if the mass ratio $\mu = m_2/(m_1 + m_2)$ satisfies the condition $\mu(1 - \mu) < 1/27$. The coefficients a and b in the celestial case depend only on the coefficient μ

$$a(\mu) = -\sqrt{1 - 3\mu(1 - \mu)}/2 - 1/2, \quad (5.4)$$

$$b(\mu) = +\sqrt{1 - 3\mu(1 - \mu)}/2 - 1/2, \quad (5.5)$$

so they that are constrained to the line $a+b = -1$ and they belong to the stability island in Fig. (3.1) if one of the masses is very small compared to the other mass, $\mu < 1/2 - \sqrt{23/108} = 0.03852$, or, $\mu > 1/2 + \sqrt{23/108} = 0.96148$. The mass

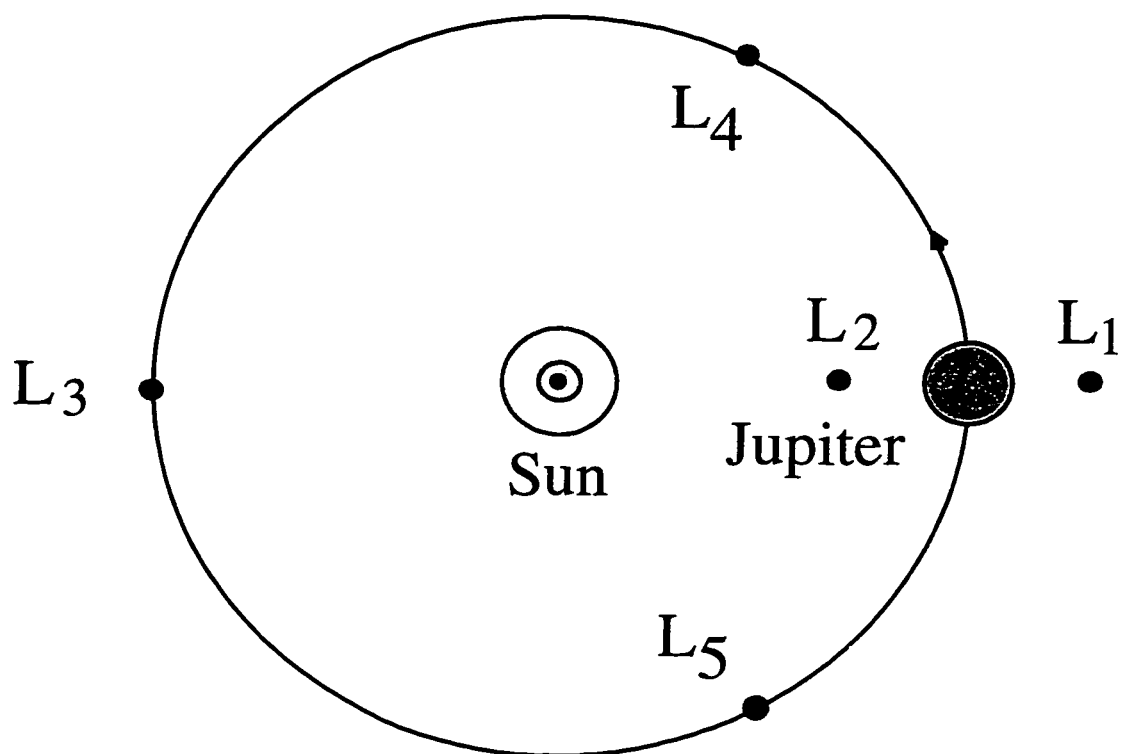


Fig. 5.1. Lagrange equilibrium points in celestial mechanics. The collinear points L_1 , L_2 and L_3 are always unstable. The equilateral points L_4 and L_5 are stable for $\mu(1 - \mu) < 1/27$ and they are the points of accumulation of Trojan asteroids in the sun-Jupiter system.

of Jupiter, slightly less than one-thousandth of the solar mass, meets the first criterion and the two clusters of Trojan asteroids undergo stable oscillations in the rotating frame with the frequencies $\omega_+ = 2\pi/147.4\text{yr}$ and $\omega_- = 2\pi/11.9\text{yr}$. Jupiter in this case is the source of a time dependent gravitational field in full analogy to the external C.P. field while the Sun as the source of an attractive gravitational force corresponds to the heavy hydrogenic nucleus.

We have confirmed the presence of Trojan wave packets in two dimensional grid simulations by solving the time dependent Schrödinger equation in the laboratory frame using so-called split-operator method [44]. The initial wave function was chosen in the form (3.47) for $\omega = 1/60^3$ and $q = 0.9562$ corresponding to best confinement in the y direction (maximum of the coefficient $A(q)$) and we obtained modest agreement with the harmonic approximation. In Fig. 5.2 we show snapshots of packet probability contour lines at various values of time.

A great improvement in shape stability (Fig. 5.3) is achieved using the corrected harmonic approximation in cylindrical coordinates with the wave function (3.63) used for the initial condition with the parameters A , B and C obtained from the numerical solution of the nonlinear system of equations (3.65), (3.68). In order to make our observations quantitative, we monitored the total probability $P(t)$ inside a circle with radius approximately twice the radius of the corresponding classical orbit. It is given by the function

$$P(t) = \int \int \Phi^*(r, \phi; t) \Phi(r, \phi; t) r dr d\phi, \quad (5.6)$$

for the area of integration is restricted to this circle, with $\Phi(r, \phi; t)$ our numerical solution. Fig. 5.4 shows a negligible rate of ionization (probability of ionization ≈ 0.0007 per cycle, averaged over the first 10 cycles). We have also made test of the approximation (3.63) by calculating the correlation function $C(t)$ between the

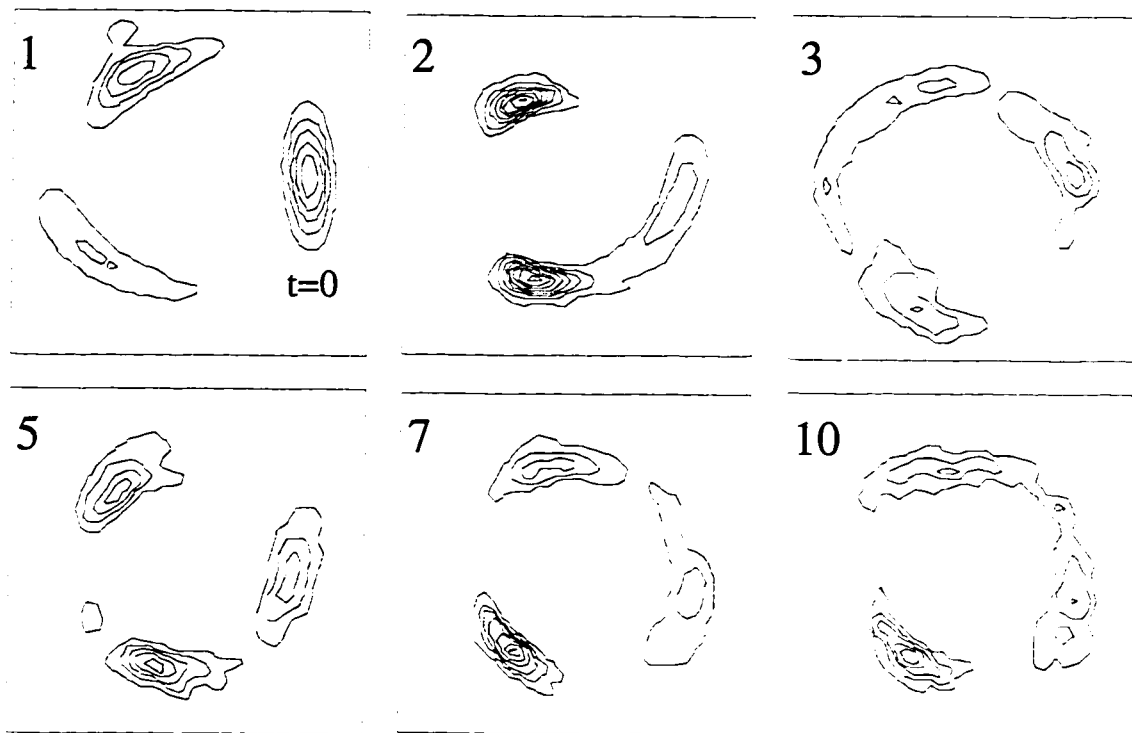


Fig. 5.2. Time evolution of the wave packet in the laboratory frame prepared at $t = 0$ according to (3.47) for $\omega = 1/60^3$ and $q = 0.9562$, i.e., for the maximum of $A(q)$. Snapshots of the contour lines of the probability distribution are taken three times per cycle for the cycles 1, 2, 3, 5, 7, and 10. Each square covers the space region of the size 11250×11250 atomic units.

approximate and numerical solutions defined as

$$C(t) = \left| \int \int \Phi^*(r, \phi; t) \Psi(r, \phi; t) r dr d\phi \right|, \quad (5.7)$$

where $\Psi(r, \phi; t)$ is the approximate solution given by (3.63). Values of C near to 1, as in Fig. 5.5, indicate excellent agreement between theoretically predicted and numerically generated functions for angular momentum of the packet as low as $l_0 = 60$.

We have also compared various approximations for even lower angular momenta. Figs. 5.6 and 5.7 show contour plots of two dimensional versions of Trojan wavepacket intensity (electron probability density) obtained from various approximations for the scaled field $\mathcal{E}_{sc} = 0.016$ for $n_0 = 10$ and $n_0 = 20$. Plots (a) show the result of the harmonic approximation discussed in Section 3.2. In plots (b) we show Trojan packets obtained from the modified Gaussian approximation given by formula (3.63). Results of the Mathieu function approach and the aligned states expansion (Section 4.2) are shown in plots (c) and (d). One can see that the difference increases when the value of n_0 decreases, but qualitatively all approaches give the same result. One expects the wave function obtained from the plain harmonic approximation to be the least accurate, since it significantly violates periodic boundary conditions for this value of the field.

5.2 Anti-Trojan wavepackets

The classical dynamics predicts the existence of two circular trajectories (2.21) with the motion shifted in phase by π which are equivalent to one stable and one unstable fixed point in the rotating frame. Since the stable point is capable to support Trojan packet discussed in the previous section, the natural question raises if there are special quantum states associated with the unstable point. No

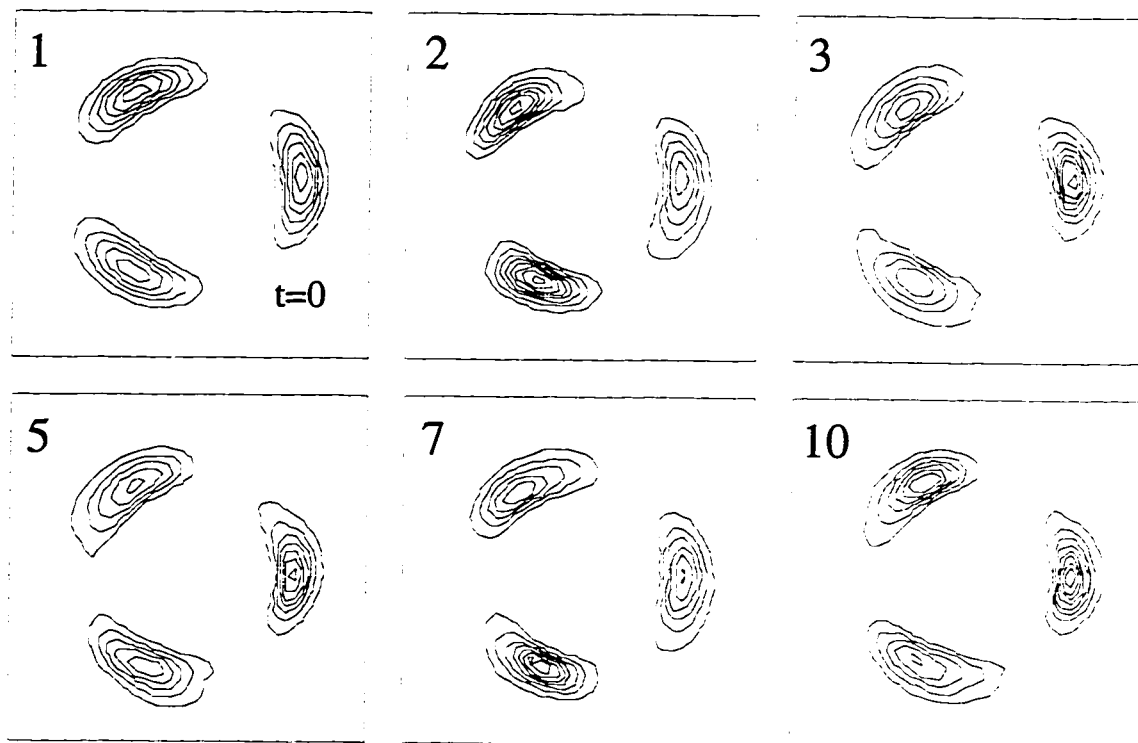


Fig. 5.3. Time evolution of the wave packet in the laboratory frame prepared at $t = 0$ according to (3.63) for $l_0 = 60$, $\omega = 1.09/60^3$ and $\mathcal{E}_{sc} = 0.050$, i.e., for the maximum of A obtained numerically from the modified Gaussian approximation. Snapshots of the contour lines of the probability distribution are taken three times per cycle for the cycles 1, 2, 3, 5, 7, and 10. Each square covers the space region of the size 11250×11250 atomic units.

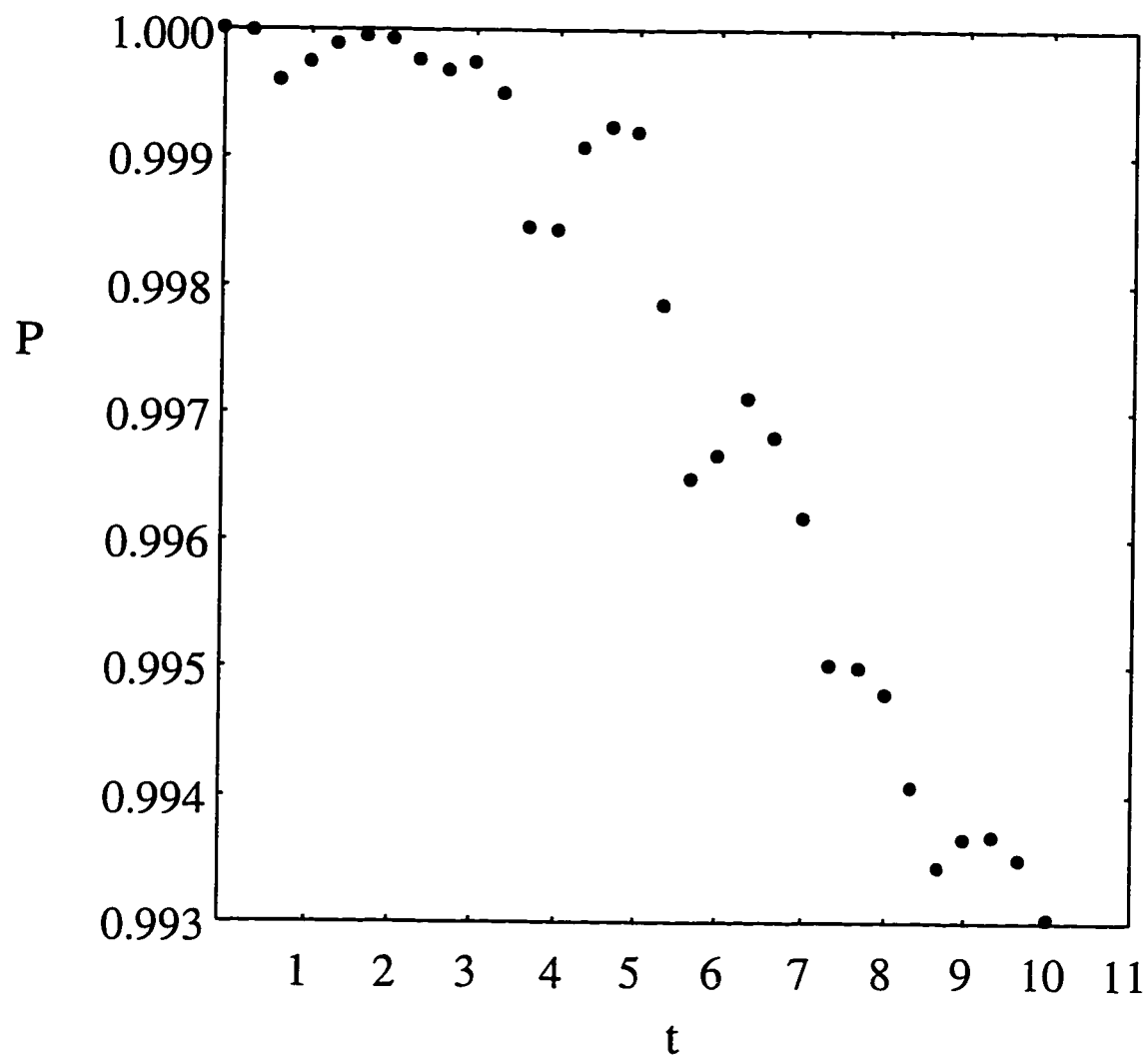


Fig. 5.4. Values of $P(t)$, the total probability inside the circle with radius approximately twice the radius of the classical orbit for the time evolution plotted in Fig. 5.3.

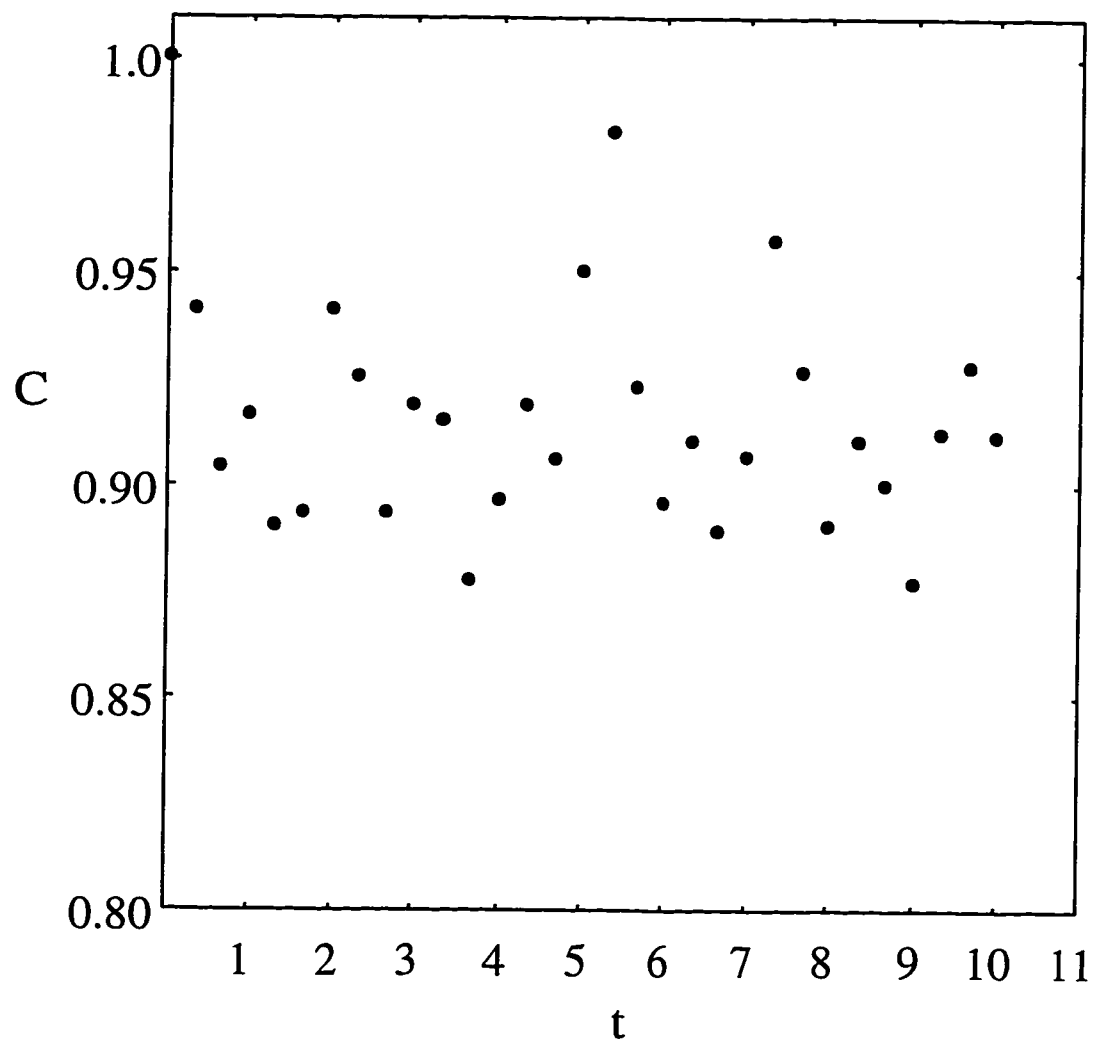


Fig. 5.5. Values of the correlation function $C(t)$, defined in (5.7) as the absolute value of the scalar product between the theoretical and numerical solutions for the time evolution plotted in Fig. 5.4.

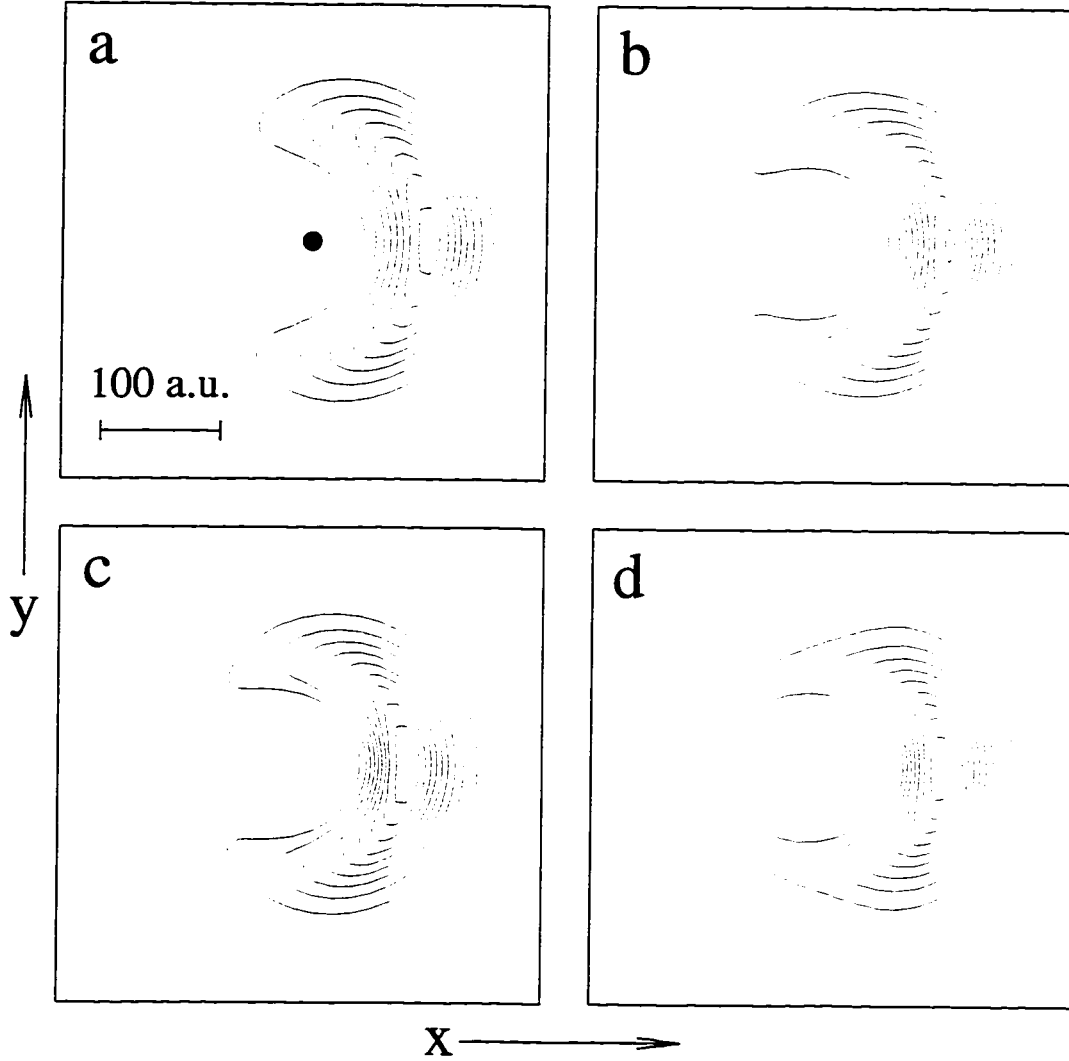


Fig. 5.6. Trojan wave packet for $\mathcal{E}_{sc} = 0.016$ and $\omega = 1/10^3$ obtained from (a) harmonic approximation from formula (3.58), (b) modified Gaussian approximation given by (3.63), (c) Mathieu functions approach from expression (4.37), and (d) the numerical solution in the aligned states basis (4.9). Functions (c) and (d) correspond to the two large points on the energy diagrams in Figs. 4.7 and 4.9. The black dot in the center indicates the position of the nucleus ($x = y = 0$).

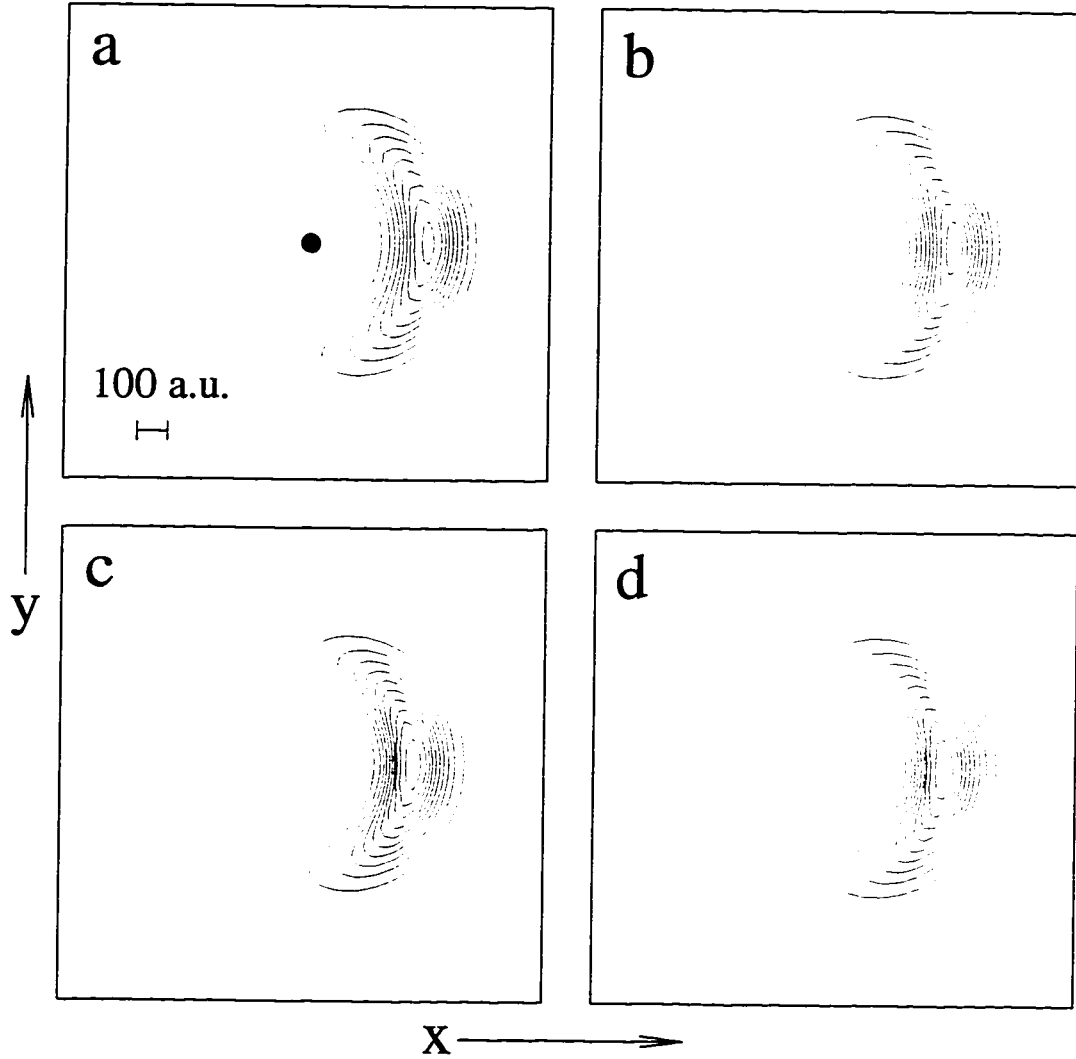


Fig. 5.7. Trojan wave packet for $\mathcal{E}_{sc} = 0.016$ and $\omega = 1/20^3$ obtained from (a) harmonic approximation from formula (3.58), (b) modified Gaussian approximation given by (3.63), (c) Mathieu functions approach from expression (4.37), and (d) the numerical solution in the aligned states basis (4.9). Functions (c) and (d) correspond to the two large points on the energy diagrams in Figs. 4.8 and 4.10. The black dot in the center indicates the position of the nucleus ($x = y = 0$).

harmonic approximation can give the answer to this question, however the non-linear theory presented in Chapter 4 does. The point is that for the quantum pendulum the localization of the wave function occurs not only around $\phi = 0$ but also $\phi = \pi$. The first point of state localization is the Trojan stable point at $\mathbf{r} = [n_0^2, \phi = 0]$, and localization there corresponds to the *highest* excited state of the effective pendular hamiltonian defined by the Schrödinger equation (4.26) for the generating function f

$$H_{EFF} = \frac{3}{2} \frac{1}{r_0^2} \frac{\partial^2}{\partial \phi^2} + \mathcal{E} r_0 \cos \phi, \quad (5.8)$$

(recall the negative effective mass).

The second localization point is of a different character. It is predicted by our pendulum theory to be located opposite the first point, at $\mathbf{r} = [m_0^2, \phi = \pi]$. State localization around the second point cannot be explained on the basis of classical mechanics. It is an example of probability density enhancement of certain eigenstates around classically unstable orbits called the quantum scar effect, known from the properties of quantum systems that are classically chaotic [60]. A local maximum in the density of levels is an imprint of localization of the eigenstate with the corresponding energy, around the trajectory in question [60]. As Fig. 4.1 shows, there is a fold or kink around the energy line $\kappa = -r_0 \mathcal{E}$ ($\alpha = 2p$). This corresponds to the separatrix in pendulum phase space and shows a larger density of levels in the vicinity of this energy. This partly heuristic arguments can also be checked directly from the properties of the symmetric Mathieu function $e_{2j}(\xi)$ [47]. The localization property can be seen from the approximate form of the Mathieu function [47] given by

$$e_{2i}(\xi) \approx \frac{C}{(\alpha_j - 2p \cos 2\xi)^{\frac{1}{4}}} \cos[(\alpha_j + 2q)^{\frac{1}{2}} E_1(\gamma, \xi)], \quad (5.9)$$

where C is a constant and $E_1(\gamma, \xi)$ is the incomplete elliptic integral of the first kind. It exhibits combined amplitude and frequency modulation [47] and the amplitude factor peaks around $\xi = 0$ in the strongest way when $\alpha_j \approx 2p$. In the laboratory the corresponding wave function describes a non-spreading wave packet moving around the nucleus on the circle $r_0 = n_0^2$ located 180° in phase advance with respect to the corresponding Trojan wave packet. We called those states “anti-Trojan” states because the theory indicates that they should be found exactly opposite each Trojan on its orbit. Note that anti-Trojan wave packets do not belong to a single energy line but to different lines close to the spectrum folding around $\alpha = 2p$.

The interval of field strengths for which the Trojan (stable-point-related) packet exists has been expressed in terms of the scaled field $\mathcal{E}_{sc} < 2/9^{4/3} \approx 0.1068$. A sufficient condition can also be obtained for anti-Trojan packets using the known properties of the Mathieu functions and the asymptotic, Gaussian form of the radial part of the circular states wave functions. The Fourier coefficients a_n^j in (4.37) of the Mathieu function of the order j with the energy near the separatrix which generates anti-Trojan state peak as discrete function of n for $n \approx j$ and $n \approx -j$. Circular states $|n_0 + j, n_0 + j - 1, n_0 + j - 1\rangle$ and $|n_0 - j, n_0 - j - 1, n_0 - j - 1\rangle$ are in this case the main components of the function (4.37). Also for sufficiently large n_0 the radial part of the circular state can be approximated by a Gaussian [19]

$$R_{n_0, n_0-1}(r) \approx N e^{-(r-n_0^2)^2/2n_0^3} \quad (5.10)$$

so centered around n_0^2 and with a full width $\Delta r = 2\sqrt{2}n_0^3/2$. Moreover from (5.10) for $j \ll n_0$ two circular states $|n_0 + j, n_0 + j - 1, n_0 + j - 1\rangle$ and $|n_0 - j, n_0 - j - 1, n_0 - j - 1\rangle$ are centered approximately $\Delta r_0 = 4n_0 j$ apart. Therefore the

wave function (4.37) will exhibit also clear radial localization when

$$\Delta r_0 / \Delta r < 1 \quad (5.11)$$

i. e. two of the leading components overlap significantly. Furthermore the flat dispersion $\alpha(p)$ below the separatrix (Fig. 4.1) allows to extrapolate $\alpha^j(0) \approx \alpha^j(p) \approx 2p$ for the $\alpha^j(p)$ near separatrix. From the result (4.31) this extrapolation leads to the relation

$$\frac{3j^2}{2r_0^2} \approx r_0 \mathcal{E} \quad (5.12)$$

which together with (5.11) leads the sufficient condition for anti-Trojan localization

$$\mathcal{E}_{sc} < \mathcal{E}_{cr} \equiv 3/4n_0. \quad (5.13)$$

In contrast to the condition for the existence of Trojan packets, the anti-Trojan critical field \mathcal{E}_{cr} is not independent of n_0 . In particular the critical field vanishes when $n_0 \rightarrow \infty$, which is consistent with the quantum-mechanical nature of anti-Trojan wave packets. In Chapter 7 we present the results of numerical simulations which confirm the existence of anti-Trojan states.

Chapter 6

The Case of Linear Polarization

6.1 Corrected RWA approximation

In this chapter we discuss the extension of our theory of hydrogen in a C.P. field to the case of the linear polarization [61]. We start from the time dependent Schrödinger equation with the hamiltonian of the hydrogen atom in a linearly polarized electromagnetic field

$$H_{LP} = \frac{\nabla^2}{2} - \frac{1}{r} + \mathbf{E}(t) \cdot \mathbf{r}, \quad (6.1)$$

with the oscillating electric field $\mathbf{E}(t) = \hat{x}\mathcal{E}[e^{-i\omega t} + e^{i\omega t}]$. The Rotating Wave Approximation [11] can be done by decomposing the electric field vector $\mathbf{E}(t)$ into two circularly polarized fields rotating with opposite helicity, namely

$$\mathbf{E}(t) = \mathbf{E}_+(t) + \mathbf{E}_-(t), \quad (6.2)$$

where the corresponding components are

$$\begin{aligned} \mathbf{E}_+(t) &= \mathcal{E}[\hat{x} \cos \omega t + \hat{y} \sin \omega t], \\ \mathbf{E}_-(t) &= \mathcal{E}[\hat{x} \cos \omega t - \hat{y} \sin \omega t]. \end{aligned} \quad (6.3)$$

and neglecting one of the components, which reduces the problem the hydrogen atom in C.P. field. One should point out however that the negligence of one of the components of $\mathbf{E}(t)$ is strictly equivalent to RWA only for the states which are well described for C.P. field within our nonlinear theory from Chapter 4, i.e., those which populate only the basis states from a single $\{k, s\}$ manifold with n in the

neighborhood of n_0 , like Trojan packets. If one includes other states, for example, “counter-rotating” states with $m = -l$, fast oscillatory terms will remain even in C.P. field which can be neglected within RWA.

Therefore for each circularly polarized component of the external field, considered separately, there are solutions of the type described in Chapter 4. Obviously the relative rotational frequency between the other component of the field and the motion of the packet is equal to twice the frequency of the circular motion of the field. One can expect that this “counterrotating” term does not have a large influence on the dynamics and this is correct. In order to estimate this influence carefully it is useful to change the reference frame to one moving with the free electron in the presence of one of the two components of the field, for instance, $\mathbf{E}_-(t)$. This is just the Kramers-Henneberger (KH) frame [12] associated with this component of the field. The corresponding (KH) hamiltonian can be obtained by the superposition of unitary transformations

$$U_A = e^{i d\tilde{\alpha}_-(t)/dt \cdot \mathbf{r}}, \quad (6.4)$$

$$U_B = e^{-i\tilde{\alpha}_-(t) \cdot \nabla}, \quad (6.5)$$

as

$$\begin{aligned} H_{KH+} &= U_B U_A H U_A^\dagger U_B^\dagger = -\frac{\nabla^2}{2} - \frac{1}{|\vec{r} + \tilde{\alpha}_-(t)|} + \mathbf{E}_+(t) \cdot [\vec{r} + \tilde{\alpha}_-(t)] \quad (6.6) \\ &= -\frac{\nabla^2}{2} - \frac{1}{|\vec{r} + \tilde{\alpha}_-(t)|} + \mathbf{E}_+(t) \cdot \vec{r} + \frac{\mathcal{E}^2}{\omega^2} \cos 2\omega t, \end{aligned}$$

where $\tilde{\alpha}_-(t)$ is the trajectory of the free electron in the field $\vec{E}_-(t)$, namely $\tilde{\alpha}_-(t) = -[\mathcal{E}/\omega^2][\hat{x} \cos \omega t - \hat{y} \sin \omega t]$, which obeys the classical equation of motion for the free electron in C.P. field

$$\frac{d^2 \tilde{\alpha}_-(t)}{dt^2} = \vec{E}_-(t). \quad (6.7)$$

In the region of the space for which $|\vec{\alpha}_-(t)|/|\vec{r}| < 1$ one can use the standard multipole expansion of the time dependent K-H potential [63]. When restricted to the plane $z = 0$ and written in circular coordinates this takes the form

$$\frac{1}{|\vec{r} + \vec{\alpha}_-(t)|} = \sum_{l=0}^{\infty} \sum_{m=-l}^l (3\delta_{m,0} - 2) \frac{a^l}{r^{l+1}} \frac{(l-m)!}{(l+m)!} \times [P_l^m(0)]^2 \cos[m(\phi + \omega t)], \quad (6.8)$$

where

$$P_l^m(0) = 2^m \pi^{-1/2} \frac{\Gamma[(l+m+1)/2]}{\Gamma[(l-m+2)/2]} \cos\left[\frac{1}{2}(l+m)\pi\right] \quad (6.9)$$

and $r = |\vec{r}|$, $\alpha_0 = |\vec{\alpha}_-(t)| = |\mathcal{E}|/\omega^2$. Therefore in zero order approximation valid for $\alpha_0/r \ll 1$ one can ignore higher multipoles and take $1/|\vec{r} + \vec{\alpha}_-(t)| = 1/r$. The resulting hamiltonian becomes

$$H_{KH+} = -\frac{\nabla^2}{2} - \frac{1}{|\vec{r}|} + \vec{E}_+(t) \cdot \vec{r} + \frac{\mathcal{E}^2}{\omega^2} \cos(2\omega t), \quad (6.10)$$

which is up to the last term equal to the hamiltonian of the hydrogen atom in a circularly polarized electromagnetic field. Therefore the time dependent solution $\Psi_{KH+}(t)$ of the Schrödinger equation with the hamiltonian H_{KH+} differs from those in C.P. field only by a time dependent phase. The hamiltonian (6.10) is written in the K-H frame associated with the component $\vec{E}_-(t)$ of the field. Therefore one should not to forget to transform the wave function $\Psi_{KH+}(t)$ to the laboratory frame using U_A and U_B

$$\Psi_+(\vec{r}, t) = U_B^\dagger U_A^\dagger \Psi_{KH+}(\vec{r}, t) \quad (6.11)$$

The full wave function in the laboratory and frame is given by

$$\Psi_+(\vec{r}, t) = e^{iF_1(t)} e^{-i\alpha_0\omega r \cos(\omega t + \phi)} \Psi_{KH+}[\vec{r} - \vec{\alpha}_-(t), t], \quad (6.12)$$

with time dependent phase F_1 .

For the Trojan wave packet given within the modified harmonic approximation (3.63) in the K-H frame by

$$\begin{aligned}\Psi_{KH+}(\vec{r}, t) = & N e^{iF(t)} e^{il_0\phi} \exp\{-(l_0/2r_c^2) \\ & \times [2r_c^2 A(1 - \cos(\phi - \omega t)) + B(r - r_c)^2 \\ & + 2iCr_c(r - r_c) \sin(\phi - \omega t)]\},\end{aligned}\quad (6.13)$$

the influence of the counter rotating term is now clear. In contrast to the case when the external field is circularly polarized, the center of the wave packet moves around a trajectory which is the sum of a circular motion with the large radius r_0 and a circular motion with the small radius α_0 having the opposite helicity, which can be written parametrically

$$\begin{aligned}x(t) &= (r_0 + \alpha_0) \cos \omega t, \\ y(t) &= (r_0 - \alpha_0) \sin \omega t.\end{aligned}\quad (6.14)$$

These expressions define an ellipse with the major axis $r_0 + \alpha_0$ and minor axis $r_0 - \alpha_0$.

Obviously we can make a comparable analysis by exchanging $\vec{E}_-(t)$ and $\vec{E}_+(t)$, and can obtain a second approximate solution

$$\Psi_-(\vec{r}, t) = e^{iF(t)} e^{i\alpha_0\omega r \cos(\omega t - \phi)} \Psi_{KH-}[\vec{r} - \vec{\alpha}_+(t), t],\quad (6.15)$$

with $\vec{\alpha}_+(t) = -[\mathcal{E}/\omega^2][\hat{x} \cos \omega t + \hat{y} \sin \omega t]$ and where $\Psi_{KH-}(\vec{r}, t)$ is the corresponding solution of obtained from (3.63), which is

$$\Psi_{KH-}(\vec{r}, t) = N e^{iF_1(t)} e^{-il_0\phi} \exp\{-(l_0/2r_c^2)$$

$$\begin{aligned}
& \times [2r_c^2 A(1 - \cos(\phi + \omega t)) + B(r - r_c)^2 \\
& - 2iCr_c(r - r_c) \sin(\phi + \omega t)] \}.
\end{aligned}
\tag{6.16}$$

The second solution is just a mirror reflection of the first one with respect to the plane of the electric field polarization. It originates from the fact, that the hamiltonian (6.1) we started with is invariant under the transformation $y \rightarrow -y$.

In order to test the quality of our approximate analytic solution we have solved the time dependent Schrödinger equation numerically with the function $\Psi_+(\vec{r}, 0)$ taken for the initial condition. The parameters of the packet have been taken the same as in the former case of circular polarization discussed in Section 4.1. Fig. 6.1 shows the time evolution of the probability density calculated from this wave function. The shape stability of the packet is a little worse than in the case with circular polarization. This can be explained by the influence of the time dependent terms in the expansion (6.8). Compared to the case for C.P. field, the stable behavior of the predicted solution is disturbed mainly by the higher terms of the multipole expansion of the time dependent Coulomb potential. Those small terms lead to a small deviation of the trajectory of the wave packet from the predicted ellipse, and shape oscillation of the packet. However for the field we took, $\alpha_0/r_0 = 0.05026$ is small and therefore appropriate as a parameter of expansion.

In addition we calculated the time dependence of the total probability P inside the circle with radius equal to $2r_0$ as well as the correlation function C as defined in Section 4.2. As shown in Fig. 6.2, faster decay of P indicates a little higher rate of ionization than found for C.P. case. This increase can also be explained by the influence of the small time dependent terms which are not included in

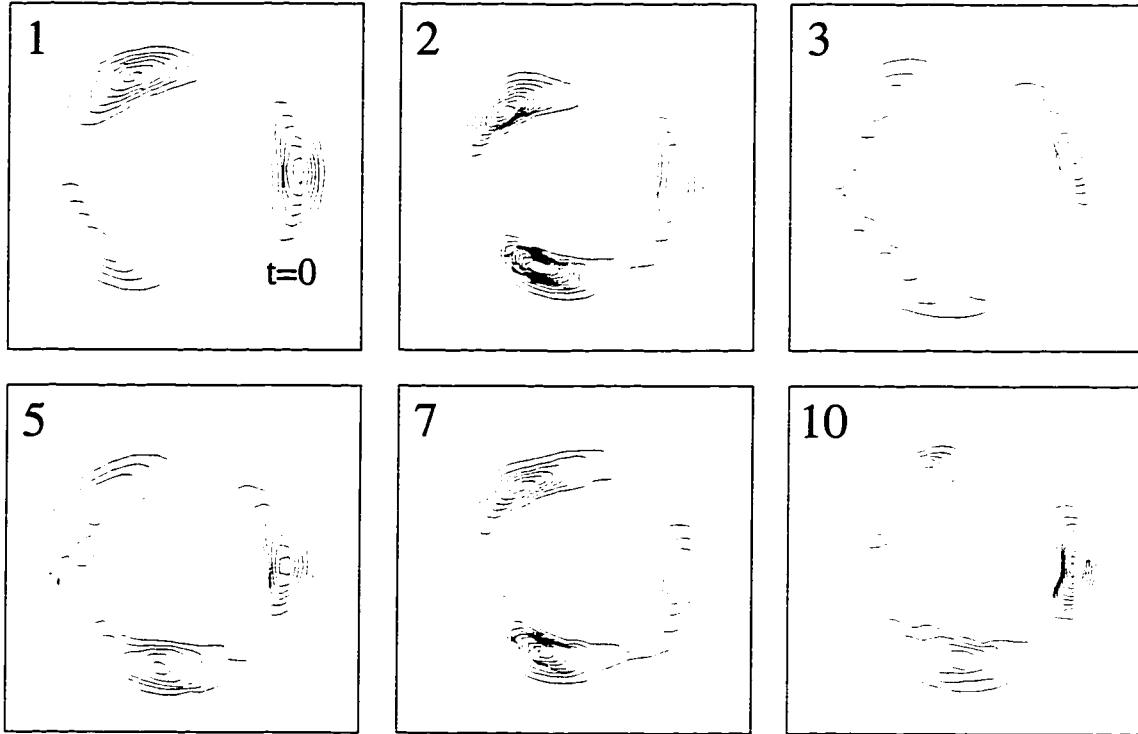


Fig. 6.1. Contour plot of the probability density for the single packet in the lab-stationary frame prepared at $t = 0$ according to the modified RWA formula (6.13) and $l_0 = 60$, $\omega = 1.09/60^3$ and $\mathcal{E}_{sc} = 0.050$. Snapshots are plotted every $1/3$ of the optical cycle for cycles number 1, 2, 3, 5, 7 and 10. Each square covers the space region of the size 11250×11250 atomic units.

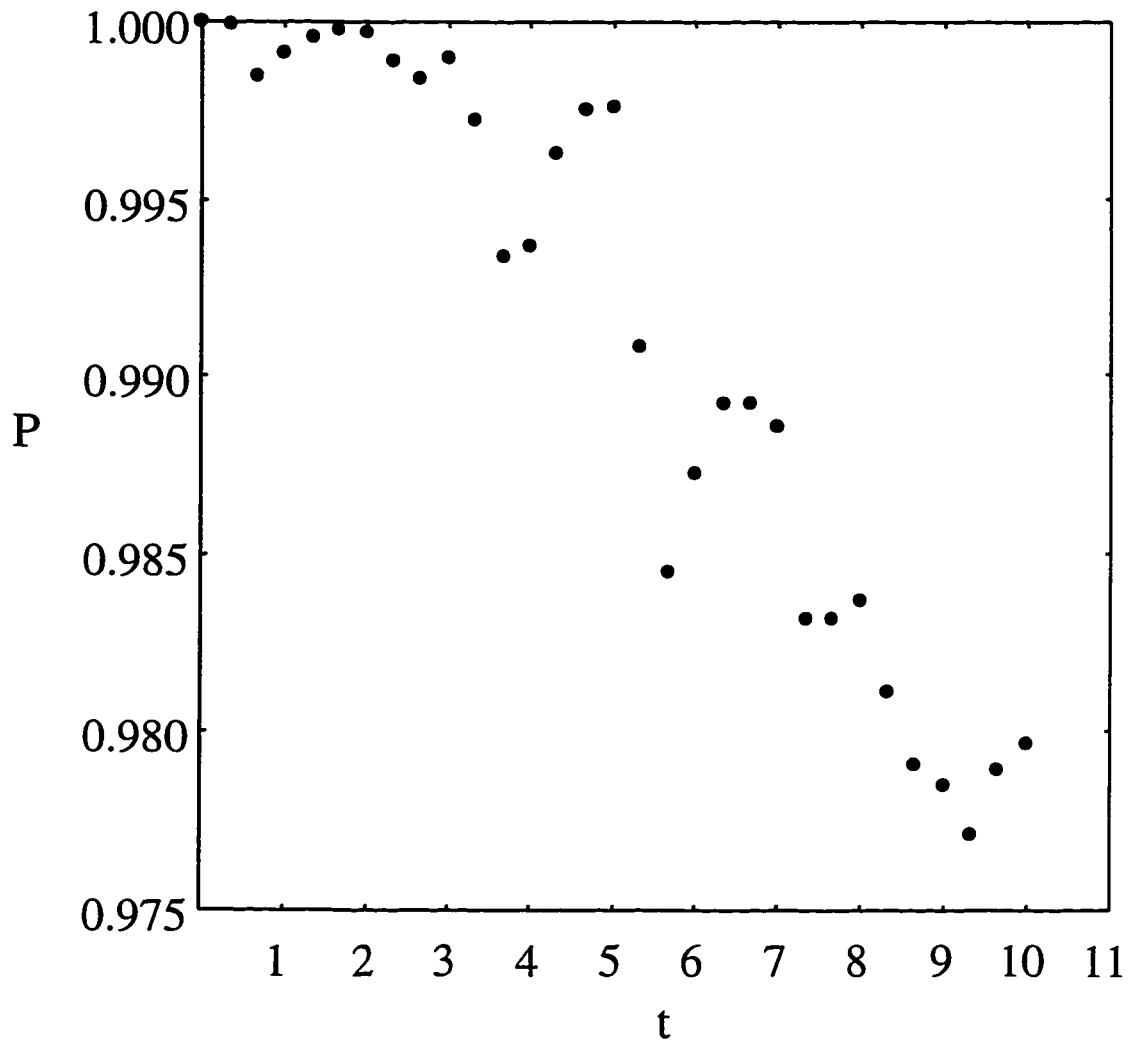


Fig. 6.2. Values of $P(t)$, the total probability inside the circle with radius approximately twice the radius of the classical orbit for the time evolution plotted in Fig. 6.1.

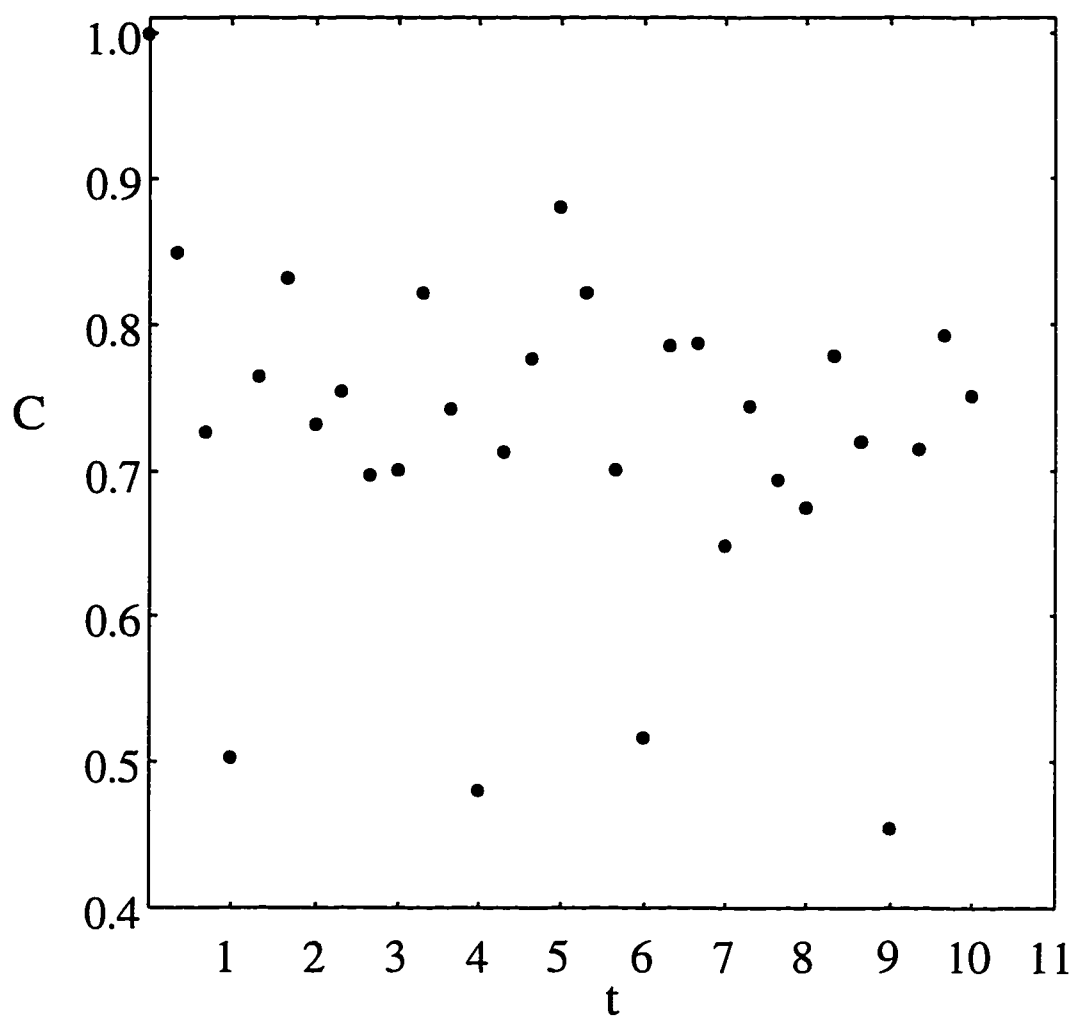


Fig. 6.3. Values of the correlation function $C(t)$, defined in (5.7) between the theoretical solution (6.13) and the numerical solution for the time evolution plotted in Fig. 6.1.

the derivation of our analytic solution. The lifetime of such a solution should be compared with the period of the orbit and in these terms the decay is still negligible.

6.2 Three-dimensional Schrödinger's cat states

The direct consequence of the linearity of the Schrödinger equation is that a coherent superposition of those states, with for example equal amplitudes

$$\Phi_{CAT}(\mathbf{r}, t) = \frac{[\Psi_-(\vec{r}, t) + \Psi_+(\vec{r}, t)]}{\sqrt{2}} \quad (6.17)$$

will also be an approximate solution of the Schrödinger equation with the hamiltonian (6.1). Both the functions $\Psi_-(\vec{r}, t)$, $\Psi_+(\vec{r}, t)$, if constructed for Trojan packets, have semiclassical character. However their coherent superposition (6.17) is a purely quantum mechanical state. The component functions are “macroscopically” distinguishable in the sense that, when considered alone, they represent well confined clouds of electron probability moving along classical orbits and therefore the superposition (6.17) can be considered as a time dependent three dimensional atomic analog of the Schrödinger cat state [62]. This coherent superposition will strongly interfere twice during one optical cycle, when the well localized components of the state “collide” and pass through each other. Fig. 6.4 shows numerical simulation of this kind of this state for $\omega = 1/20^3$, and $\mathcal{E}_{sc} = 0.016$.

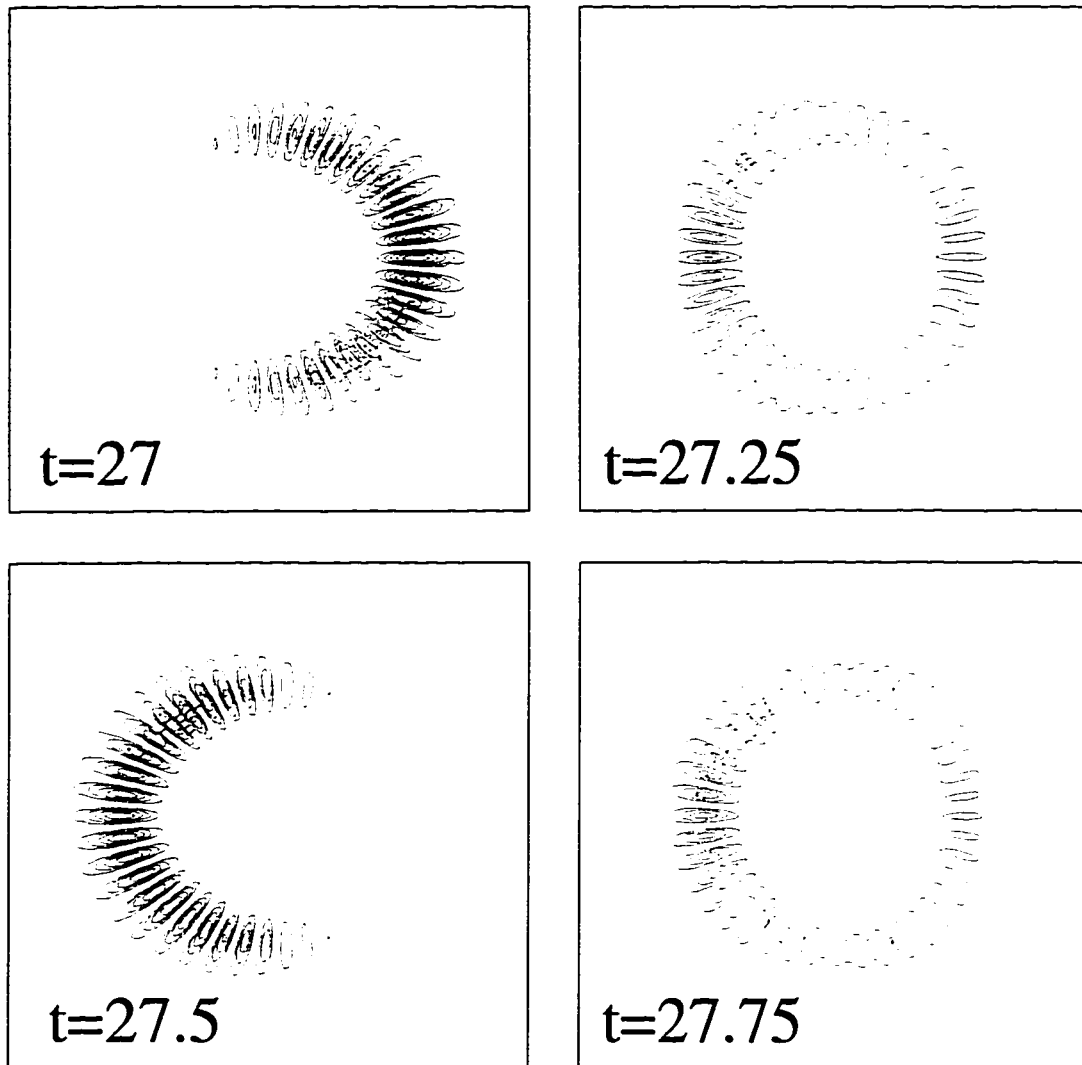


Fig. 6.4. Typical one cycle steady field ($\mathcal{E}_{sc} = 0.016$) evolution of two-packet state (6.17) ($\omega = 1/20^3$) obtained in numerical simulation. Strong interference pattern appears twice a period when the two packet components pass through each other.

Chapter 7

Application to Quantum Control

7.1 Adiabatic connection to zero-field states

The direct prediction of nonlinear theory presented in Chapter 4 is that for a fixed excitation j . The eigenvalues E^j of the rotating frame of the hamiltonian (2.29) depend continuously on the field strength \mathcal{E} . In particular in the limit $\mathcal{E} = 0$ the corresponding eigenstates correspond to hydrogenic eigenfunctions. This follows directly from the expression for the energy spectrum (4.31) and the properties of the Mathieu equation. The discrete eigenvalues $\alpha^j(p)$ and Mathieu functions [47] depend continuously on the parameter p for fixed excitation j (Fig. 4.1). Therefore the eigenstates with the same quantum numbers s and k are adiabatically connected to hydrogenic eigenstates with a fixed deviation from circularity.

Most interesting from the point of view of applications is the adiabatic connection of Trojan and anti-Trojan wave packets since the atom in those states has a well localized Rydberg electron moving around a circular orbit with controllable uncertainty of the position and the momentum. In the case when direct resonance is possible, i.e., $\Delta = 0$ and with no quantum defect $\delta = 0$ (Section 4.6), it follows directly from formula (4.31) that Trojan wave packets are adiabatically connected to circular Rydberg states with the principal quantum number n_0 , for which the Kepler frequency equals the frequency of the C.P. field:

$$\omega = \frac{1}{n_0^3}. \quad (7.1)$$

For delta $0 < |\Delta| < 3/2r_0^2$ the weak binding (4.60) predicts Trojan wave packets

to be adiabatically connected to the circular states with the closest resonant n_0 as defined in Section 4.6. For $\Delta \approx 3/2r_0^2$ the Trojan level has a weakly avoided crossing with the first deexcited level, which is adiabatically connected to the nearest circular state with $n = n_0 - 1$. In tight binding approximation (4.61) this crossing becomes strongly avoided and two neighboring Trojan packets with near resonant or resonant n_0 and $n_0 + 1$ are also adiabatically connected in the frequency domain.

In contrast to Trojan wave functions, anti-Trojan wave functions converge in the zero field limit ($p \rightarrow 0$) to hydrogenic eigenstates for which the resonant condition $\omega = 1/n^3$ is not satisfied exactly even when $\Delta = 0$. This is caused by the nonlinearity of the Coulomb spectrum, represented within our pendulum model by the kinetic energy term in the hamiltonian (5.8) which originates from the second order expansion of the hydrogenic energy around the resonant n_0 .

7.2 Three-dimensional localization of Rydberg electron

By the adiabatic theorem [55] the adiabatic connection between a Gaussian-like Trojan packet and its parent circular state implies that the approximate time dependent solution of the Schrödinger equation

$$\left[\frac{\mathbf{p}^2}{2} - \frac{1}{r} + x\mathcal{E}(t) - \omega L_z \right] \Psi(t) \equiv H(t)\Psi(t) = i \frac{d\Psi}{dt} \quad (7.2)$$

with the initial condition

$$\Psi(0) = \langle \mathbf{r} | n_0, n_0 - 1, n_0, -1 \rangle \quad (7.3)$$

can be found as

$$\Psi(t) = \Psi_{010}[\mathbf{r}, \mathcal{E}(t)] e^{iG(t)} \quad (7.4)$$

where $\Psi_{010}[\mathbf{r}, \mathcal{E}(t)]$ is a Gaussian Trojan wave packet (4.65) and $G(t)$ a time dependent phase. The approximation works fine [55] if the transition to the first deexcited Trojan state is small

$$|a_{110}| = \langle \Psi_{110} | \frac{\partial H(t)}{\partial t} | \Psi_{010} \rangle / (E_{010} - E_{110})^2 \ll 1 \quad (7.5)$$

The quantity $|a_{110}|$ estimates the population transferred to the neighboring state during a quasi adiabatic process [55]. In the low field limit and generalized detuning $\Delta = 0$ this may be estimated in terms of dimensionless variables, using the formula (7.5)

$$\left| \frac{d\mathcal{E}_{sc}}{d\tau} \right| \ll \frac{9\pi}{n_0^3}, \quad (7.6)$$

where we have introduced the scaled time $\tau = t\omega/2\pi$. For larger field in the harmonic regime we get the condition

$$\frac{1}{\mathcal{E}_{sc}(t)} \left| \frac{d\mathcal{E}_{sc}}{d\tau} \right| \ll \frac{12\pi}{n_0} \quad (7.7)$$

Note that the strong field adiabaticity condition implies that the best envelopes are exponential envelopes since the left side of inequality (7.7) is constant for the exponential $\mathcal{E}_{sc}(t)$. This is a direct consequence of the square-root dependence of the levels spacing σ given by (4.36) on the electric field.

The adiabatic condition (7.5), together with the extension of our nonlinear theory to the case with the generalized detuning in Section 4.6, also implies the importance of the direct resonance condition $\omega = 1/n_0^3$ for the quality of the Trojan packet state. It also predicts that the influence of the quantum defect in other single-electron atoms should be canceled by the frequency tuning such that $\Delta = 0$ for the best confinement of the electron. The use of the weak binding formula (4.60) in condition (7.5) implies that the quality of the packet generation

can be defined as

$$Q = 1 - |a_{110}|^2 \approx 1 - \frac{r_0^2}{(3/2r_0^2 - |\Delta|)^4} \left(\frac{d\mathcal{E}}{dt} \right)^2 \quad (7.8)$$

For a given envelope of the field this function is decreasing fast with growing Δ , which shows that the worse quality packet will be generated for the same envelope when the frequency is detuned from direct resonance.

The passage through such an avoided crossing is described by the Zener theory [64]. The probability to jump over such a crossing is given by

$$P = \exp \left[-\frac{2\pi|\varepsilon_{12}|^2}{|d[E_1(t) - E_2(t)]/dt|} \right] \quad (7.9)$$

where ε_{12} is a matrix element of the perturbation leading to the repulsion between the levels which otherwise cross directly. The matrix element ε_{12} is related to the energy gap between them, $\Delta_{12} = 2\varepsilon_{12}$, and $E_1(t)$ and $E_2(t)$ are the energies of the “repulsing” states which depend parametrically on time t .

For the Trojan energy line, we can estimate for the large fields from (4.36)

$$\left| \frac{d[E_1(t) - E_2(t)]}{dt} \right| \approx r_0 \frac{d\mathcal{E}}{dt} \quad (7.10)$$

since the linear term in \mathcal{E} is leading and other levels interact weakly with the Trojan line and are almost parallel to the field axis because of the smallness of the matrix elements directly from our theory. The later feature also allows us to estimate the interaction with those irrelevant levels, which leads to avoided crossings, as

$$\varepsilon_{12} < \frac{\mathcal{E}r_0}{10} \quad (7.11)$$

This estimate leads to the condition

$$\frac{1}{\mathcal{E}_{sc}^2} \left| \frac{d\mathcal{E}_{sc}}{dr} \right| > n_0 \frac{\pi^2}{50} \quad (7.12)$$

as a sufficient condition for diabatic passage over avoided crossings not included within our nonlinear theory. The condition (7.12), together with conditions (7.6) and (7.7), defines the adiabatic-rapid passage which is sufficient to generate Trojan packet from the resonant circular state.

We have solved the time dependent Schrödinger equation numerically with a two dimensional version of the circular state $n_0 = 20$ taken for the initial condition [45]. The frequency of the circularly polarized field was tuned to the Kepler frequency of this state, $\omega = 1/n_0^3$. The field was switched on exponentially during twenty optical cycles according to the formula $\mathcal{E}(t) = \mathcal{E}_0 e^{-0.2(t-20)}$ until the value $\mathcal{E}_0 = 0.016\omega^{4/3}$ was reached ($\mathcal{E}_{sc} = 0.016$). After the turn-on was complete we monitored an additional ten cycles of evolution with the constant value of the amplitude $\mathcal{E} = \mathcal{E}_0$. Fig. 7.1 confirms our prediction. It shows the formation of a sharply angularly localized packet during the adiabatic switching process.

To check this confirmation quantitatively, we have also calculated the correlation functions $C(t)$ and $P(t)$ as defined by (5.6) and (5.7). The predicted function (3.63) used in the correlation function had the following parameters.

$$\begin{aligned} l_0 &= 20, \\ r_c &= 388.69, \\ A &= 0.05706, \quad B = 0.71656, \quad C = -0.13860 \end{aligned} \tag{7.13}$$

The growth of the correlation function C plotted in Fig. 7.2 shows that a state with a large component of Trojan packet is actually generated. It is important to note that the probability (Fig. 7.3) of escape out of the circle $1 - P$ is negligible. This is represented by the decrease of the function P , which is shown in Fig. 7.3. We have also solved numerically the time-dependent and field-dependent Schrödinger equation for the anti-Trojan wave function [71]. We started from a

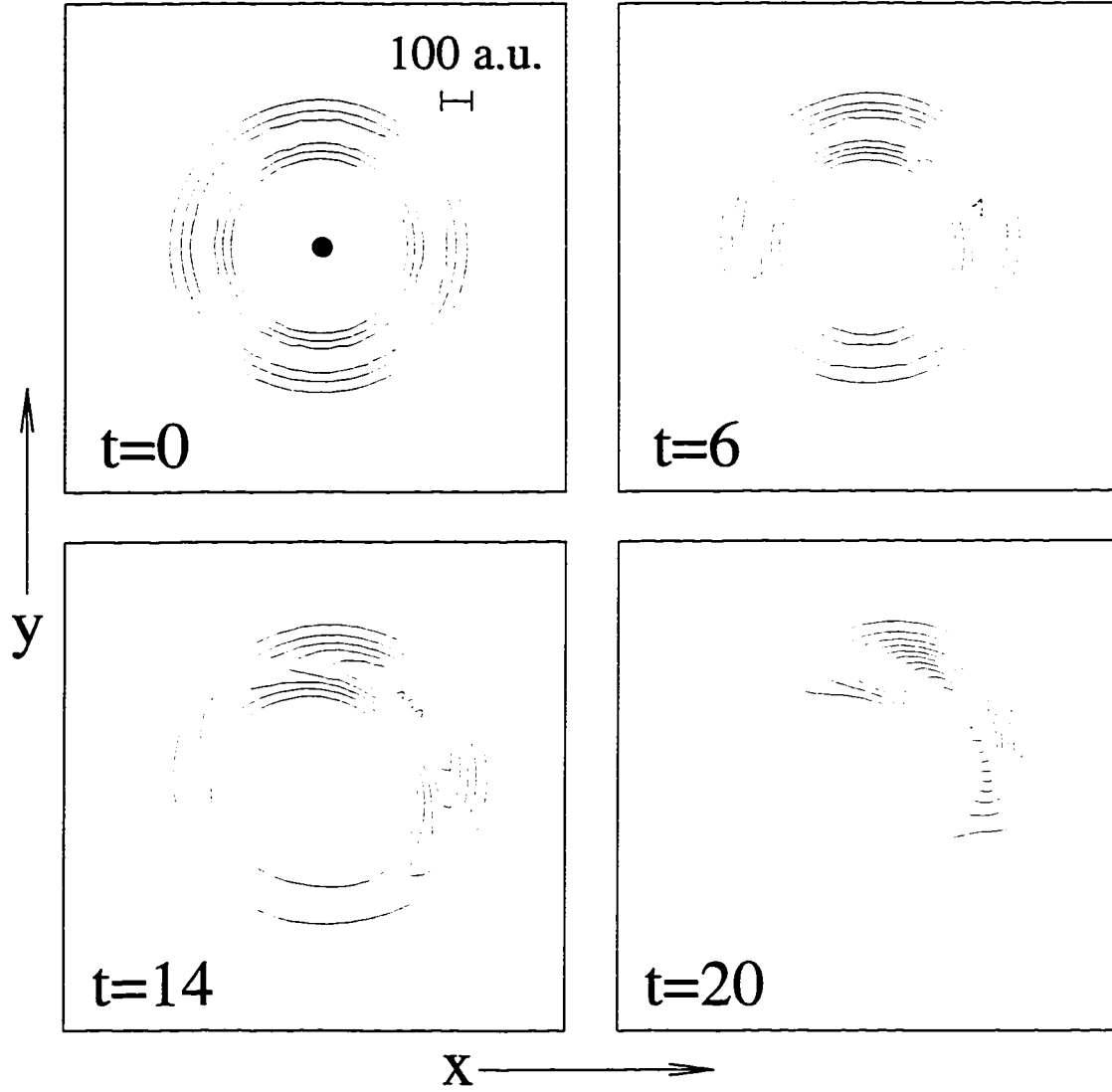


Fig. 7.1. Adiabatic angular localization of electron probability density. Snapshots of $|\Phi|^2$ at $t = 0$ and after 6, 14 and 20 cycles show increasing angular bunching during exponential switching of the field. The initial state is the circular state for $n_0 = 20$. The black dot in the center indicates the position of the nucleus ($x = y = 0$).

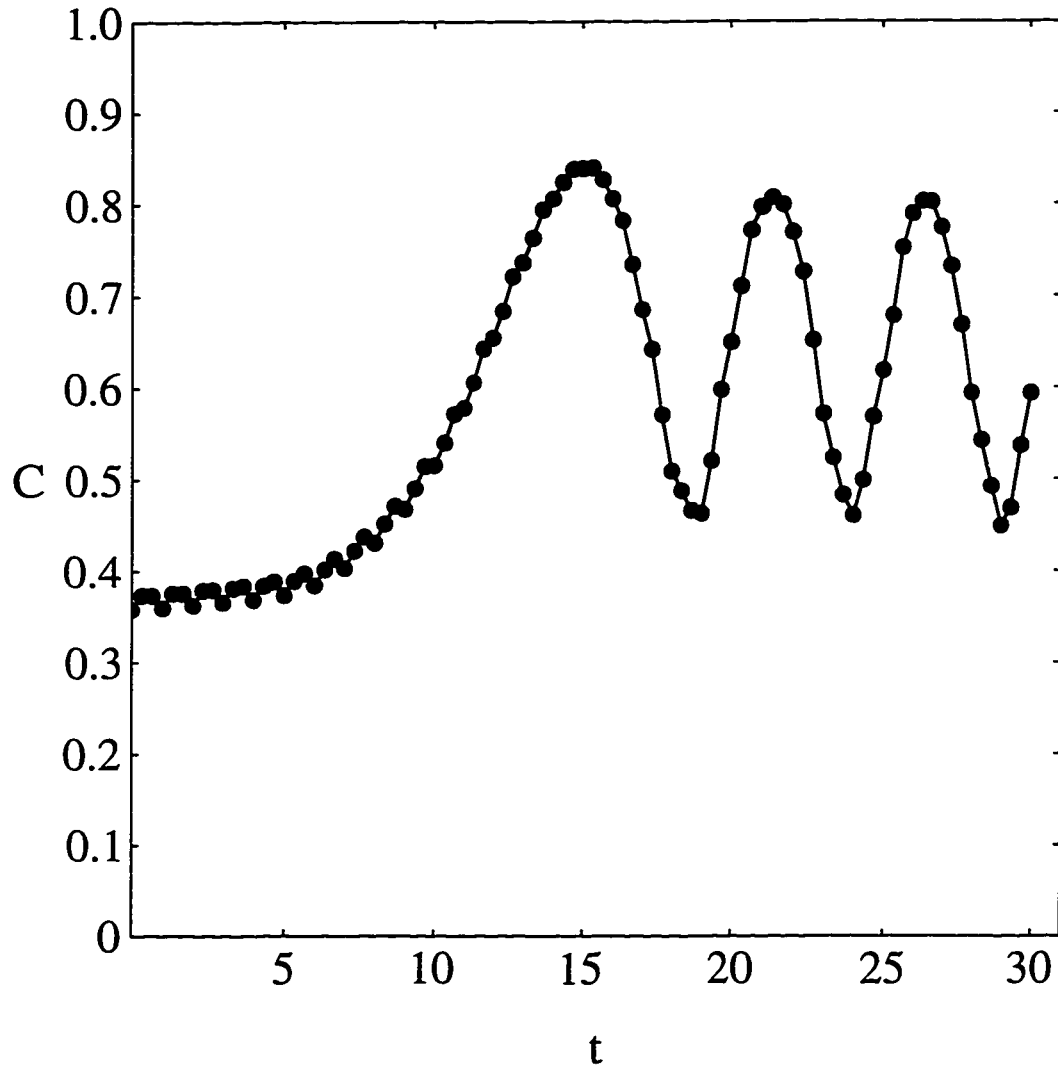


Fig. 7.2. Correlation function $C(t)$ defined in (5.7) between the numerical solution Φ and the predicted solution from the modified Gaussian approximation (3.63).

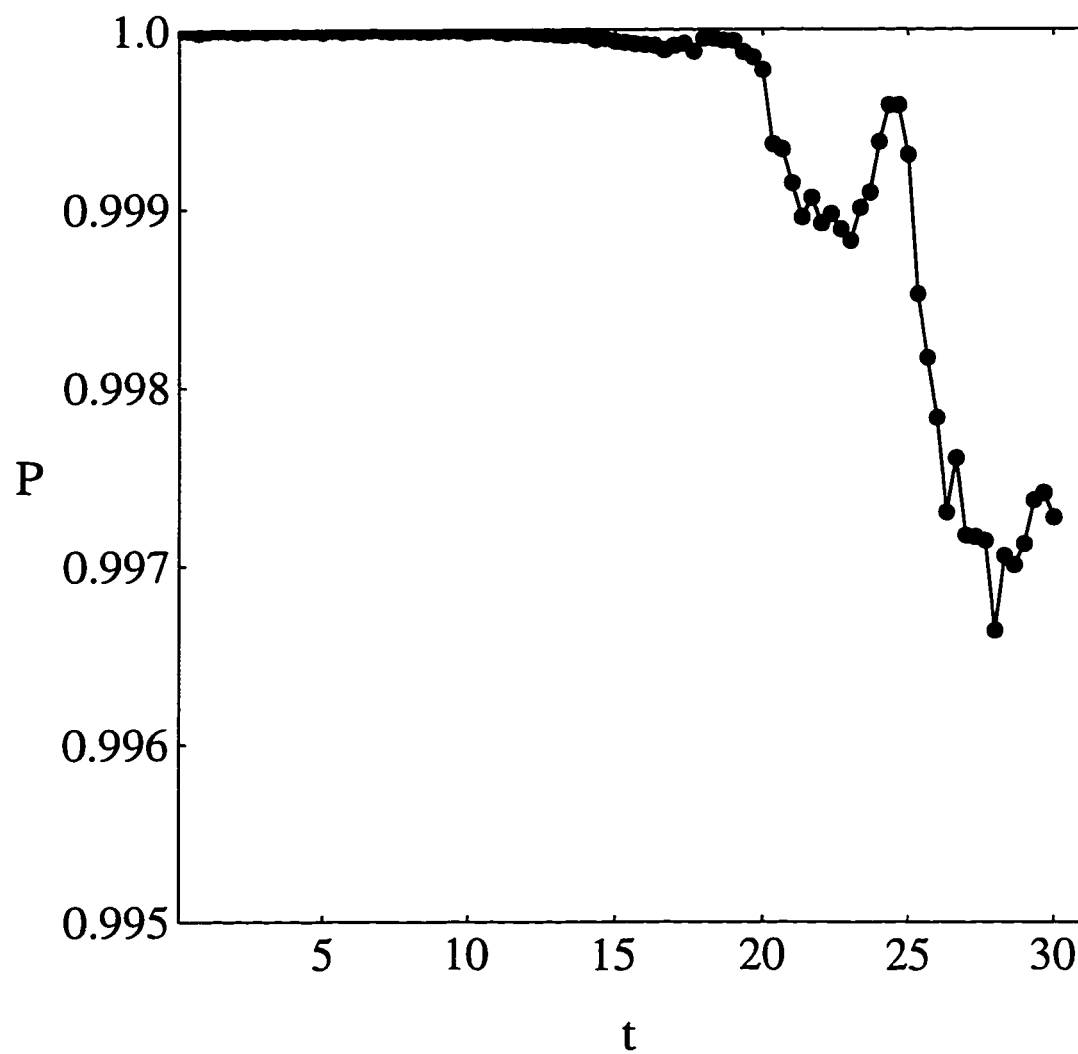


Fig. 7.3. Total electron probability $P(t)$ as defined in (5.6). The values along the P axis emphasize the negligible loss to ionization.

prepared circular state and turned on the C.P. field in a quasi-adiabatic manner for 20 C.P. field cycles and then held the C.P. amplitude constant at the value \mathcal{E}_0 for an additional 10 cycles. As in the Trojan case the frequency of the field was chosen equal to the Kepler frequency of the $n_0 = 20$ circular state.

In the anti-Trojan case we applied a field with the same frequency and $\mathcal{E}_0 = 0.0064\omega^{-4/3}$, but the initial state was the circular state with principal quantum number one atomic unit lower, i.e., $n_0 = 19$, therefore slightly out Keplerian resonance, as predicted by the theory. The field in this case also generates a packet state, shown in Fig. 7.4, which orbits around the nucleus, but the point of electron localization is shifted approximately 180° with respect to the previous case so we observe the probability density concentrated at the left side of the nucleus at the end of each cycle. Because of its non-classical stability, the anti-Trojan packet requires some weak “wings” that reach to each other around the nucleus, resulting in a characteristic “pull-tab” shape. Note that the spacing between two Kepler frequencies of two neighboring circular states is a small fraction of the driving frequency

$$\frac{1}{(n_0 - 1)^3} - \frac{1}{n_0^3} \approx \frac{3}{n_0^4} = \frac{3\omega}{n_0} \quad (7.14)$$

and this detuning from the Kepler frequency of the state $n_0 - 1$ is enough to flip the phase of the electron localization by the π -angle with respect to the driving field.

7.3 Expansion and compression of Rydberg atom

Another kind of adiabatic process may be considered when the frequency of the external field changes slowly and the field strength remains constant. In the strong field limit and in tight binding approximation (4.61), dressed energies depend

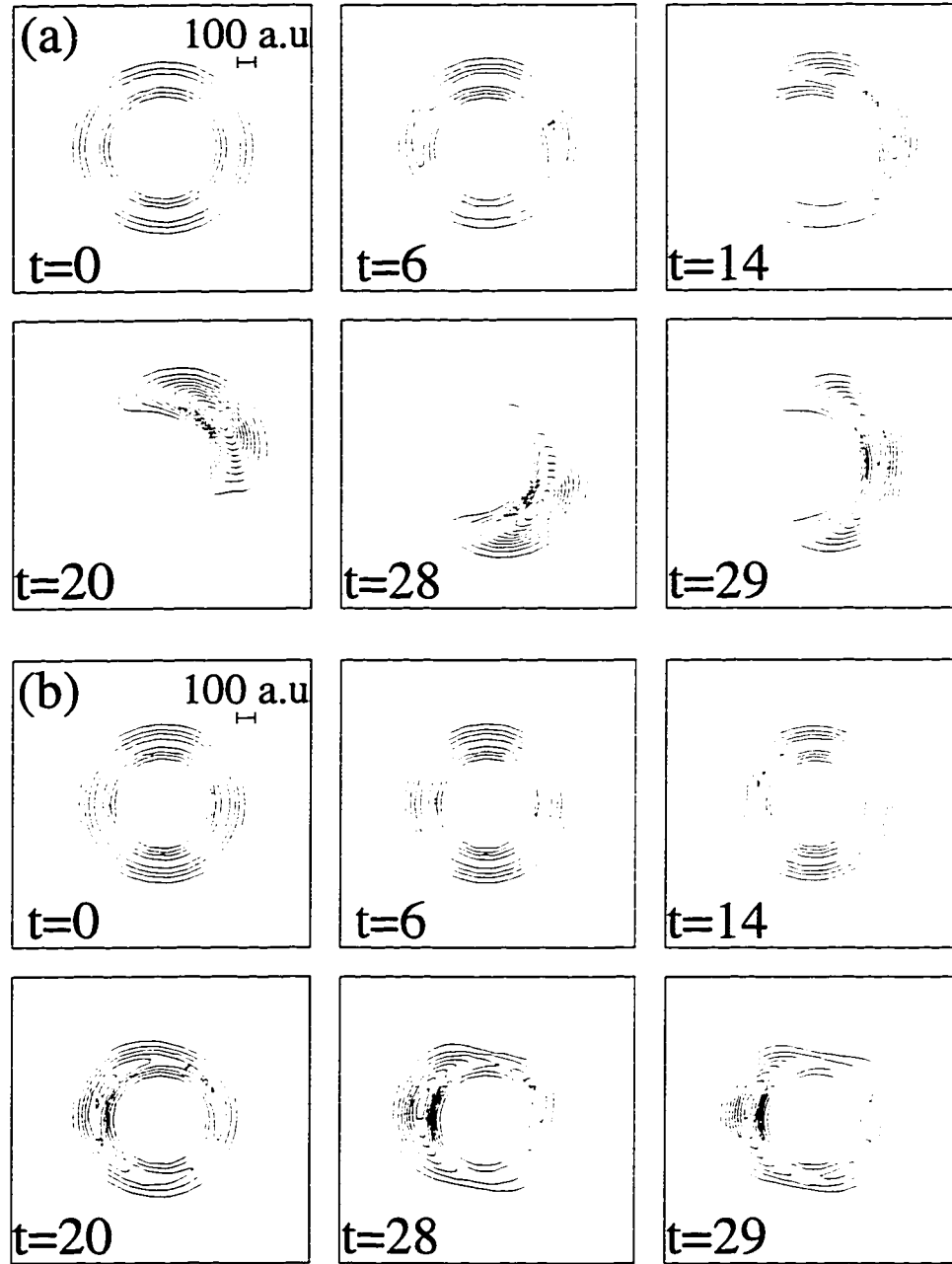


Fig. 7.4. Trojan versus anti-Trojan wave packet formation. (a) The initial state is a circular state with $n_0 = 20$. (b) Anti-Trojan wave packet formation. The initial state is a circular state with $n_0 = 19$. Note that localization occurs at the opposite side of the nucleus from the Trojan case. In both (a) and (b) the CP field was switched on quasi-adiabatically and $\omega = 1/20^3$.

linearly on the frequency of the external field and they are separated by $\sigma \approx \omega_-$.

In that case we can estimate the adiabatic condition from (7.5) as

$$\frac{\omega^{-2/3}}{3\mathcal{E}} \frac{d\omega}{dt} \ll 1 \quad (7.15)$$

which for small changes of ω close to the value $1/n_0^3$ leads to the condition in terms of the scaled variables

$$\frac{d\tilde{\omega}}{d\tau} \ll 6\pi\mathcal{E}_{sc}, \quad (7.16)$$

where we have introduced the frequency scaled to the resonant one $1/n_0^3$, $\tilde{\omega} = \omega n_0^3$.

In the weak binding limit $\mathcal{E}_{sc} \ll 3/8n_0^2$ the Trojan energy line as a function ω has a weakly avoided crossing with the first deexcited level with a gap which can be estimated within the weak binding approximation [65] as $\Delta_{12} = \mathcal{E}r_0$. In order to remain on the Trojan energy line in the weak field limit this crossing must be passed adiabatically. Using the Zener probability condition (7.9) this leads to the estimate

$$\frac{d\omega}{dt} \ll \frac{\pi}{2}(\mathcal{E}r_0)^2. \quad (7.17)$$

This condition for small changes of ω near the resonant value $\omega = 1/n_0^3$ leads to the following condition in terms of scaled variables

$$\frac{d\tilde{\omega}}{d\tau} \ll \pi^2 \frac{\mathcal{E}_{sc}^2}{n_0^4}. \quad (7.18)$$

Fig. 7.5 shows the energy levels as a function of the frequency of C.P. field ω calculated numerically using the aligned states basis between two consecutive resonant values. Figs. 7.6 and 7.7 show the levels for those resonant values as functions of the electric field. The Trojan lines have weakly avoided crossings with other levels not included within our nonlinear theory. The passage through such

crossings should be diabatic and the estimate of the interactions (7.11) leads for both the weak and strong fields to the condition for diabatic passage

$$\frac{d\omega}{dt} \gg \frac{\pi}{200} (\mathcal{E}r_0)^2 \quad (7.19)$$

which in terms of scaled variables is

$$\frac{d\tilde{\omega}}{d\tau} \gg \frac{\pi^2}{100} \frac{\mathcal{E}_{sc}^2}{n_0^4}. \quad (7.20)$$

The conditions (7.15), (7.17) and (7.19) define the adiabatic-rapid passage which should be sufficient to keep the electron in its Trojan packet state when changing the frequency of the C.P. field. Note that in the weak field limit conditions (7.17) and (7.19) may be difficult to fulfill since obeying one leads to the border of applicability of the other.

Both the formula (3.58) and (4.39) for the wave function of the Trojan packet predict that absolute spreads of a Gaussian in all spatial dimensions scale like $\omega^{-1/2} = n_0^{3/2}$. This means that by a frequency change one can compress and expand the region of the electron localization.

Fig. 7.8 shows the electron compression by linearly chirping the frequency between the values resonant with $n = 24$ and $n = 18$. Note that the electron probability density remains in its well localized packet state while being compressed and following helical trajectory.

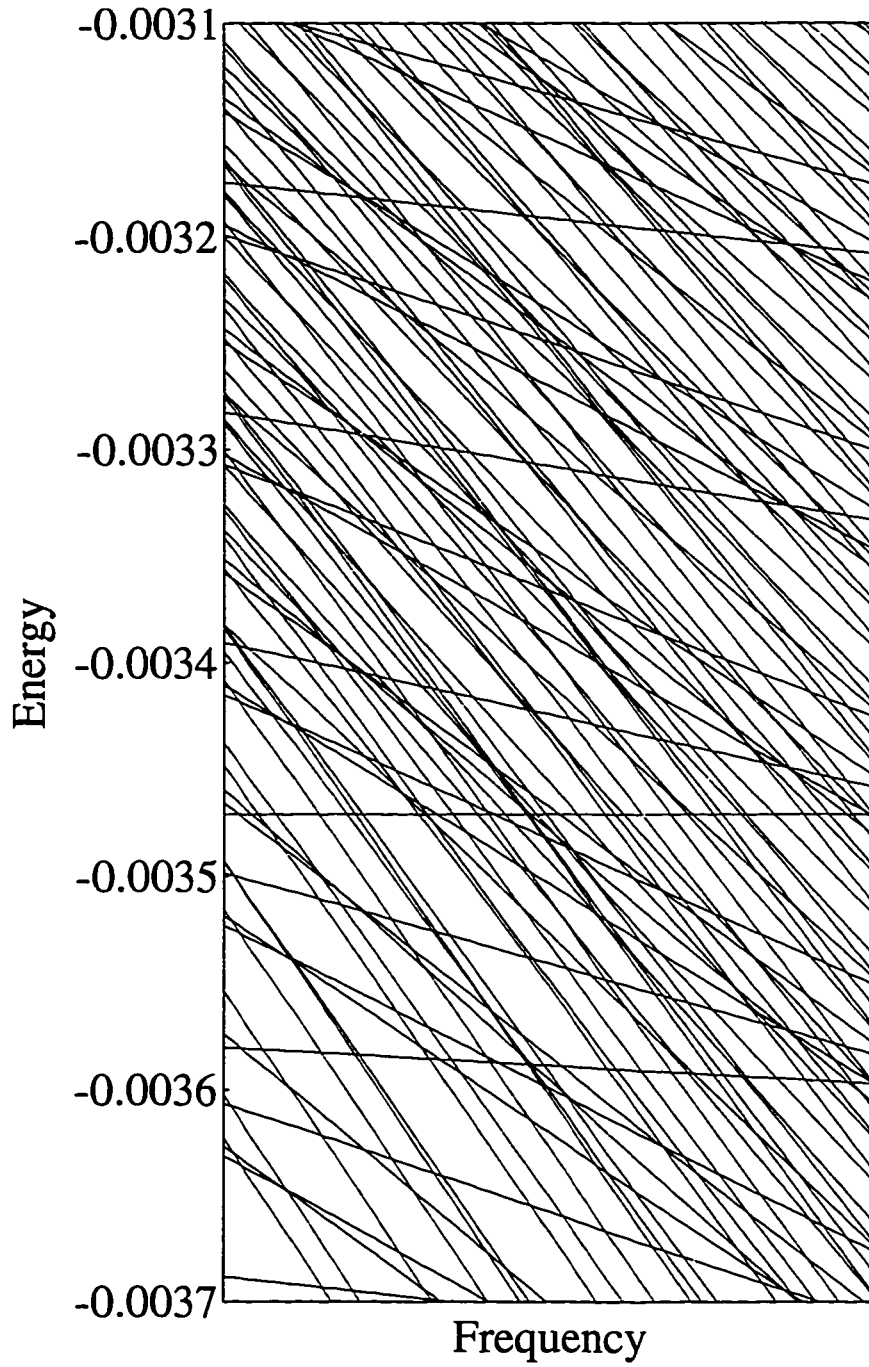


Fig. 7.5. Energy spectrum as a function of frequency between two resonant values $\omega = 1/21^3$ and $\omega = 1/20^3$ for the fixed electric field strenght $\mathcal{E} = 0.016/20^4$. Trojan lines can be identified from their proper connection with triplets for the resonant values (Figs. 7.5 and 7.6).

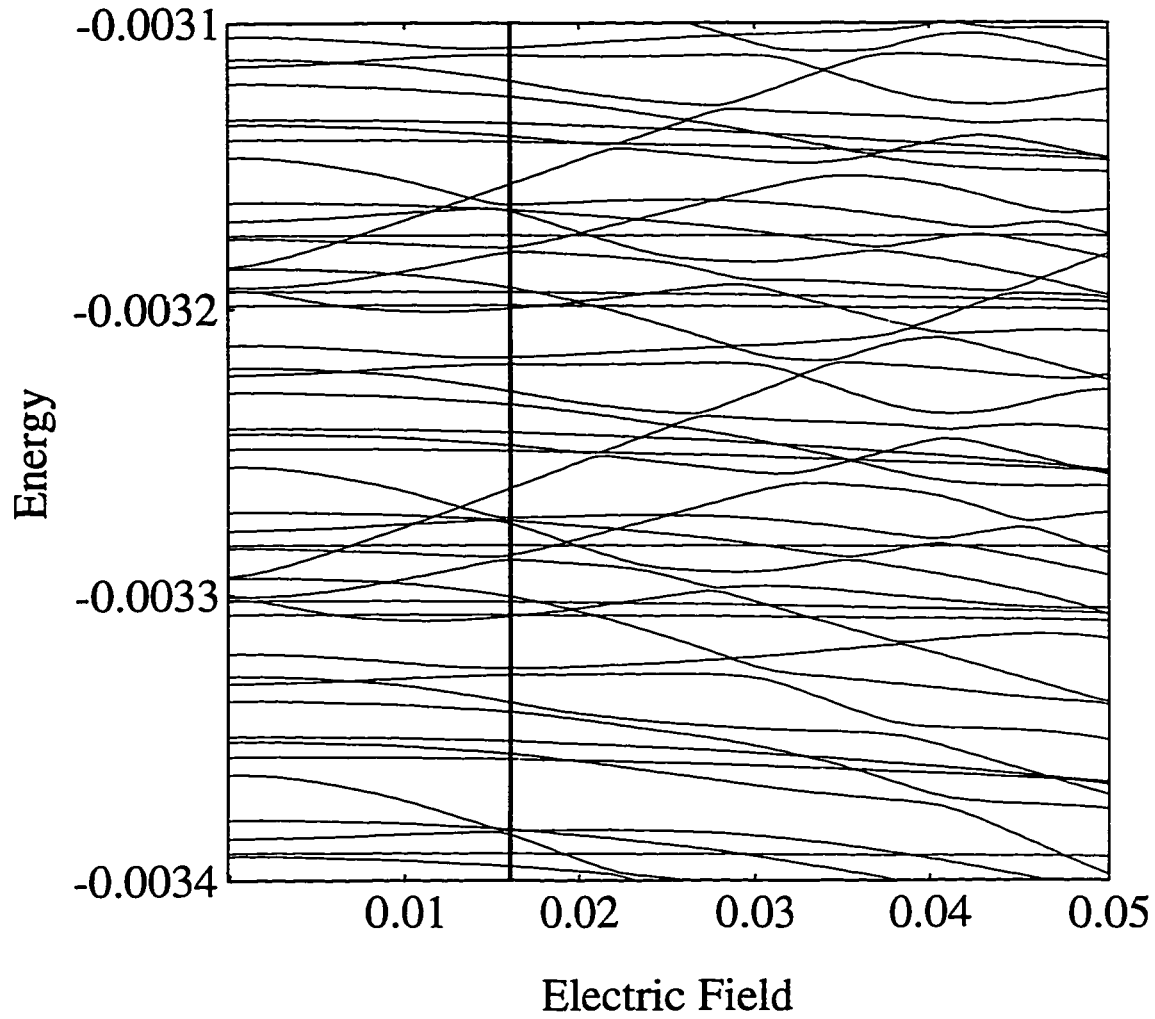


Fig. 7.6. Energy spectrum as a function of electric field scaled to $\omega = 1/20^3$ for the lower frequency boundary of Fig. 7.5 $\omega = 1/21^3$. The energies along the horizontal line coincide with the energies for the lower boundary frequency in Fig. 7.5. The crossing between the horizontal line and Trojan triplets determine starting points for Trojan lines in frequency domain in Fig. 7.5.

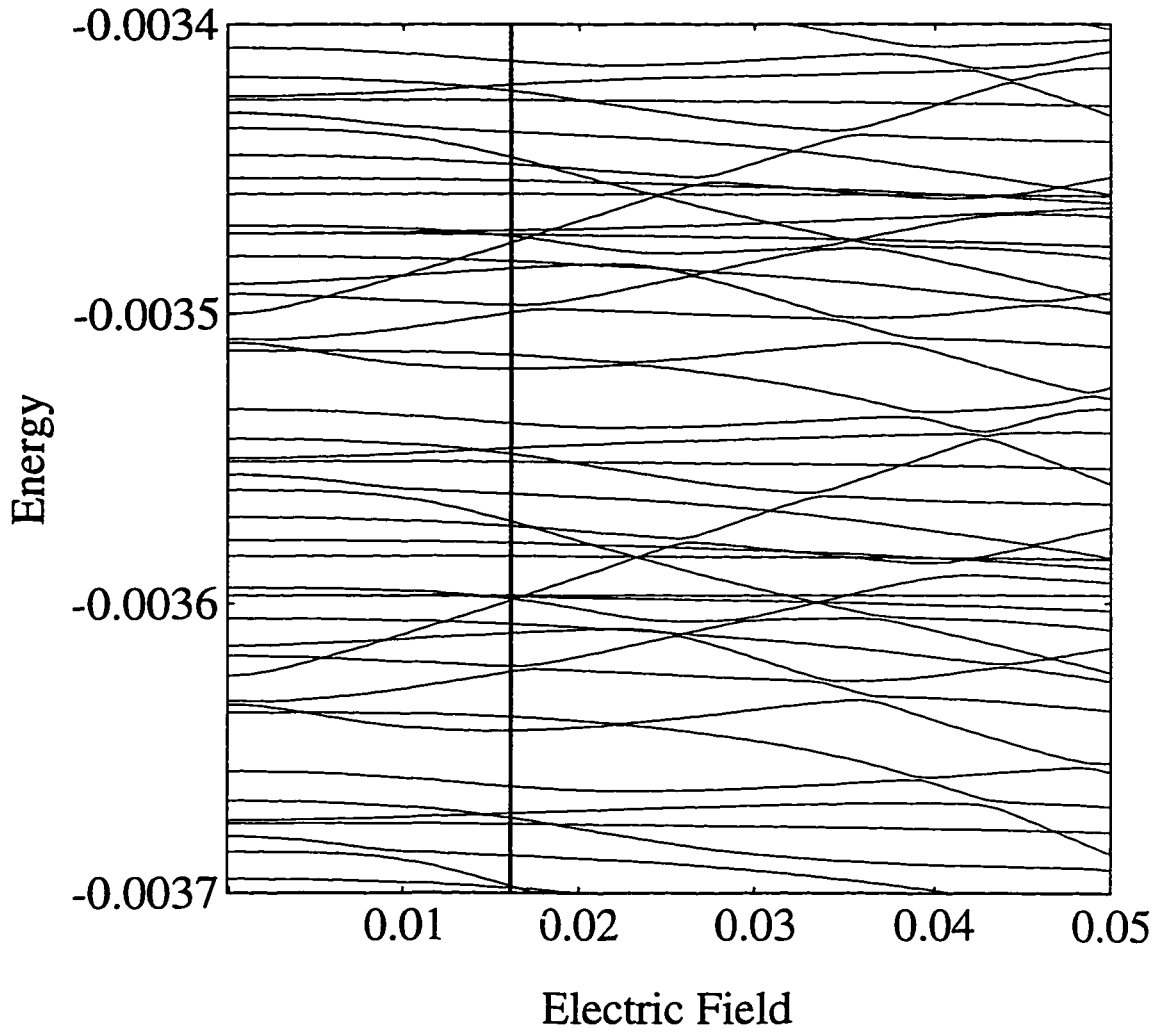


Fig. 7.7. Energy spectrum as a function of electric field scaled to $\omega = 1/20^3$ for the upper frequency boundary of Fig. 7.5 $\omega = 1/20^3$ (same as Fig. 4.8). The energies along the horizontal line coincide with the energies for the upper boundary frequency in Fig. 7.5. The crossing between the horizontal line and Trojan triplets determine ending points for Trojan lines in frequency domain in Fig. 7.5.

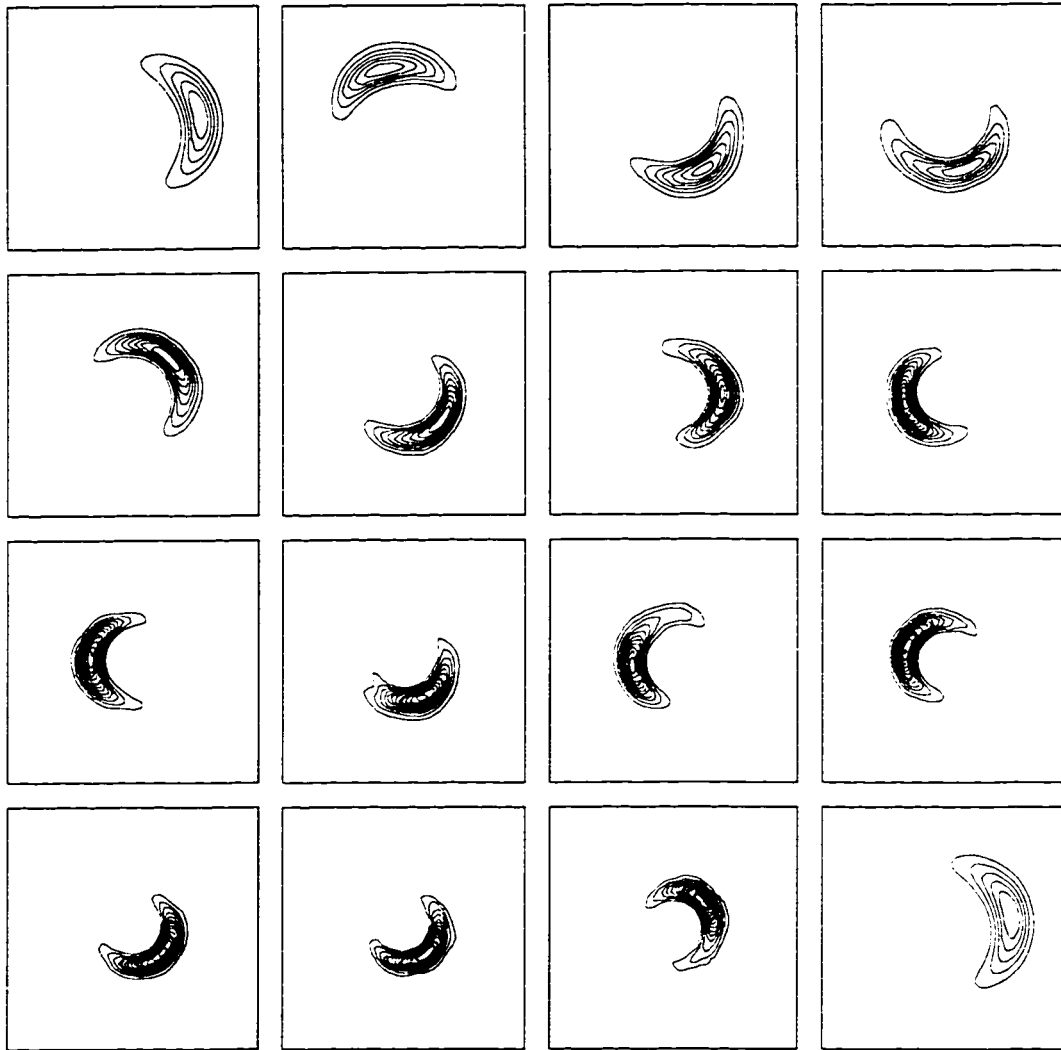


Fig. 7.8. Adiabatic compression of Trojan wave packet. The frequency of the C.P. field is growing linearly from the resonant $\omega = 1/24^3$ to the resonant $\omega = 1/18^3$ during 60-ty optical cycles for the initial frequency. The last plot shows again the packet at $t = 0$ for comparison with compressed proceeding packet at the end of compression. The field strength is $\mathcal{E} = 0.016/24^4$ all the time during frequency chirping. Each square covers the region 1800×1800 atomic units.

Chapter 8

Theory of Detection of Localized States

8.1 Effect of a short pulse on the quantum state

The new experimental technique of generating half-cycle pulses has made it possible both to create atomic wavepackets and to probe their momentum distributions [66]. The condition of a successful probing is that the duration of the pulse must be much shorter than the characteristic time related to the wavepacket dynamics.

Now we consider ionization of the state (4.38) by such an ultra short half-cycle pulse at the time t . When the pulse is much shorter than a period of the linearly polarized field it can be represented by an extra potential [67]

$$V_\delta(\mathbf{r}, t) = -\mathbf{F} \cdot \mathbf{r} \delta(t), \quad (8.1)$$

where \mathbf{F} is the total impulse given to the electron by the pulse. The Schrödinger equation with the total hamiltonian.

$$[H(t) + V_\delta(\mathbf{r}, t)]\Psi_\delta = i \frac{d\Psi_\delta}{dt} \quad (8.2)$$

for small time t can be written in the interaction picture with $\Psi_{I\delta} = e^{-iH(0)t}\Psi_\delta$

$$[e^{-iH(0)t}V_\delta(\mathbf{r}, t)e^{iH(0)t}]\Psi_{I\delta} = i \frac{d\Psi_{I\delta}}{dt} \quad (8.3)$$

and now easily integrated over infinitesimal time ϵ . Thus the quantum state just after the action of the δ -pulse is

$$\Psi_\delta(\mathbf{r}, t + \epsilon) = e^{i\mathbf{F} \cdot \mathbf{r}} \Psi_\delta(\mathbf{r}, t). \quad (8.4)$$

This equation reflects the intuitively clear fact that the momentum has been transferred to the electron by the δ -pulse which leads to an additional phase factor of the wave function.

8.2 Scattering cross section for δ -pulse ionization

Having the result of the action of the short pulse on the quantum state we can now calculate the cross section for the electron ejection in given direction. Further we assume that in the ionization experiment electron is no longer subjected to the influence of the C.P. field so we may use Coulomb continuum states as the scattering states. If $\phi_k(\mathbf{r})$ is a continuum state, the differential ionization cross section for δ -pulse ionization is [68]

$$\frac{d\sigma}{d\Omega} = \rho(k) \left| \int \phi_k^*(\mathbf{r}) \Psi_c(\mathbf{r}, t + \epsilon) d\mathbf{r} \right|^2 \quad (8.5)$$

where $\rho(k)$ is the density of states around ϕ_k . A particularly simple expression given by (8.5) may be obtained for the Trojan wave packet within the Gaussian approximation (3.47) after approximating the continuum state by a plane wave $\phi_k(\mathbf{r}) = e^{i\mathbf{k}\mathbf{r}}/2\pi^{3/2}$, which can be done for sufficiently large momentum k since (8.5) contains the Fourier transform of a Gaussian.

If we assume the ionizing pulse in the direction of the x axis, $\mathbf{F} = -F\hat{x}$, we obtain

$$\begin{aligned} \frac{d\sigma}{d\Omega}(k_x, k_y, k_z, t) &= \frac{N^2 k^2}{(2\pi)^3 [(AB + C^2)D\omega^3]} \exp - \frac{(k'_x - F \cos \omega t)^2}{B\omega} \\ &\times \exp - \frac{(k'_x - F \cos \omega t)^2 C^2 + (k'_y - F \sin \omega t - \omega x_0)^2 B^2}{\omega(AB^2 + C^2 B)} \\ &\times \exp \frac{-k_z^2}{D\omega}, \end{aligned} \quad (8.6)$$

where

$$\begin{aligned} k'_x &= k_x \cos \omega t - k_y \sin \omega t \\ k'_y &= k_x \sin \omega t + k_y \cos \omega t \end{aligned} \quad (8.7)$$

In the plane of the packet motion $k_z = 0$ and in the direction parallel to the ionizing pulse $k_y = 0$ this cross section has two maxima per period as a function of time. For $t = \pi(j + 1/4)/\omega$, the maximum value is reached for the resonant momentum transfer $k_x = F \pm \omega x_0$. It means that the ionization in the direction of the ionizing pulse is the largest when the Trojan packet momentum and the impulse of the δ -pulse are parallel to each other. This result immediately suggests the detection of the Trojan packet state in an experiment analogous to the pump-probe experiment suggested for the detection of the circular-orbit wave packets in bare hydrogen or performed for the detection of the angularly localized wave packets [69]. In this experiment the launching of the ionizing δ -pulse should be timed to the phase of the circularly polarized field which generates the Trojan packet, and spatially resolved measurement of the ionization should be performed.

For any rotating frame eigenstates given by (4.37) the differential cross section (8.5) can be calculated analytically using the exact states of the Coulomb continuum $|\kappa\rangle$

$$\begin{aligned} \langle \mathbf{r} | \kappa \rangle &= \frac{1}{(2\pi)^{3/2}} \exp(\pi/2\kappa) \Gamma(1 + i/\kappa) \exp(i\vec{\kappa} \cdot \mathbf{r}) \\ &\times {}_1F_1(-i/\kappa, 1, -i\vec{\kappa} \cdot \mathbf{r} - i\kappa r), \end{aligned} \quad (8.8)$$

where ${}_1F_1$ is a confluent hypergeometric function of the first kind. This can be done since the matrix elements $\langle \kappa | e^{i\mathbf{F} \cdot \mathbf{r}} | n, n - k, n - k - s \rangle$ in the projection

$$\begin{aligned} \langle \kappa | e^{i\mathbf{F} \cdot \mathbf{r}} | jks \rangle(t) &= \exp[-iE_{ks}^j t] \\ &\times \sum_n \langle \kappa | e^{i\mathbf{F} \cdot \mathbf{r}} | n, n - k, n - k - s \rangle a_{nks}^j \exp[-i(n - k - s)\omega t] \end{aligned} \quad (8.9)$$

with $|jks\rangle$ by $\langle \mathbf{r}|jks\rangle = \Psi_{jks}(\mathbf{r}, t)$, have explicit analytical form. The latter follows from the expansion

$$\begin{aligned} \langle \kappa | e^{i\mathbf{F}\cdot\mathbf{r}} | n, n-k, n-k-s \rangle = \\ \sum_{n_1=0}^{n-|m|-1} \langle n_1, n_2, m | n, n-k, n-k-s \rangle \langle \vec{\kappa} | \exp(i\mathbf{F}\cdot\mathbf{r}) | n_1, n_2, m \rangle, \end{aligned} \quad (8.10)$$

where $|n_1, n_2, m\rangle$ are the parabolic states and $n_1 + n_2 = n - |n-k-s| - 1$. Further [68] the transformation matrix $\langle n_1, n_2, m | n, l, m \rangle$ can be expressed in terms of the standard Clebsch-Gordan coefficients $C(j_1, j_2, j; m_1, m_2, m)$ [55]

$$\begin{aligned} \langle n_1, n_2, m | n, l, m \rangle = (-1)^{n_1+(3|m|-m)/2} \\ C[(n-1)/2, (n-1)/2, l; (m+n_2-n_1)/2, (m+n_1-n_2)/2, m] \end{aligned} \quad (8.11)$$

and the matrix elements $\langle \vec{\kappa} | \exp(i\mathbf{F}\cdot\mathbf{r}) | n_1, n_2, m \rangle$ are known [68]. An especially simple expression can be obtained for the states spanned by the circular states manifold $k=1, s=0$, i.e., the ones which include the Trojan packets $j=0$, and by approximating the Coulomb continuum by plane waves $|\vec{\kappa}\rangle \approx |\mathbf{k}\rangle$. For $\mathbf{k} = (k_x, 0, 0)$ we get

$$\begin{aligned} \langle \mathbf{k} | e^{i\mathbf{F}\cdot\mathbf{r}} | jks \rangle = \exp[-iE_{ks}^j t] \\ \frac{\sqrt{2}}{2\pi} \sum_n a_{n10}^j e^{-i(n-1)\omega t} \frac{1}{(n-1)!} \frac{2^{2n}}{n^{n+1}} (k_x - F)^{n-1} \left[(k_x - F)^2 + \frac{1}{n^2} \right]^{-n} \end{aligned} \quad (8.12)$$

Fig. 8.1 shows a sample differential cross section (8.5) as a function of time and k_x for $k_z = k_y = 0$ as obtained from the formula (8.6). Fig. 8.2 shows the cross section obtained from the formula (8.12) and Fig. 8.3 from the numerical solution.

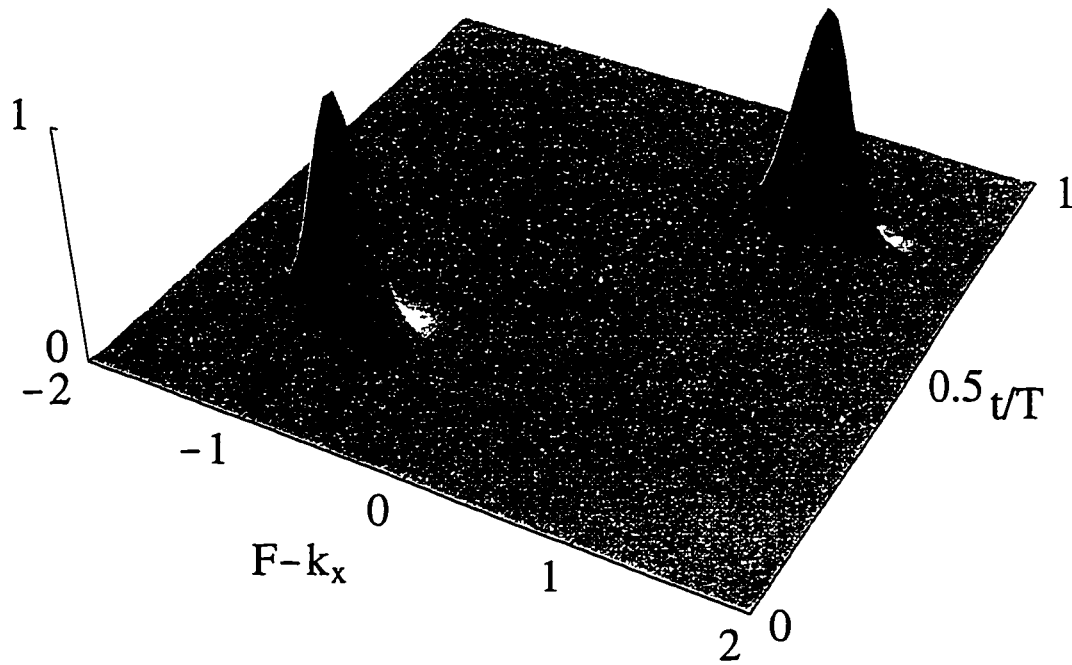


Fig. 8.1. Normalized differential cross section (8.6) (divided by the density of levels) in the direction parallel to the ionizing δ -pulse calculated with the plane-wave continuum and Gaussian wave function (3.47) for $\omega = 1/20^3$ and $\mathcal{E}_{sc} = 0.016$ as a function of time during one optical cycle. Note that a single flash appears during the cycle in each direction. One unit of the wave vector k_x is the momentum of the Trojan packet ωr_0 .

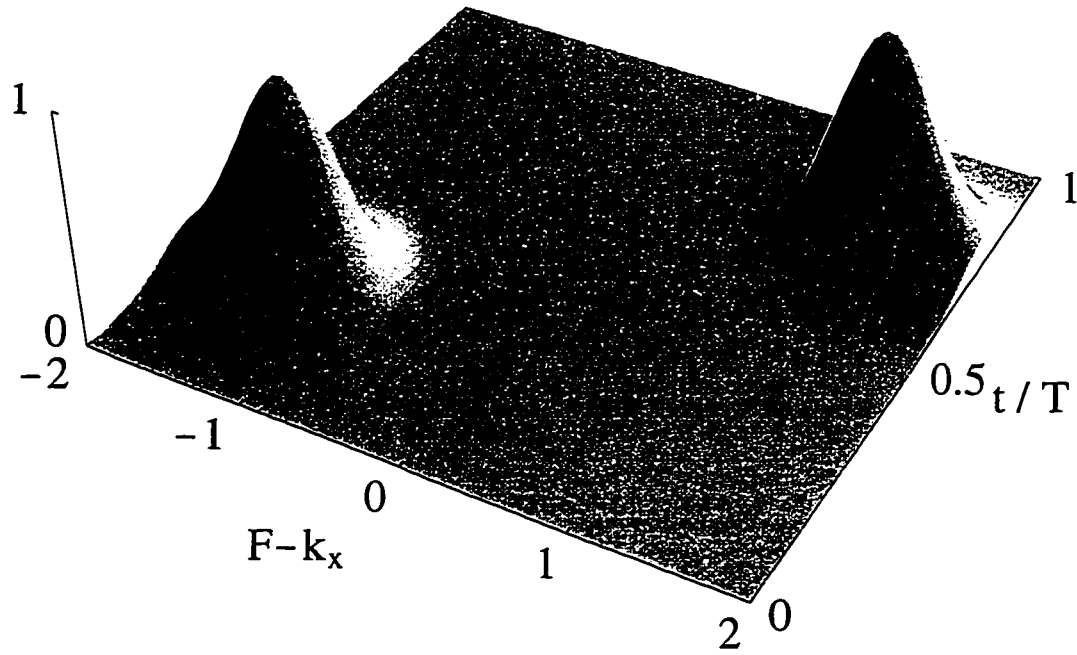


Fig. 8.2. Normalized differential cross section from the expansion (8.12) (divided by the density of levels) in the direction parallel to the ionizing δ -pulse calculated with the plane-wave continuum and the Trojan state within nonlinear approach (4.37) for $\omega = 1/20^3$ and $\mathcal{E}_{sc} = 0.016$ as a function of time during one optical cycle. The deviation of the packet from Gaussian form in Cartesian coordinates leads to broadening of the peaks in the time domain. One unit of the wave vector k_x is the momentum of the Trojan packet ωr_0 .

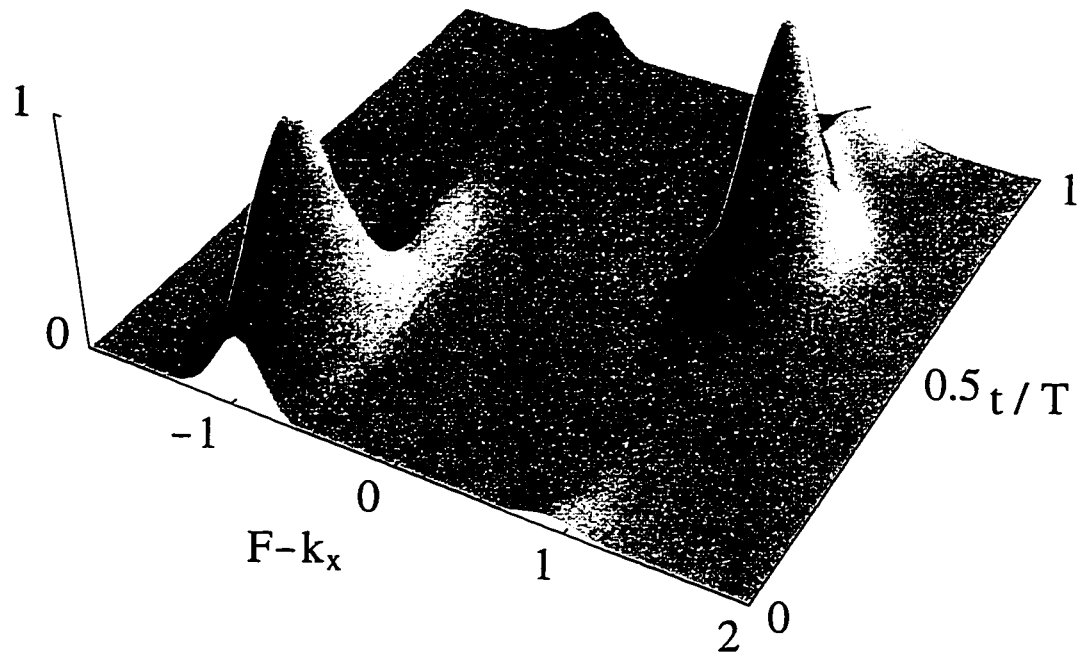


Fig. 8.3. Normalized differential cross section (8.5) (divided by the density of levels) in the direction parallel to the ionizing δ -pulse calculated numerically with the plane-wave continuum for $\omega = 1/20^3$ and $\mathcal{E}_{sc} = 0.016$ as a function of time during one optical cycle (between $t = 20$ and $t = 21$) for the wave packet generated in the adiabatic turn-on shown in Fig. 7.1. One unit of the wave vector k_x is the momentum of Trojan packet ωr_0 .

Chapter 9

Summary

The theory presented here describes the quantum dynamics of a hydrogenic single electron atom in the case when the frequency of a monochromatic driving field is nearly equal to the spacing between unperturbed Rydberg levels and the quantum states have large angular momentum. By a new choice of basis states we have managed to reduce a complicated quantum system to a simple pendulum with wave functions well understood as solutions of Mathieu's equation. The only dynamical parameter of the theory, $p = 4\mathcal{E}/3\omega^2$, has a clear physical interpretation as $4/3$ of the ratio between the Volkov radius and the Bohr radius. The theory predicts the existence of two classes of eigenstates that are well-localized packets which move in the laboratory frame along circular orbits. The so-called Trojan states, for larger electric fields, can be accurately predicted within a simpler harmonic approximation, however anti-Trojan states are a direct prediction of nonlinear theory.

In the theory the inverse of the principal quantum number $1/n$ is assumed to be very small. This fact however should not lead to the conclusion that the existence of the localized states can be explained on the basis of classical mechanics. For both Trojan and anti-Trojan wave packets the phase space distributions calculated from the quantum mechanical wave functions significantly overlap with regions where the corresponding classical dynamics is chaotic [70, 71]. This allowed us to associate anti-Trojan states with quantum scars [71] and gave new insight into the quality of classical versus quantum-mechanical harmonic approximations [70]. Both the pendular and harmonic approximations work better on the

quantum mechanical level and this can be well understood within the hydrodynamic approach to quantum dynamics [72]. For bound quantum states quantum mechanics is never a small correction to classical mechanics as the classical forces exactly balance effective quantum mechanical forces.

The strongest and most striking prediction of our theory, beyond just the existence of two classes of localized states, is that the nonlinear response of the electron localization is enormously sensitive to the relation between the quantum number of these states and the frequency of this field. This imprint of Trojan nonlinear, resonant dynamics may be very helpful for the detection of both Trojan and anti-Trojan states. This feature can also be used to control the relative phase of the induced electron dipole moment of the Rydberg atom with respect to the driving C.P. field. The adiabatic extension of the theory for the case when the frequency changes slowly predicts that compression and expansion of the electron orbit accompanies this process. An extension of the theory using the RWA predicts that a linearly polarized electromagnetic field is also sufficient to support and generate well localized states

Extensions of the harmonic theory have been made to the case when a magnetic field is perpendicular to the plane of polarization of the C.P. field [73]. This combination of fields is also able to support coherent propagation of nondispersing Gaussian-like wave packets. Also the very small ionization of localized states, which is neglected in our theory, exhibits interesting behavior [74] closely related to conductance fluctuation in mesoscopic rings. The peculiar localization properties of Trojan states also motivated us to test hydrogen in a linearly polarized field as a magnetic-field-sensitive quantum magnetometer [75].

Another related class of problems arises with the question whether localized electron wavepackets exist, where the electron probability cloud is frozen in shape

without any external fields and moves periodically along a well defined trajectory. These have been predicted both in molecules with a permanent dipole moment of the core [76] as well as in a two-electron atom [77] which would be a true quantum realization of the “Rutherford atom”.

The only ultimate test of each theory is an experiment, and we hope that both Trojan and anti-Trojan packets will be observed in the laboratory in near future.

References

- [1] See, for example, P. Agostini and G. Petite, *Contemp. Phys.* **29**, 57 (1988); A. L'Huillier, L. A. Lompré, G. Mainfray and C. Manus, in *Atoms in Intense Laser Fields*, edited by M. Gavrilá (Academic Press, 1992).
- [2] T. W. Ducas, M. G. Littman, R. R. Freeman and D. Kleppner, *Phys. Rev. Lett.* **35**, 366 (1975); P. Koch, *Phys. Rev. Lett.* **41**, 99 (1978); M. L. Zimmermann, M. G. Littman, M. M. Kash and D. Kleppner *Phys. Rev. A* **40**, 485 (1989); A. ten Wolde and L. D. Noordam, *Phys. Rev. A* **40**, 485 (1989); L. D. Noordam, T. F. Gallagher, *J. Opt. Soc. Am. B* **8**, 882 (1991); J. A. Yeazell, G. Raithel, L. Marmet, H. Held and H. Walther, *Phys. Rev. Lett.* **70**, 2884 (1993).
- [3] A. Yeazell and C. R. Stroud, Jr., *Phys. Rev. Lett.* **60**, 1494 (1988); J. A. Yeazell, M. Mallalieu, J. Parker, C. R. Stroud, Jr., *Phys. Rev. A* **40**, 5040 (1990); J. A. Yeazell, M. Mallalieu and C. R. Stroud, Jr., *Phys. Rev. Lett.* **64**, 2007 (1990); M. W. Noel and C. R. Stroud, Jr., *Phys. Rev. Lett.* **75**, 1252 (1995).
- [4] J. H. Eberly, J. Javanainen and K. Rzazewski, *Phys. Rep.* **204**, 331 (1991).
- [5] Q. Su, J. H. Eberly and J. Javanainen, *Phys. Rev. Lett.* **64**, 862 1990; K. C. Kulander, K. J. Schafer and J. L. Krause, *Phys. Rev. Lett.* **66**, 2601 (1991); J. H. Eberly and K. C. Kulander, *Science* **262**, 1229 (1993).
- [6] See, for example, *Atoms in Strong Light Fields*, N. B. Delone and V. P. Krainov (Springer-Verlag, 1985).
- [7] D. M. Volkov, *Z. Phys.* **94**, 250 (1935).

- [8] R. Grobe, C. I. Moore, Q. Su, W. G. Greenwood and J. H. Eberly, *Ann. Phys.* **48**, 87 (1991); R. Grobe and J. H. Eberly, *Phys. Rev. A* **47**, 1605 (1993).
- [9] G. M. Huang, T. J. Tarn and J. W. Clark, *J. Math. Phys.* **24**, 2608 (1983); M. Dahleh, A. P. Peirce and H. Rabitz, *Phys. Rev. A* **42**, 1065 (1990); Y. Yan, R. E. Gillilan, R. M. Whitnell, K. R. Wilson and S. Mukamel, *J. Phys. Chem.* **97**, 2320 (1993).
- [10] S. Basile, F. Trombetta and G. Ferrante, *Phys. Rev. Lett.* **61**, 2435 (1988); H. R. Reiss and V. P. Krainov, *Phys. Rev. A* **50**, R910 (1994).
- [11] See, for example, *Optical Resonance and Two-Level Atoms*, L. Allen and J. H. Eberly (Dover Publications Inc., 1987).
- [12] W. C. Henneberger, *Phys. Rev. Lett.* **21**, 838 (1968).
- [13] H. R. Reiss, *Phys. Rev. A* **22**, 1786 (1980).
- [14] T. F. Gallagher, *Rydberg Atoms* (Cambridge University Press, 1994).
- [15] J. E. Bayfield and P. M. Koch, *Phys. Rev. Lett.* **33**, 258 (1974); J. E. Bayfield and D. W. Sokol, *Phys. Rev. Lett.* **61**, 2007 (1988); B. E. Sauer, M. R. W. Bellermaun and P. M. Koch, *Phys. Rev. Lett.* **68**, 1633 (1992).
- [16] G. Casati, B. V. Chirikov, I. Guarneri and D. L. Shepelyansky, *Phys. Rev. Lett.* **59**, 2927 (1987); A. Buchleitner and D. Delande, *Phys. Rev. Lett.* **70**, 33 (1992); J. Zakrzewski, D. Delande and J. C. Gay, *Phys. Rev. A* **47**, 2468 (1993).
- [17] R. G. Hulet and D. Kleppner, *Phys. Rev. Lett.* **51**, 1430 (1983); J. Hare, M. Gross and P. Goy, *Phys. Rev. Lett.* **61**, 1938 (1988); P. Nussenzveig, F.

- Bernardot, M. Brune, J. Hare, J. M. Raimond, S. Haroche and W. Gawlik, Phys. Rev. A **48**, 3991 (1993); R. J. Brecha, G. Raithel, C. Wagner and H. Walther, Opt. Comm. **102**, 257 (1993); C. H. Cheng, C. Y. Lee and T. F. Gallagher, Phys. Rev. Lett. **73**, 3078 (1994).
- [18] H. Klar, Z. Phys. D **11**, 45 (1989).
- [19] L. S. Brown, Amer. J. Phys. **41**, 525 (1973).
- [20] H. Goldstein, *Classical Mechanics* (Addison-Wesley, 1980).
- [21] M. Abramowitz and I. A. Stegun, *Handbook of Mathematical Functions* (Dover, 1969).
- [22] J. H. Howard, Phys. Rev. A **46**, 364 (1992).
- [23] D. Farrelly and T. Uzer, Phys. Rev. Lett **74**, 1720, (1995).
- [24] K. Sacha and J. Zakrzewski, Phys. Rev A **55**, 568 (1997).
- [25] B. V. Chirikov, Phys. Rep. **52**, 265 (1979).
- [26] A. J. Lichtenberg and M. A. Lieberman, *Regular and Chaotic Dynamics* (Springer-Verlag, 1992).
- [27] W. Pauli, Z. Phys. **36**, 339 (1926).
- [28] D. Wintgen, Z. Phys. D **18**, 125 (1991).
- [29] L. I. Schiff, *Quantum Mechanics* (McGraw-Hill, 1968).
- [30] M. Kalinski, E. A. Shapiro and J. H. Eberly, (in preparation).
- [31] M. Nauenberg, Phys. Rev. A **40**, 1133 (1989).

- [32] I. W. Herb, Phys. Rev. Lett. **41**, 67 (1978).
- [33] H. J. Silverstone, Phys. Rev. A **18**, 1853 (1978).
- [34] K. Helfrich, Theoret. Chim. Acta **24**, 271 (1972).
- [35] L. D. Landau and E. M. Lifshitz *Quantum Mechanics, Non-relativistic Theory* (Pergamon, 1958).
- [36] M. C. Gutzwiller, *Chaos in Classical and Quantum Mechanics* (Springer-Verlag, 1990).
- [37] M. L. Zimmerman, M. M. Kash and D. Kleppner, Phys. Rev. Lett. **45**, 1092 (1980).
- [38] D. Wintgen and H. Friedrich, J. Phys. B **19**, 1261 (1986).
- [39] E. A. Solov'ev, Zh. Eksp. Theor. Fiz. **82**, 1762 (1981).
- [40] D. R. Herrick, Phys. Rev. A **26**, 323 (1982).
- [41] D. Delande and J.C. Gay, J. Phys. B **17**, 335 (1984).
- [42] Y. N. Demkov, B.S. Monozon and V. N. Ostrovskii, Zh. Eksp. Theor. Fiz. **57**, 1431 (1970).
- [43] J. J. Hopfield, Phys. Rev. A **122**, 1555 (1958).
- [44] I. Bialynicki-Birula, M. Kalinski and J. H. Eberly, Phys. Rev. Lett. **73**, 1777 (1994).
- [45] M. Kalinski and J. H. Eberly, Phys. Rev. A **53**, 1715 (1996).
- [46] M. Kalinski, J. H. Eberly and I. Bialynicki-Birula, Phys. Rev. A **52**, 2460 (1995).

- [47] N. W. McLachlan, *Theory and Application of Mathieu Functions* (Oxford University Press, 1947).
- [48] H. A. Bethe and E. E. Salpeter, *Quantum mechanics of one and two-electron atoms* (Springer-Verlag, 1957).
- [49] R. M. More and K. H. Warren, *Ann. Phys.* **207**, 282 (1991).
- [50] I. C. Percival and D. Richards, *Adv. At. Mol. Phys.* **11**, 1 (1975).
- [51] D. Farrelly and T. Uzer, *Phys. Rev. Lett.* **74**, 1720 (1995).
- [52] D. Delande, J. Zakrzewski and A. Buchleitner, *Europhys. Lett.* **32**, 107 (1995).
- [53] X. L. Yang, S. H. Guo and F. T. Chan, *Phys. Rev. A* **43**, 1186 (1991).
- [54] E. Merzbacher, *Quantum Mechanics* (John Wiley & Sons, 1970).
- [55] L. I. Schiff, *Quantum Mechanics* (Mc-Graw Hill, 1968).
- [56] U. Fano, *Phys. Rev. A* **2**, 353 (1970).
- [57] C. Kittel, *Introduction to Solid State Physics* (John Wiley & Sons, 1959).
- [58] See *Letters on Wave Mechanics*, edited by K. Przibram (Philosophical Library, 1967), pp 55-75.
- [59] Revivals were first indenified in the context of cavity QED: J. H. Eberly, N. B. Narozhny and J. J. Sanchez-Mondragon, *Phys. Rev. Lett.* **44**, 1323 (1980). Fractional revivals appeared in studies of Rydberg wave packets: J. Parker and C. R. Stroud, Jr., *Phys. Rev. Lett.* **56**, 716 (1986); Y. A. Yeazell and C. R. Stroud, Jr., *Phys. Rev. A* **43**, 5153 (1991) and were first explained

- by Averbuch: I. S. Averbuch and N. F. Perelman, Phys. Lett. A **139**, 449 (1989).
- [60] E. Heller, Phys. Rev. Lett. **53**, 1515 (1984).
- [61] M. Kalinski and J. H. Eberly, Phys. Rev. A **52**, 4285 (1995).
- [62] G. V. Varada and G. S. Agarwal, Phys. Rev. A **48**, 4062 (1993).
- [63] J. D. Jackson, *Classical Electrodynamics* (John Wiley & Sons, 1975).
- [64] C. Zener, Proc. Roy. Soc. London A **137**, 696 (1932).
- [65] G. Schön and A. D. Zaikin, Phys. Rep. **198**, 237 (1990).
- [66] R. R. Jones, Phys. Rev. Lett. **76**, 3927 (1996).
- [67] V. Enss, V. Kostykin and R. Schrader, Phys. Rev. A **50**, 1578 (1994).
- [68] D. Belkic, J. Phys. B **16**, 2773 (1983).
- [69] J. A. Yeazell and C. R. Stroud, Jr., Phys. Rev. A **35**, 2806 (1987); J. A. Yeazell and C. R. Stroud, Jr., Phys. Rev. A **43**, 5153 (1991).
- [70] I. Bialynicki-Birula, M. Kalinski and J. H. Eberly, Phys. Rev. Lett. **75**, 973 (1995).
- [71] M. Kalinski and J. H. Eberly, Phys. Rev. Lett. **77**, 2420 (1996).
- [72] I. Bialynicki-Birula, M. Cieplak and J. Kaminski, *Theory of Quanta* (Oxford University, 1992), p. 88.
- [73] E. Lee, A. F. Brunello and D. Farrelly, Phys. Rev. A **55**, 2203 (1997).

- [74] J. Zakrzewski, D. Delande and A. Buchleitner, Phys. Rev. Lett. **75**, 4015 (1995).
- [75] M. Kalinski, Phys. Rev. A (submitted for publication).
- [76] I. Bialynicki-Birula and Z. Bialynicka-Birula, Phys. Rev. Lett. **77**, 4298 (1996).
- [77] M. Kalinski, J. H. Eberly, J. A. West and C. R. Stroud, Jr., Phys. Rev. Lett. (submitted for publication).